WATER: A TALE OF TWO LIQUIDS

P. Gallo

Dipartimento di Matematica e Fisica,
Universitá Roma Tre, via della Vasca Navale 84,
I-00146 Rome, Italy and INFN Sez. Roma Tre,
Via della Vasca Navale 84, I-00146 Rome, Italy

K. Amann-Winkel

Department of Physics, AlbaNova University Center,
Stockholm University, SE-106 91, Stockholm, Sweden

C. A. Angell

Department of Chemistry and Biochemistry,
Arizona State University, Tempe, Arizona 85287, USA

M. A. Anisimov

Institute for Physical Science and Technology and
Department of Chemical and Biomolecular Engineering,
University of Maryland, College Park, MD 20742, USA

F. Caupin

Laboratoire de Physique de la Matière Condensée et Nanostructures,
Université Claude Bernard Lyon 1 et CNRS, Institut Universitaire de France,
43 boulevard du 11 novembre 1918, 69100 Villeurbanne, France

C. Chakravarty

Department of Chemistry, Indian Institute of Technology Delhi,
Hauz Khas, New Delhi 110016, India

T. Loerting

Institute of Physical Chemistry, University of Innsbruck, 6020 Innsbruck, Austria

A. Z. Panagiotopoulos

Department of Chemical and Biological Engineering,
Princeton University, Princeton, NJ 08544, USA

J. Russo and H. Tanaka
Institute of Industrial Science, University of Tokyo,
4-6-1 Komaba, Meguro-ku, Tokyo 153-8505, Japan

J. A. Sellberg
Laboratory of Molecular Biophysics,
Department of Cell and Molecular Biology,
Biomedical Center, SE-752 37 Uppsala Sweden

H. E. Stanley and E. Lascaris
Center for Polymer Studies and Department of Physics,
Boston University, Boston, MA 02215, USA

C. Vega
Departamento de Quimica Fisica, Facultad de Ciencias Quimicas,
Universidad Complutense de Madrid, 28040 Madrid, Spain

L. Xu
International Center for Quantum Materials,
Peking University, Beijing 100871, China

L. G. M. Pettersson
Dept. of Physics, AlbaNova University Center,
Stockholm University, SE-106 91, Stockholm, Sweden

CONTENTS

I. INTRODUCTION

Water is the most abundant liquid, exhibits the most anomalous behavior, and is a prerequisite for life on this planet and probably for life elsewhere [1–10]. It shows a density maximum at 4°C (277 K) under ambient conditions and the solid phase has a lower density than the liquid (ice floats on top of liquid water) [11, 12, 14]. Its thermodynamic response functions, such as specific heat C_P, compressibility κ_T, and thermal expansion coefficient α, all of which can be determined by entropy or volume fluctuations, i.e.

$$\left\langle (\Delta V)^2 \right\rangle = V k_B T \kappa_T, \tag{1}$$

$$\left\langle (\Delta S)^2 \right\rangle = N k_B C_P,$$

and

$$\langle \Delta V \Delta S \rangle = V k_B T \alpha,$$

also show anomalous behaviors [4–6, 14–19].

For example, at atmospheric pressure κ_T increases when $T < 46$°C (319 K) but exhibits normal behavior when $T > 46$°C. Similarly, at atmospheric pressure C_p increases when $T < 35$°C (308 K) and the value of α becomes negative, indicating that the volume expands below 4°C. One characteristic of the three thermodynamic properties shown in Eq. (1) is that they are related to fluctuations in liquid water that *increase* upon cooling below a certain temperature instead of decrease as in simple liquids. Figure 1 shows how this anomalous behavior becomes more pronounced in the deeply supercooled region and seems to diverge when T approaches -45°C (228 K) [12].

Here we review the behavior of water in the anomalous regime from ambient conditions to the deeply supercooled region. The regime above 232 K (temperature of homogeneous ice nucleation) and below the crystallization temperature 160 K (at ambient pressure) has provided the most information since it is more accessible. Among several theoretical scenarios, a liquid-liquid phase transition and an associated critical point (LLCP) are conjectured [13] and are assumed to lie in the regime between 232 K and 160 K, the so-called "no-man's land" in the phase diagram, so called because ice nucleation occurs too rapidly for conventional measurement techniques. We connect the thermodynamic behavior of liquid water—its restructuring, anomalous behavior, and dynamics in the ambient and moderately supercooled

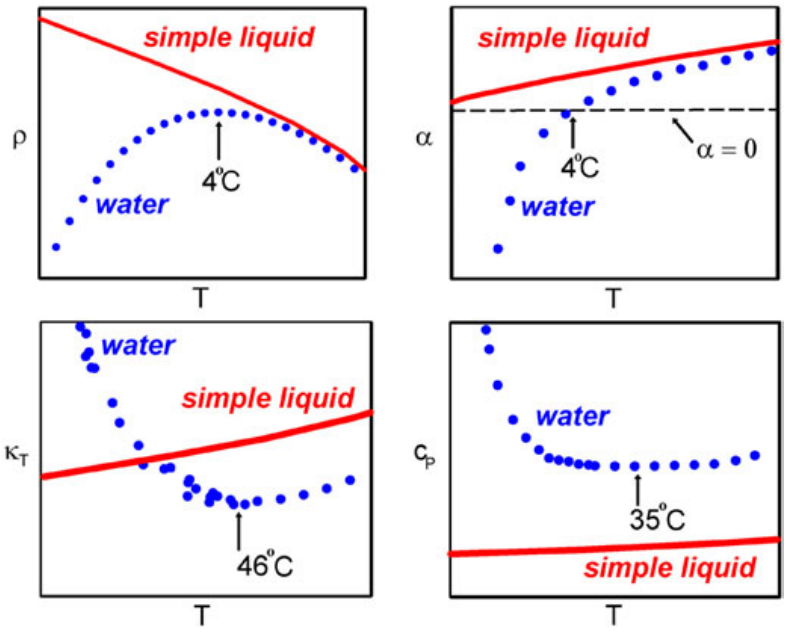

FIG. 1. Anomalous thermodynamic properties of water compared to simple liquids. Schematic comparison of the isobaric temperature dependence of the density ρ, thermal expansion coefficient α, isothermal compressibility κ_T, and isobaric heat capacity C_P for water and a simple liquid. Reproduced with permission from ref. [4].

regimes where experimental and simulation data are more accessible—to its behavior in the deeply supercooled region where an LLCP, real or virtual, may be located.

II. SEVERAL SCENARIOS

Over the past years, different scenarios have been proposed to explain the origin of the anomalies briefly described in the preceding section [13, 20–24]. The first was in 1982 in a remarkable paper by Robin Speedy [25], which has become known as the "Speedy stability limit conjecture". It has the same form of metastable water phase diagram as that yielded by empirical equations of state for water produced by the water and steam engineers. It was followed in 1992 by the famous "second critical point hypothesis" of Poole et al. [13] on the basis of molecular dynamics simulations of the ST2 model. This has been by far the most influential scenario and has been supported, explained, and contested, by various authors, e.g., Tanaka [26–28], Anisimov [29–31], Stanley and coworkers [13, 32–34], Limmer and Chandler [35, 36] to name a few. Then, among scenarios that are qualitatively distinct,

there is the "critical-point-free" scenario, initially presented in 1994 as one of two cases within a bond-modified van der Waals model of the tetrahedral liquid state by Poole et al. [37] and recently revisited by one of the present authors [24]. This was followed in 1996 by the "singularity free" scenario of Sastry et al. [23], based on lattice model calculations.

The essential differences between these four scenarios are depicted in the series of phase diagrams of Figure 2, adapted from the recent paper of Pallares et al. [38], and may be summarized as follows (see also the Figure caption).

In the "stability limit conjecture" scenario, Figure 2A, the boundary of the liquid state at high temperatures, (the well-known spinodal limit to the stability of the superheated liquid state that terminates at the liquid gas critical point) is seen as reversing its temperature dependence where the line of density maxima meets the liquid-vapor spinodal at negative pressure. It then retraces to establish the limit to supercooling of the ambient pressure and low pressure liquid. Debenedetti [4] correctly argues that the intersection between a liquid-vapor spinodal and the metastable continuation of the liquid-vapor equilibrium line must be a critical point, whose existence is not expected. However, we note that this is not necessary if the line of instability at positive pressure is not a liquid-vapor spinodal, but rather a line of instability toward another phase. The critical-point free scenario [23, 24] (Fig. 2C) provides such a line (see below).

Figure 2B shows the second critical point scenario in its most familiar form, wherein a second critical point exists at positive pressure, which terminates a line of liquid-liquid transition. From the second critical point emanates a Widom line, the locus of extrema of the correlation length. This scenario also includes other lines of response function maxima, extending to lower and negative pressures. Near the critical point these lines asymptotically approach the Widom line, but they fan out further away from the critical point.

In Fig. 2C is depicted the "critical point free" scenario by which is meant that the liquid-liquid transition exists but the LLCP has moved sufficiently to negative pressures that it meets the liquid-vapor spinodal and the fluctuations characteristic of each merge and lose identity.

Finally, the "singularity-free" scenario (Fig. 2D), is characterized by sharp but non-divergent maxima in the different response functions, occurring at different temperatures but without a liquid-liquid transition and with a critical point only at 0 K.

Only in the first of the above scenarios does the form agree with that of the various

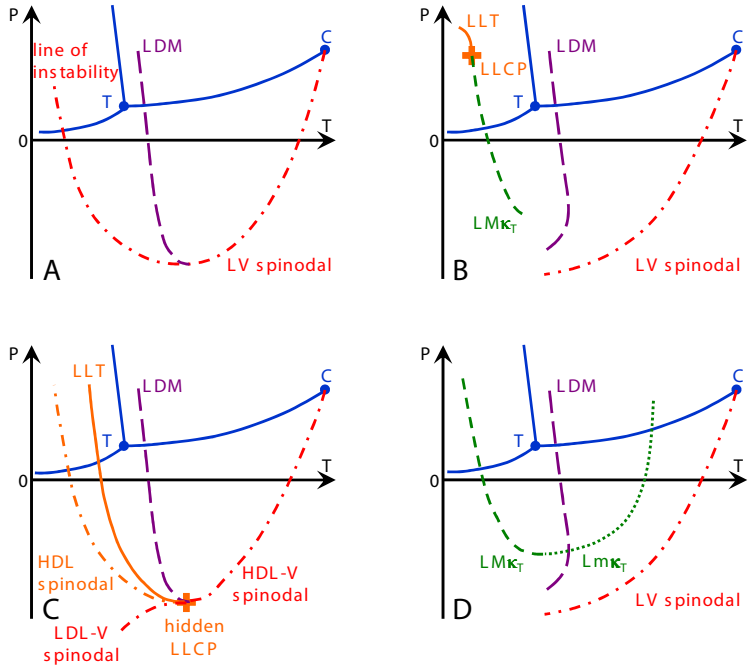

FIG. 2. Scenarios that might account for the behavior observed in Figure 1. **A**. Speedy's reentrant spinodal, **B**. Poole et al.'s 2nd critical point **C**. Poole et al.'s "weak bond" modified van der Waals model, now the "critical point free" scenario **D**. Sastry et al.'s "singularity free" scenario. Continuous blue curves show the known equilibrium coexistence lines between liquid, solid and vapor. Liquid-vapor equilibrium terminates at the critical point C. The long-dashed purple line shows the line of density maxima (LDM), the short-dashed and dotted green line the lines of isothermal compressibility maxima (LMkT) and minima (LmkT), respectively. The dash-dotted lines show lines of instability. When the scenario comprises a liquid-liquid transition, it is displayed with a continuous orange line (LLT) and the liquid-liquid critical point is shown as an orange plus. Adapted from ref. [38].

multiparameter empirical equations of state, for which the spinodal limit to liquid stability reverses its position in pressure and retraces to positive pressures. Only in the second and third of these scenarios does a liquid-liquid coexistence line exist. And only in one of these does a second critical point exist.

III. LIQUID-LIQUID TRANSITION

Among the scenarios presented in Section II, the second critical point scenario [13] (Fig. 2B) with the possible existence of a liquid-liquid critical point (LLCP) and its associated critical fluctuations, which are considered as the source of water anomalies [5, 6, 20–22, 33, 39, 40], has been investigated extensively both in amorphous glassy water and in deeply supercooled liquid water, see for example [40–43]. The second critical point scenario and its associated liquid-liquid phase transition (LLPT) will be the focus of the present review.

In 1985, Mishima et al. [44] amorphized ice Ih at 77 K by compression beyond 1.1 GPa, and observed a first-order-like phase transition from high-density amorphous ice (HDA) to low-density amorphous ice (LDA) by heating the pressure-amorphized material at ambient pressure. LDA and HDA differ in structure and density where both states consist of fully hydrogen bonded, tetrahedral networks, but in HDA five first neighbors exist where the fifth molecule sits on an interstitial place between the first and second shell [46]. The radial distribution functions of LDA and HDA are examined in the article "X-ray and Neutron Scattering of Water" [47] contained within this volume.

The idea that water is a "mixture" of two different structures dates back to the 19th century [48, 49] and was reinvigorated in the late 20th century [50–52]. In 1992, in a seminal paper [13], using molecular dynamics simulations on the ST2 model of water, Poole, Sciortino, Essman, and Stanley found a first-order phase transition from low-density liquid (LDL) to high-density liquid (HDL) with an LLCP located at $T_C \sim 235$ K and $P_C \sim 200$ MPa [20–22]. In this scenario the LLPT is determined by extending the HDA and LDA first-order phase transition into the higher temperature and lower pressure region of the phase diagram [32, 44, 45, 53–57], see Fig. 3. Mishima and Stanley base their estimate of the LLCP location on the discontinuity of the melting curve of ice IV at $T_C = 220$ K and $P_C = 100$ MPa [39]. Using neutron diffraction, first Bellissent-Funel [58] and then Soper and Ricci [57] verified the structure transformation in liquid water from LDL to HDL with increasing pressure, see Fig. 4. They found that the main difference between LDL and HDL lies in the second shell, i.e. the second shell of LDL sits at approximately the tetrahedral distance, but the second shell of HDL substantially collapses with interstitial molecules and contributions from less specific, bifurcated hydrogen bonds [59]. Using similar techniques, Bellissent-Funel et al. further demonstrated that the structure of liquid water becomes HDA

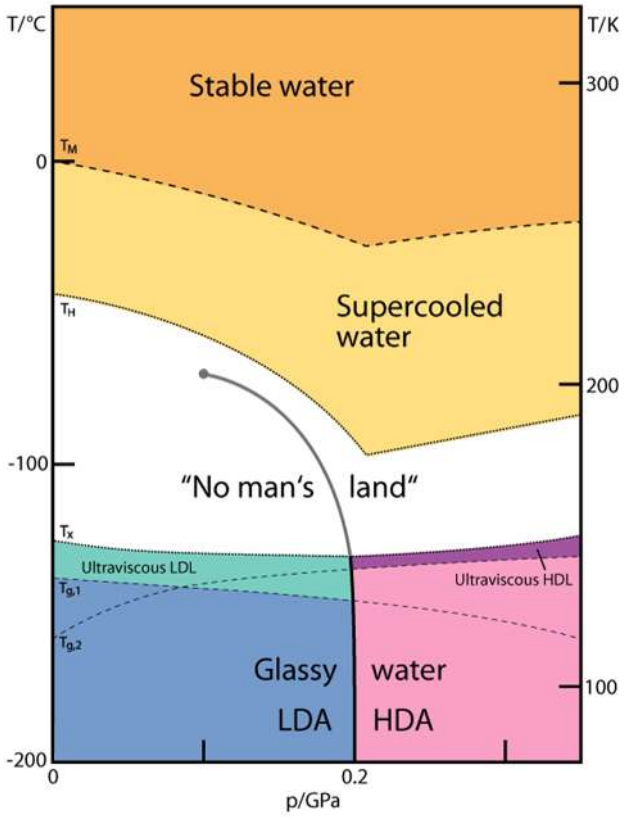

FIG. 3. Phase diagram of non-crystalline water (adapted from ref. [60], courtesy of Stephan Fuhrmann and Thomas Loerting). The "No man's land" indicates the region in which only crystalline ices have been observed so far. It is enclosed by the homogeneous crystallization line T_H from the top and the crystallization line T_X from the bottom. Two ultraviscous liquid domains, low- and high-density liquid water (LDL and HDL), can be found just below T_X. The two corresponding glass transition temperatures $T_{g,1}$ and $T_{g,2}$ separating the glassy solids LDA and HDA from the ultraviscous liquids LDL and HDL are taken from refs. [61] and [62], respectively. Please note the metastable extension of $T_{g,1}$ into the stability region of HDA and of $T_{g,2}$ into the stability region of LDA/LDL. A first-order liquid-liquid phase transition line (LLPT) ends in the purported liquid-liquid critical point (LLCP).

when cooled at high pressures but changes to LDA when cooled at low pressures. This again indicates a continuation of the LDA–HDA transition line to a LLPT in water [54, 55], and is consistent with results obtained using dilatometry and powder x-ray diffraction [56, 57].

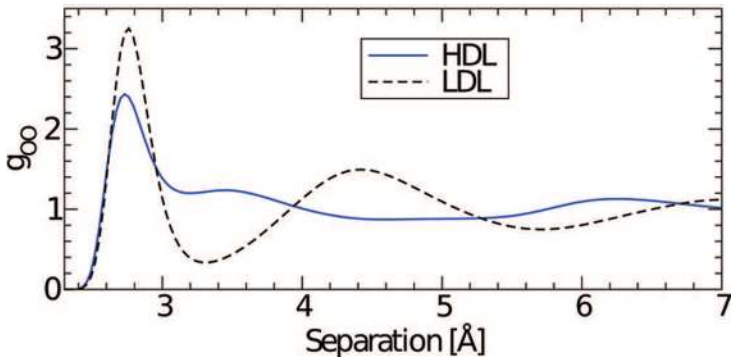

FIG. 4. Radial oxygen-oxygen pair-distribution functions for HDL and LDL demonstrating the structural difference between high- and low-density water. Adapted from ref. [57]

The transition between HDA and LDA under pressure was studied by Mishima and Suzuki [63], Klotz et al. [64], and Yoshimura et al. [65]. Their experiments demonstrate the first-order nature of the transition by revealing phase-boundaries between two phases, phase-coexistence, and a discontinuous change of structural properties at the transformation. Going beyond these studies Winkel et al. [66, 67] saw evidence of a first-order transition in the ultraviscous liquid domain at $\approx$ 140 K and 100 MPa on the downstroke. The location of the ultraviscous liquid domains for HDL and LDL is mapped by several experiments on the glass transition of amorphous ices, see Fig. 4 in Ref. 62 and Refs. 61 and 68.

A glass transition onset temperature of $\approx$ 136 K was detected in LDA by following the change in heat capacity upon heating LDA ice at ambient pressure at a rate of 10 K/min [69–71]. Although LDA can be prepared in several ways—by vapor deposition, by hyperquenching, and by the transformation from HDA described above—all studies find a similar increase in heat capacity, ΔC_p of $\approx$ 1 $JK^{-1}mol^{-1}$ [72]. The real nature of this extremely weak signal has been discussed for decades [24, 73]. The main point of the controversy concerns the question of whether a liquid nature is reached prior to crystallization [74] and the question whether translational motion [75] or rather defect-dynamics as in a crystalline system [76] is observed above T_g. More recently the interpretation that LDA undergoes a glass-liquid transition at the calorimetric glass transition near 136 K has received considerable support [77–79]. In the most recent scenario, the feeble signal is explained by the suspected strong or even superstrong nature of the low-density liquid near the glass transition temperature [24, 73, 80]. This suspicion found recent confirmation by dielectric

measurements indicating that LDL is actually the strongest of all known liquids [81, 82].

The glass transition of high-density amorphous ices was studied by *in situ* high-pressure methods by Mishima [83, 84], Andersson [68, 85, 86], and Loerting et al. [87, 88]. These measurements were recently reviewed in Ref. 62. All measurements indicate that the glass transition at elevated pressures of $p > 200$ MPa appears to be at $T_g > 140$ K. These measurements also indicate that the glass transition in HDA can be observed even at pressures < 200 MPa, where LDA is thermodynamically favored over HDA [89], i.e. metastability alone does not preclude the observation of glass transitions if the time scale of the transformation to the thermodynamically more stable phase is significantly longer than the time scale of equilibration. The transformation time scales can in fact greatly exceed those required for the equilibration of HDA, even at ambient pressure. Thus measurements of HDA become possible in an extended temperature range and reveal an ambient-pressure heat capacity step and a dielectric relaxation time that indicates a glass transition at 116 K [81]. This glass transition in HDA is 20 K lower than the glass transition in LDA and thus represents water's second glass transition. The possibility that two distinct glass transitions occur has been further supported by the simulation results of Xu et al. [90, 91] and Giovambattista et al. [61], which indicate that the experimental observations are qualitatively consistent with water and water-like models having a LLPT, e.g., the ST2 water model, but not with models lacking two liquid phases, e.g., SPC/E water.

The hypothesized LLCP is located in the deeply supercooled region, the "No-Man's Land" below the homogeneous nucleation [13, 20–22, 33, 39, 40]. Various potential model studies [20–22, 29, 30, 92–107] have demonstrated the existence of an LLCP, and Table I provides the reported locations of the LLCP in the various long-range all-atom models.

Some models show a number of water's anomalies but do not have an LLCP, e.g., the short-range monoatomic mW model [108, 109].

On the other hand other short-range monoatomic models, e.g., the Jagla model, do show the presence of an LLCP [110]. The use of the technique of successive umbrella sampling grand canonical Monte Carlo and of finite-size scaling has allowed to prove rigorously that the Jagla LLCP is a second-order critical point that belongs to the Ising universality class and to determine with great precision its location [111]. Importantly the estimate of the LLCP position that was previously obtained by molecular dynamics (MD) simulation [110] is in very good agreement with the true location of the LLCP in the model, as found

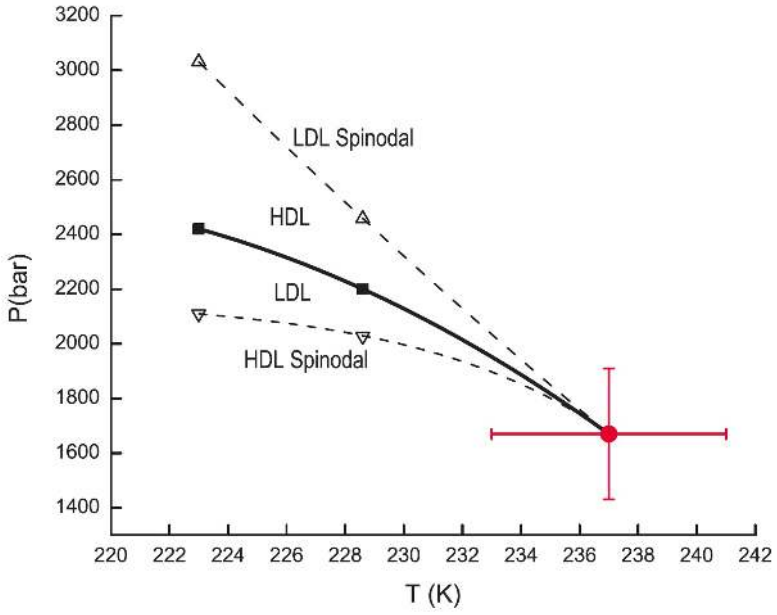

FIG. 5. Pressure-temperature projection of the metastable phase behavior of the ST2b model for water from Liu et al. [112] showing the liquid-liquid coexistence curve (black squares), the LDL spinodal (up-triangles), and the HDL spinodal (down-triangles). Solid and dashed lines are a guide to the eye and the red circle is the critical point from Ref. [113]. Copyright ©2012 by the American Institute of Physics.

with the rigorous finite-size scaling approach [111]. These results prove that the techniques for locating the LLCP at the maximum temperature of the spinodals in MD finite size simulations are valid and lead to the same result as the rigorous technique.

The liquid-liquid transition phenomenon for a one-component liquid also applies to other network-forming, tetrahedrally-coordinated liquids where simulations show the possible existence of an LLCP, see for example Refs. [114–119].

The landmark paper by Poole, Sciortino, Essman and Stanley [13] that first proposed the possibility of an LLPT in a molecular model of water described their molecular dynamics simulations as using the 5-site, rigid ST2 model [120] that includes both Coulombic and van der Waals forces. Long-range interactions for the Coulombic forces were taken into account using the reaction-field method. We label this variant of the model ST2c to distinguish it from the two other variants that we will introduce below. Poole et al. observed that at sufficiently low temperatures the liquid isotherms exhibit behavior consistent with an

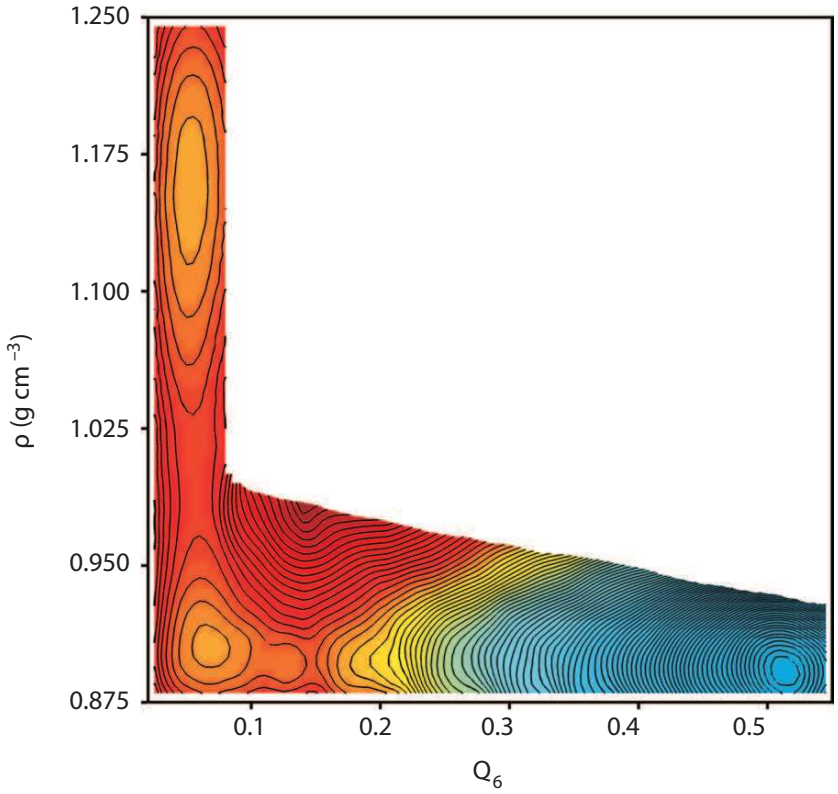

FIG. 6. The free energy surface of the ST2 model with vacuum boundary conditions at 228.6 K and 2.4 bar from Palmer et al. [121]. These conditions correspond to liquid-liquid equilibrium. Contours are spaced 1 k_BT apart. Copyright ©2014 by Macmillan Publishers.

approach to a critical point, which they proposed would terminate a liquid-liquid coexistence line in the deeply supercooled region of the phase diagram. More recently Liu et al. [113] used grand canonical Monte Carlo to study the ST2 model with an Ewald summation of electrostatic interactions. This approach determines the free energy of the system as a function of density, but does not permit the precise control of other order parameters.

An Ewald summation of Coulombic interactions requires an assumption about the dielectric properties of the medium surrounding the system at infinite distance. Reference [113] used vacuum boundary conditions ($\epsilon_\infty = 1$), which we will refer to as the ST2b model. Limmer and Chandler [35, 36] studied different versions of the ST2 model using a hybrid Monte Carlo approach in which both the density ρ and the orientational order parameter Q_6 that discriminates between disordered liquid and crystalline environments can be controlled. They did not find evidence of an LLPT for any model variation and suggested that results pointing to an LLPT were due to insufficient equilibration and sampling. A subse-

Potential	T_c (K)	P_c (MPa)	ρ_c (g/cm^3)
ST2 [13]	235	200	1
ST2 [94]	245	180	0.94
ST2a [112]	-	-	-
ST2b [97]	237 ± 4	167 ± 24	0.99 ±0.02
ST2c [122]	247 ± 3	185 ± 15	0.955 ± 0.010
TIP4P [107]	190	150	1.06
TIP4P/2005 [98]	193	135	1.012
TIP4P-EW [96]	210	310	1.09
TIP5P [93]	217 ± 3	340 ± 20	1.13 ± 0.04
TIP5P-E [95]	210	310	1.09
SPC/E [92]	160	200	1.07

TABLE I. Critical temperature T_c, pressure P_c and density ρ_c reported using different water potentials. ST2a, ST2b and ST2c are variants of ST2 as described in the text.

quent study by Liu et al. [112] used NPT Monte Carlo sampling and a weighted histogram analysis method to obtain the free energy as function of ρ, Q_6, and temperature T. The existence of an LLPT for the ST2b ($\epsilon_\infty = 1$) model was confirmed (see Fig. 5). For the ST2a ($\epsilon_\infty \to \infty$) model, rapid crystallization to an unphysical high-density ($\rho \sim 1.5$ to 1.7 g/cm^3) dipolar-ordered ice phase was observed. A phase diagram similar to that shown in Fig. 5 (shifted to slightly higher temperatures and pressures) was obtained by Cuthbertson and Poole [122] and Poole et al. [123] for the ST2c (reaction field) model using molecular dynamics and umbrella sampling Monte Carlo, respectively. The most comprehensive study to date of an LLPT in a molecular model of water was reported recently by Palmer et al. [121] who focused on the ST2b ($\epsilon_\infty = 1$) model. Six different computational protocols were used to obtain the free energy as a function of ρ, Q_6, and temperature T, and all three basins (HDL, LDL, and crystal) were sampled reversibly (see Fig. 6). The free energy barrier between HDL and LDL was obtained as a function of system size and found to be consistent with the $N^{2/3}$ scaling law expected for a first-order phase transition.

At LLPT conditions, both liquids are metastable with respect to crystallization, and if the time is sufficiently long and the system size sufficiently large, crystallization will occur.

Unlike the mW model [124], crystallization time scales for the ST2 model of water are longer than the time scales for equilibration of the liquid. For example, in a study of the ST2c (reaction field) model using an N = 4000 molecule system, Yagasaki et al. [125] observed liquid-liquid coexistence at $T = 235$ K for approximately 800 ns, followed by ice nucleation and crystal growth. In this study a rectangular simulation box was used to minimize the interfacial energy and allow liquid-liquid coexistence to develop. These results were later criticized by Overduin and Patey [126] who found that the density differences that are observed for TIP4P/2005 and TIP5P water using smaller simulation cells disappear when larger cells (N = 32,000) are considered.

Using the same force-field model as Yagasaki et al., Kesselring et al. [127, 128] performed many 1 μs simulations of systems ranging in size from 216 to 729 molecules, and found LDL to be stable with respect to the crystal in over 98% of their runs. Small crystal nuclei ("crystallites") are easily detected using the bond order parameter d_3 introduced by Ghiringhelli et al. [129]. This parameter characterizes the bond between two molecules and is designed to distinguish between a fluid and a diamond structure. A molecule is typically considered part of a crystal if three of its four bonds exhibit $d_3 < 0.87$. In all of the simulations done by Kesselring et al., tiny crystallites grew and then melted within 1 μs. Based on the few crystallization events that occurred, they estimated that the critical size of a crystallite is approximately 70 ± 10 molecules before spontaneous crystallization occurs.

Two recent studies by Sciortino and coworkers rigorously examine the LLPT for a general model of tetrahedrally coordinated liquids [115] and for variations of the ST2 model of water [130]. They show that bond flexibility affects the relative stability of the liquid and crystal phases. On increasing bond flexibility, the liquid-liquid critical point moves to a temperature where the liquid is more stable than ice. Taken together with the work of Palmer et al. [121], these studies conclusively show that the claim of Limmer and Chandler—that the liquid-liquid transition is a misinterpreted crystallization transition in all atomistic models of water—is incorrect in its generality. It is certainly true for the mW model, while for TIP4P/2005 water the situation is unclear [125, 126]. The origin of the discrepancy between different simulations using the ST2 model has still not been clearly identified, but potential contributions are discussed in Ref. [131]. We conclude this section by noting that the strong debate about the potential existence of a LLPT in real and simulated supercooled water has

driven a rapid expansion of computational methodologies and has led to rigorous sampling of low-temperature properties in several water models. However, to conclusively determine which case describes real water we will need new experimental data that go deeper into "no-man's land".

IV. MICROSCOPIC STRUCTURE AND THERMODYNAMICS

The thermodynamic behavior of water suggests that it consists of at least two structurally distinct species with relative populations varying with pressure and temperature. Beginning with the work of Whiting and Röntgen mixture models [48, 49] and two-scale models [110, 132] have often been invoked as possible explanations of the thermodynamic and dynamic anomalies of liquid water. These models posit a separation of the energy states available to water molecules into two distinct groups: one corresponding to low-energy ordered configurations, and the other to high-energy configurations. The complexity of water is thus modeled by a mixture of these two structural motifs.

Conceptually similar but differently formulated approaches have been taken using two-state models. Tanaka [26, 28, 133] recognizes that, in any liquid, locally-favored structures with low configurational entropy are formed in a sea of random normal-liquid structures with high configurational entropy. A phenomenological two-state model approximates this picture as a bimodal distribution of possible molecular configurations and sees cold and supercooled liquid water as a "mixture" of two distinct competitive states, and the fraction of each state is controlled by pressure and temperature. Anisimov and coworkers [30, 31, 134] describe a competition between an ideal entropy of mixing and a non-ideal part of the Gibbs energy of mixing. From a phenomenological point of view, even without a microscopic understanding of the differences between these alternative configurations, this two-state model yields an equation of state of supercooled water that agrees remarkably well with experimental results [26, 31, 133, 135] (see Fig. 7).

A difficulty associated with correlating data that are obtained in the experimentally accessible region (above the ice homogeneous nucleation temperature) is accurately locating the liquid-liquid critical point and determining the critical pressure. Using the optimization shown in Fig. 8, any critical pressure value above 100 MPa is excluded and the lower limit is uncertain. This is in contrast to the extensively-studied water models, the ST2 model and

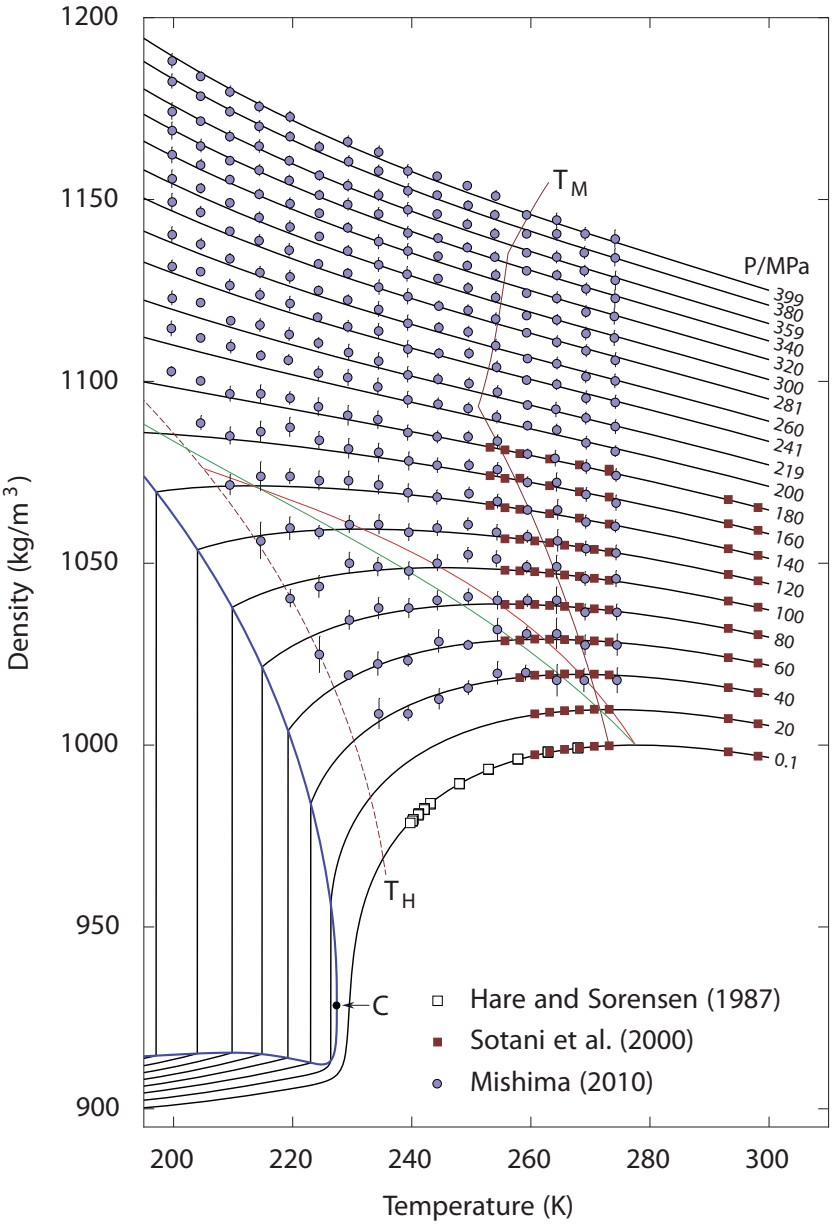

FIG. 7. Density of cold and supercooled water as a function of temperature along isobars. Symbols represent experimental data [136–138]. Black curves are the predictions of the two-state model [31]. T_M (dark red) indicates the melting temperature and T_H indicates the homogeneous nucleation temperature. The thick blue line is the predicted liquid-liquid equilibrium curve, with the critical point C. The red line is the line of maximum density, and the green line is the line of a constant LDL fraction of about 0.12.

the TIP4P/2005 model proposed by Abascal and Vega [139], for which the critical points are located at about 180 and 135 MPa, respectively, see Table I. However, any attempt to

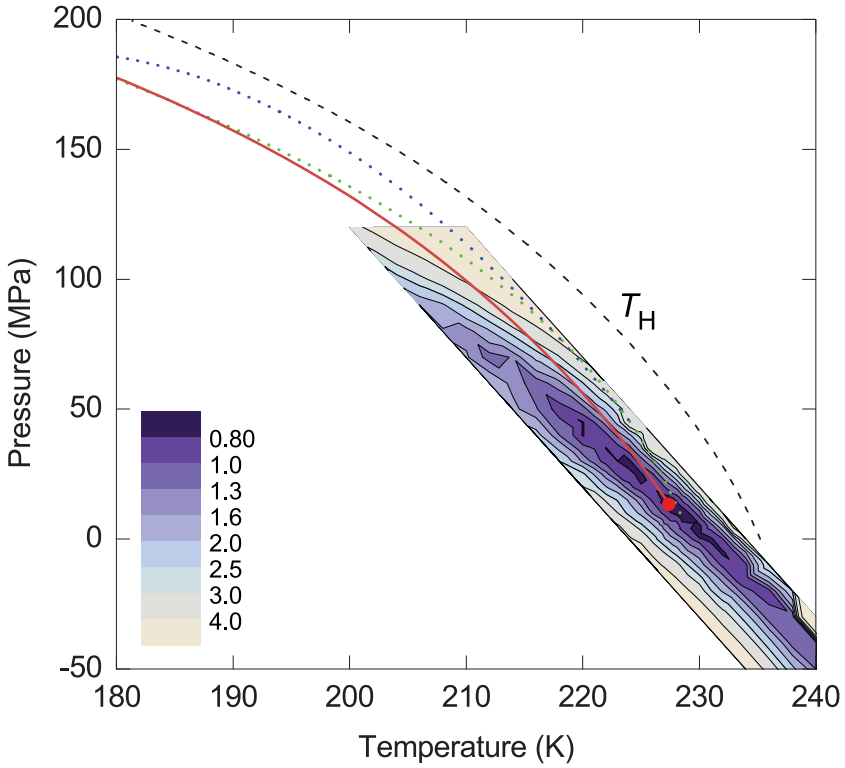

FIG. 8. Optimization of the critical-point location [31]. The colored map shows the reduced sum of squared residuals. The solid red line is the hypothesized liquid-liquid transition curve. The dashed curve shows the temperature of homogeneous ice nucleation. The blue dotted curve is the liquid-liquid transition curve suggested by Mishima [137] and the green dotted curve is the 'singularity' line suggested by Kanno and Angell [19].

predict the location of a possible LLCP becomes highly uncertain because the anomalous behavior intensifies as it moves into regions of lower temperature and higher pressure where measurements are lacking (see Fig. 8). Indeed, we note the uncertainty in the location of a possible LLCP in the TIP4P/2005 model as there have been different proposals [98, 125] and the existence of an LLCP in the model has even been questioned [126, 140].

Thus pseudo-binary models are used to explain both the anomalies and the possible liquid-liquid phase transition. From a molecular point of view, water does not consist of distinct species. It is the nature of the hydrogen-bonding network that implies that fluctuations in density, correlated with local tetrahedral ordering, give rise to structurally distinct regions of local order that in turn give rise to pseudo-binary behavior. Indeed, data from small-angle x-ray scattering (SAXS) have been interpreted in terms of density inhomogeneities

in the liquid—with an average spatial extent of $\sim$ 1 nm at ambient conditions [141]—that grow upon supercooling [142]. Although this has not avoided controversy [143–145], it has received support from a purely statistical mechanical perspective [146].

X-ray absorption spectroscopy (XAS) has also indicated the presence of two types of local structure in liquid water: very tetrahedral and very disordered [147–149]. The former would correspond to LDL and the latter to HDL. There is general agreement that the pre- (535 eV) and main-edge peaks (537 to 538 eV) in the XAS of liquid water are the fingerprints of distorted H-bonds, whereas the post-edge (540 to 541 eV) is associated with strong H-bonds and is further enhanced for tetrahedral H-bond structures [147–152]. Interpretations of the spectra in terms of structure either emphasize the ultrafast nature of the x-ray probe and suggest small, instantaneous distortions around a mainly tetrahedral network [152–155] or propose fluctuations that are of a sufficiently long duration and are sufficiently extended that a distinction in terms of local HDL and LDL environments becomes meaningful [141, 143, 156, 157].

The most direct evidence of bimodality in terms of local structures is found in x-ray emission spectroscopy (XES) in which the sharp, non-bonding lone-pair peak of gas phase water becomes broadened and shifted down in energy in crystalline ice. In water we observe *two* sharp peaks that interconvert but do not broaden with increasing temperature [141, 158–163] (see Fig. 9). The peak close to the peak in tetrahedral ice is assigned to local LDL-like tetrahedral coordination and the other peak, close to the gas phase position, is assigned to disordered HDL-like local structures with broken or weakened H-bonds. The origin of the split is under debate [165, 166], with one interpretation in terms of differences in final state [158, 159] and the other in terms of differences in the initial state [141, 162, 167]. However both interpretations require the existence of two different local environments. As further support for a bimodal distribution of structures, we note the recent time-resolved Optical Kerr Effect (OKE) measurements by Taschin et al. [168]. OKE involves low-energy vibrations in the H-bonding network where there are clearly identified signatures of HDL and LDL with the same temperature dependence as in the other spectroscopies.

A two-order parameter model provides a framework for understanding the spectroscopic results and the various thermodynamic features in terms of two competing order parameters: a density-dependent order metric that promotes close-packed structures in both the crystal and the liquid and an anisotropic or bond-driven order parameter that promotes open,

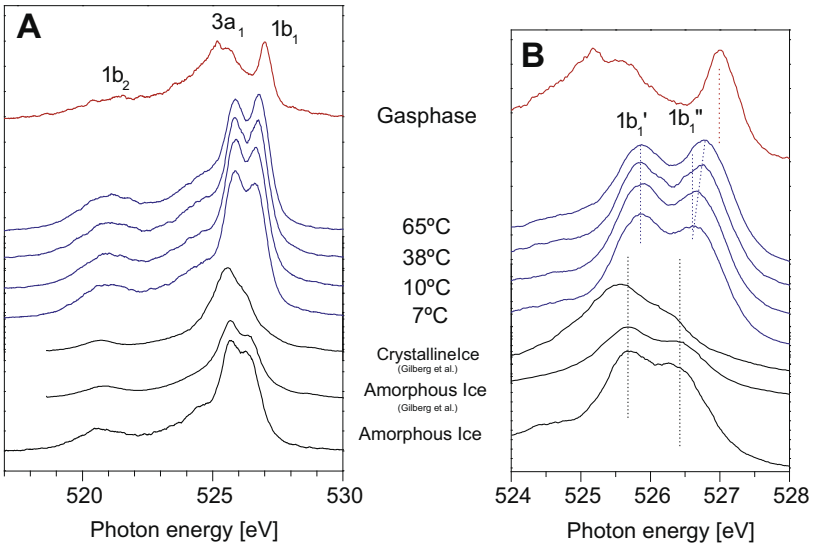

FIG. 9. O 1s soft x-ray emission spectra of gas phase water, liquid water at different temperatures and amorphous and crystalline ice, with an energy scale displaying the full spectrum (A) or only the lone-pair, $1b_1$ region (B). The excitation energy is 550 eV, well above the ionization threshold. Peak components are labeled based on the molecular orbitals for a water molecule. The highest peak ($1b_1$) splits into double peaks ($1b_1'$ and $1b_1''$). The XES spectra of amorphous (–190 °C (83 K)) and crystalline ice from Gilberg et al. [164] are included for comparison. Figure adapted from ref. [162].

tetrahedral local order.

The local structure of the liquid tends to correspond to that of the underlying crystalline phase, and a triple point is seen, i.e. a point where the low-density crystal, the high-density crystal, and the liquid are in equilibrium [27]. Glass-forming tendencies are most pronounced in the neighborhood of the triple point [169, 170] where structural frustration due to competition between the two order metrics is most pronounced [28].

The connection between the two-order parameter description of water-like liquids and an atomistic picture of liquid state structure and dynamics was first provided by Errington and Debenedetti using the rigid-body SPC/E water model [171]. This connection requires that local order metrics be defined in terms of particle positions. A suitable order metric that defines density-driven local order applicable to both simple and complex fluids is the translational- or pair-ordering metric in terms of the atom-atom pair-correlation function

g(r) [172]. In the case of H_2O, this order parameter may be defined as

$$\tau = 1/\xi_C \int_0^{\xi_C} |g_{oo}(\xi) - 1| d\xi, \tag{2}$$

where $\xi = r\rho^{1/3}$ is the distance r beween the oxygen atoms of a pair of molecules divided by the mean pair separation $\rho^{1/3}$ where ρ is the number density N/V, and $g_{OO}(\xi)$ is the oxygen-oxygen pair-correlation function. A convenient measure of local tetrahedrality associated with a given oxygen atom i is given by

$$q_{\rm tet} = 1 - \frac{3}{8} \sum_{j=1}^{3} \sum_{k=j+1}^{4} (\cos(\psi_{jk}) + \frac{1}{3})^2, \tag{3}$$

where ψ_{jk} is the angle between the bond vectors r_{ij} and r_{ik} where j and k label the four nearest oxygen atoms. At low densities or temperatures the probability distributions of tetrahedral order $\mathrm{P}(q_{\rm tet})$ have a peak at high tetrahedrality. At intermediate densities or temperatures $\mathrm{P}(q_{\rm tet})$ has a bimodal or shoulder structure with a second peak at intermediate tetrahedrality. Order maps displaying the correlation between translational and tetrahedral order provide an interaction-independent summary of the variation of structural order over a wide range of state points. In the case of SPC/E and other rigid-body models of water, one can define a structurally anomalous region in the phase diagram such that all state points in this regime fall on essentially the same curve in the ($q_{\rm tet}$, T) plane. This strong correlation between tetrahedral- and pair-order indicates that distortions from local tetrahedrality in the hydrogen-bonded network reduce pair-correlations and enhance disorder in the anomalous regime. At high densities, tetrahedral order ceases to be significant and the system behaves as a simple liquid dominated by pair-ordering.

Figure 10 uses simulations of the TIP4P/2005 water model [173] to show the structurally anomalous regime in water that encloses the region of diffusional anomaly which in turn encloses the region of density anomaly. This nested structure gives rise to the idea of a cascade of anomalies, where progressive enhancement of the degree of structural anomaly gives rise to various transport and thermodynamic anomalies. Comparisons of the cascade structure and the order maps of a number of tetrahedral liquids are now available [177–179].

Connecting entropy with structure-based order parameters for fluids, particularly in the context of biomolecular simulations, has been an active area of research [180–186]. A useful route in the context of simple and anomalous liquids is provided by the multiparticle

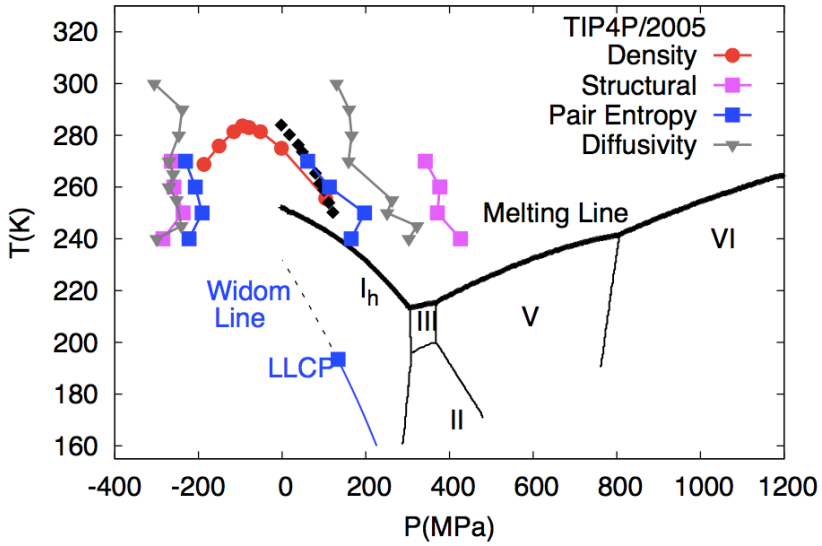

FIG. 10. Thermodynamics of the condensed phases of water, illustrated for the TIP4P/2005 rigid-body model of water [173]. The data for the phase boundaries are taken from ref. [174]. The boundaries of the structural, density, pair-entropy and diffusivity anomalies are taken from ref. [175]. The experimental TMD line shown in filled black diamonds is taken from ref. [176]. The Widom line (see the definition in Sec. VI) is taken from ref. [98].

correlation expansion of the entropy. $S_e = S_2 + S_3 + ...$, where S_n denotes the entropy contribution due to n-particle correlations [187–191]. Since the thermodynamic excess entropy can be obtained from simulations or from calorimetric data, the multiparticle expansion serves to highlight the role of pair-, triplet-, and higher-order correlations in determining the liquid entropy. The behavior of simple liquids is dominated by pair-correlations which contribute 85–90% of S_e. For multi-atomic systems, the pair-entropy term can be generalized in terms of atom-atom pair-distribution functions accessible from simulations, x-ray, or neutron scattering. For tetrahedral liquids such as water, however, the three-body or triplet correlations can be significant since they are associated with the locally anisotropic nature of the liquid-state network.

Stillinger-Weber liquids with a variable tetrahedrality parameter can be used to model molten phases of Group 14 elements (C, Si, Ge, Sn, Pb) as well as provide a coarse-grained, monoatomic (mW) model for water [108, 124, 192–195]. As a function of increasing tetrahedrality, the triplet contribution to the excess entropy is significantly higher than the pair-entropy contribution [196]. Transformation to a triplet-dominated fluid strongly favors

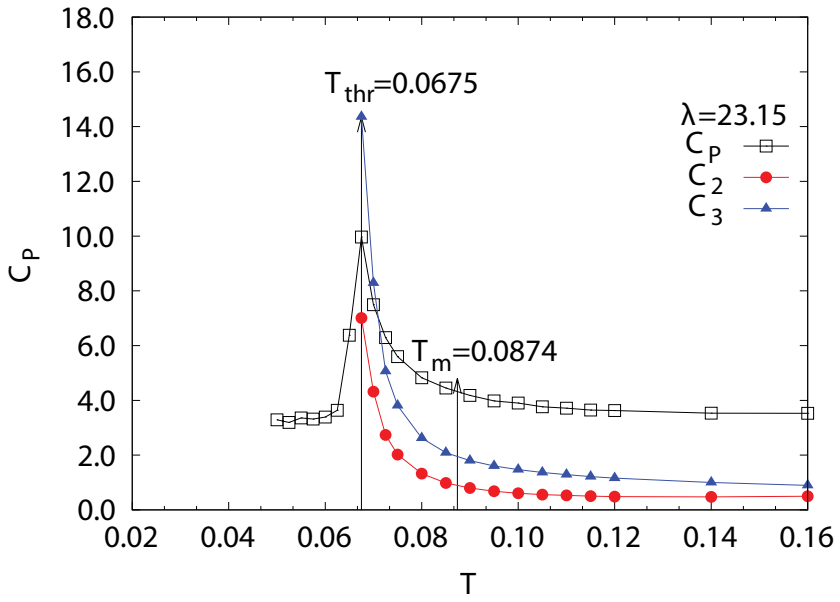

FIG. 11. Multiparticle correlation. Contributions to the entropy and the heat capacity anomaly. The total (C_P), pair (C_2), and triplet (C_3) contributions as a function of temperature (T) for the monoatomic water (mW) model at 1 atm pressure [196].

the formation of a tetrahedral crystal, as well as the existence of a heat capacity anomaly, and the local order within the first neighbor shell is a critical factor in determining the its behavior upon supercooling. The characteristic rise in heat capacity on the isobaric cooling of tetrahedral liquids is closely tracked by the pair- and triplet-contributions to the entropy (see Fig. 11), and thus provides a direct connection between structural correlations and thermodynamics. Preliminary results for triplet O–O–O correlations in pair-additive, rigid-body, atomistic models of water strongly resemble the mW water model [197].

In the section linking dynamics to thermodynamics the behavior of the two-body excess entropy s_2 will be discussed for the TIP4P water model upon supercooling [198, 199]. This quantity is easily measureable in experiments and it is connected to a dynamic crossover that in supercooled water is asociated with the presence of an LLCP.

V. COMPETITION BETWEEN TWO ALTERNATIVE STRUCTURES

The anomalies of supercooled water and the possibility of metastable liquid-liquid separation in water can be explained if water is viewed as a mixture of two inter-convertible

organizations of hydrogen bonds whose ratio is controlled by thermodynamic equilibrium [31, 133, 200, 201]. The existence of two structures does not necessarily mean that they will phase-separate [31, 134, 201]. If these structures form an ideal solution, the liquid will remain homogeneous at any temperature or pressure, while the competition between the two structures may cause the density maximum and non-diverging anomalies of the response functions [201]. However, if the solution is non-ideal, a positive excess Gibbs energy of mixing could lead to phase separation if the nonideality of mixing of these two states is strong enough. If the excess Gibbs energy is primarily associated with a heat of mixing, the separation will be energy-driven. If the excess Gibbs energy is primarily associated with excess entropy, the separation will be entropy-driven. The entropy-driven nature of this separation means that if the two states were unmixed they would allow more possible statistical configurations and thus a higher entropy.

One example of this is the Woodcock-Angell-Cheeseman (WAC) model [202] modified by Lascaris [203]. The original WAC model was for liquid silica (SiO_2), a close relative of water. Both liquids are tetrahedral and consist of large four-coordinated atoms (O in water, Si in silica) surrounded by twice as many smaller atoms (H in water, O in silica), but unlike most water models the WAC model has no explicit bonds and is simply a mixture of Si^{+4} and O^{-2} ions. It was recently found that the WAC model is remarkably close to having a LLCP [204], and it was subsequently demonstrated that by decreasing the ion charge the model can be tuned such that a LLCP appears, as indicated by the crossing of the isochores and the diverging response function maxima at the state point where the LLCP is located [34, 94]. Increasing the charge separates the isochores and greatly reduces the magnitude of the response function maxima. In addition, the response function maxima move to separate state points, indicating that the LLCP has disappeared [203]. Changing the ion charge in the WAC model has this effect due to the Gibbs free-energy mixing, $\Delta G_{\mathrm{mix}} = \Delta H_{\mathrm{mix}} - T\Delta S_{\mathrm{mix}}$. Because increasing the charge makes the Si–O bond more attractive, more Si ions are drawn into the first coordination shell. This increases the HDL entropy and thus the ΔS_{mix}. The result is that ΔG_{mix} becomes negative at all temperatures and pressures, and no liquid-liquid transition occurs. A decrease in the ion charge reverses this effect. These considerations suggest that the liquid-liquid transition in the modified WAC model may be entropy-driven, a scenario that has also been proposed for water [31].

More generally, two-state thermodynamics can explain "liquid polymorphism," defined as

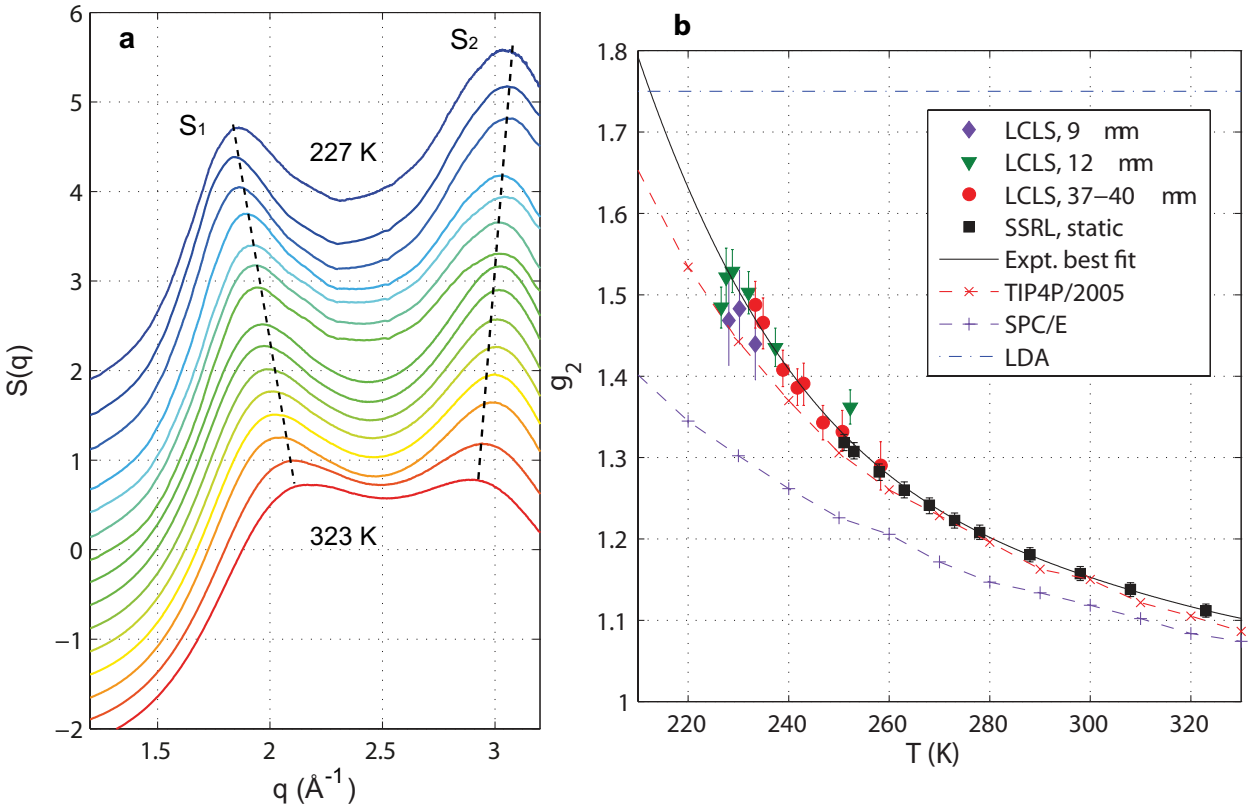

FIG. 12. Ultrafast x-ray probing of water structure below the homogeneous ice nucleation using micron-sized water droplets falling in vacuum [210] **a**. Scattering structure factor, S(q). The data reveal a continuously increasing split of the principal S(q) maximum into two well-separated peaks, S_1 and S_2 (dashed lines). **b**. Experimental tetrahedrality (g_2) values, derived from the measured split, Δq, between the two peaks in **a** as calibrated against a fit to molecular dynamics data. Error bars are estimated from the maximum and minimum Δq values allowed by the uncertainty in the S_1 and S_2 peak positions. Also shown is the fourth-order polynomial least-squares fit to the experimental data (black solid line), where the last (that is, low-T) two data points for the 12-μm-diameter droplets and the last data point for the 9-μm-diameter droplets are ignored owing to high nonlinearity in the detector response (see ref. [210]. For comparison, the temperature dependences of g_2 for the TIP4P/2005 (red dashed line) and SPC/E (purple dashed line) models are depicted along with the characteristic value of g_2 for LDA ice [211] (blue dashdot line).

the existence of a single-component substance with two different liquid forms [133, 201, 205–208]. Liquid polymorphism has been experimentally observed or theoretically suggested

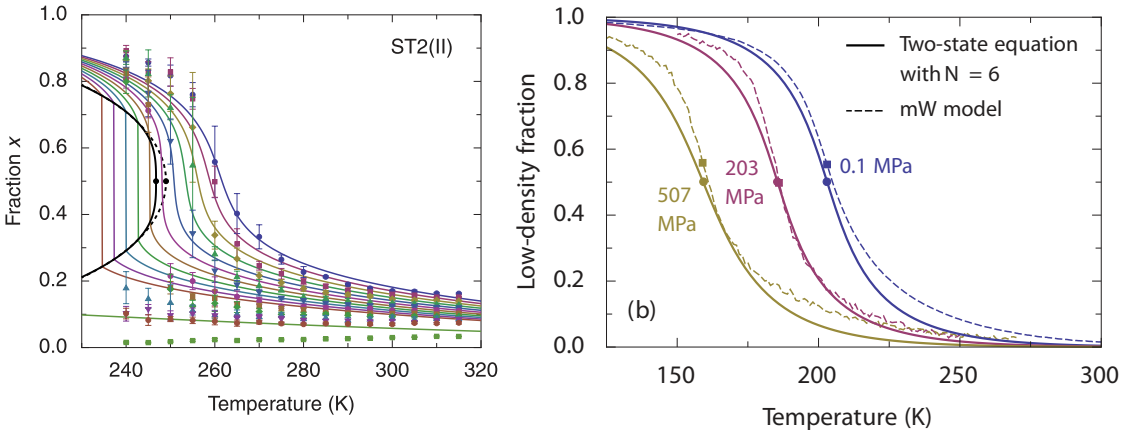

FIG. 13. Low-density fraction from simulations of water-like models and the predictions from the two-state thermodynamics: **a**. ST2(II), a version of the ST2 model [219]. Symbols are simulation data. Solid curves are theoretical predictions. Dashed curve is a mean-field approximation. **b**. mW model [109]. Solid curves are theoretical predictions which include clustering of water molecules with average aggregation number N = 6.

in molten silicon, liquid phosphorus, triphenyl phosphate, and in some other molecular-network-forming substances [119, 178, 201, 205, 206]. Recent experiments [147, 156, 162, 163, 168, 209, 210] suggest the existence of a bimodal distribution of molecular configurations in water. In particular, the transformation of water structure in micrometer-sized water droplets has been observed [210] using an x-ray free-electron laser (see Fig. 12). The droplets are injected into vacuum where they almost instantly cool through evaporation, and a diffraction pattern is obtained from individual droplets when they are hit by the 50 fs duration, fully-coherent intense x-ray pulses. The temperature of the droplets can be controlled by varying the distance between the nozzle where the droplets are generated and the region where they interact with the x-rays. If the diffraction pattern exhibits Bragg spots the droplets are ice-containing, and if it exhibits diffuse rings the droplets are liquid. The lowest temperature at which liquid droplets are still present is 227 K, i.e. 5 K below the previous upper boundary of the "no-man's land". Analysis of the data shows a continuous, but accelerated transformation of the structure towards an LDL dominated liquid [210]. Thus the structure of water is LDA when it cools through the "No-Man's Land" (to $T < 136$K) without crystallization [72, 212–215].

According to Mishima and Stanley [33], if the intermolecular potential of a pure fluid

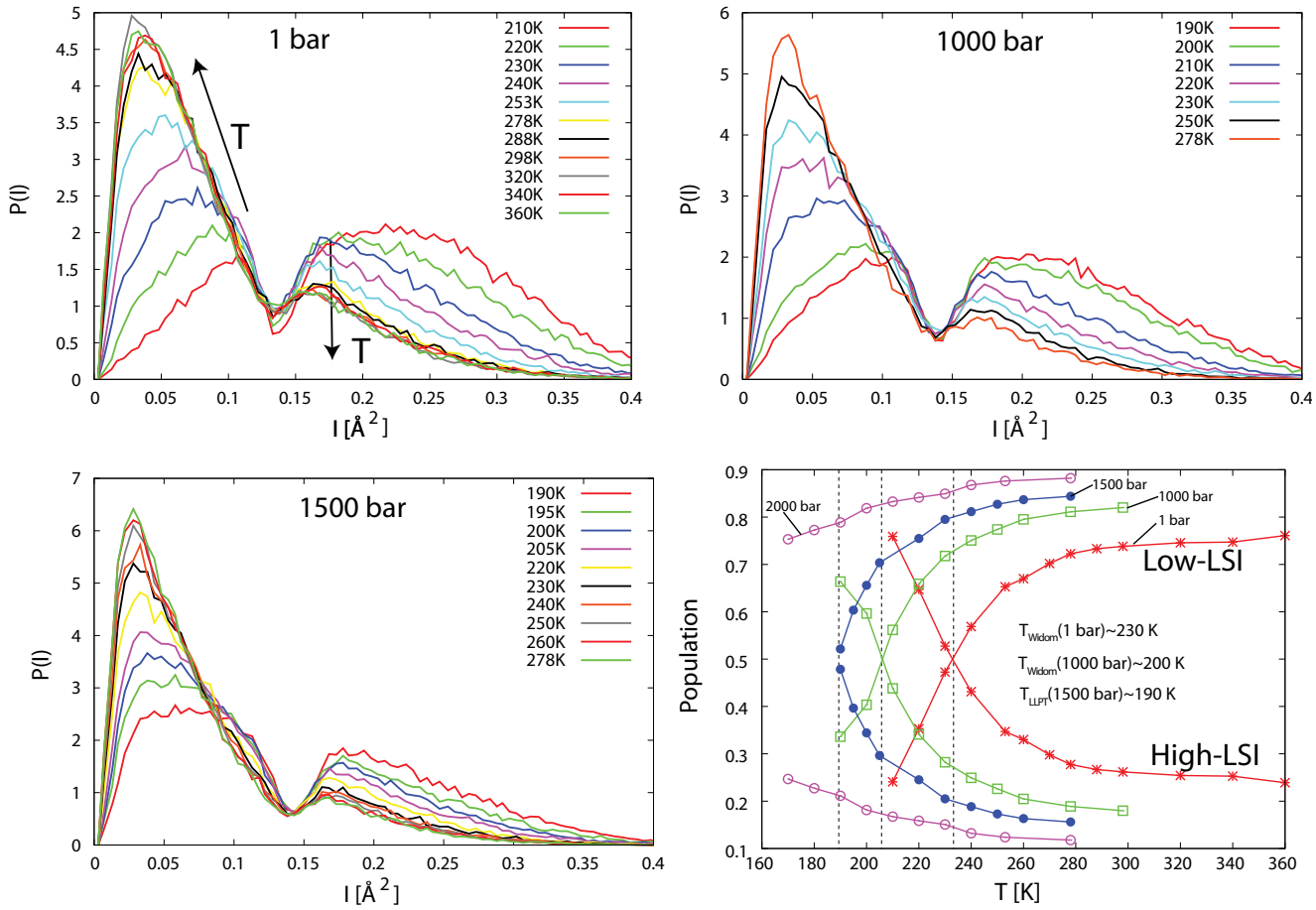

FIG. 14. Analysis of the inherent structure in simulations of TIP4P/2005 water. (A-C) Plot of the temperature dependent distributions of LSI values at (A) 1 bar, (B) 1000 bar and (C) 1500 bar. (D) Number of molecules in each distribution as function of temperature and pressure. The Widom line (see the definition in sec. VIII) at each pressure is indicated by a vertical line and corresponds to the crossing point between the high- and low-LSI distributions. Figure adapted from ref.[224].

exhibits two minima, the interplay between the two indicates that a liquid-liquid separation may be present. Another possibility is a double-step potential caused by hydrogen-bond bending, as shown by Tu et al. [216]. A liquid-liquid transition in the two-scale spherically-symmetric Jagla ramp model of anomalous liquids has been demonstrated [110], and the LLCP has rigorously been proven to be second-order and belonging to the Ising universality class [111]. Ponyatovsky et al. [217] and Moynihan [218] assume that water is a "regular binary solution" of two states, and this implies that the phase separation is driven by

energy. Cuthbertson and Poole [122] and Holten et al. [219] apply the energy-driven version of the two-state thermodynamics to describe the fraction of molecules in the high-density structure of two versions of the ST2 model of water, which exhibits liquid-liquid separation. Holten et al. [109] also describe the thermodynamic anomalies of the mW model with the same equation of state as used in Ref. [31] to correlate thermodynamic anomalies in real supercooled water. Although the direct computations of the fraction of molecules involved in the low-density structure in the ST2 and mW models are in agreement with the prediction of the two-state thermodynamics [109, 134] (see Fig. 13), in the mW model the athermal, entropy-driven non-ideality of mixing of the two alternative structures is not sufficiently strong to cause liquid-liquid phase separation. The situation in real water remains less certain, but the recent correlation of available experimental data [31, 135] (see Fig. 7) favors a nonideality in entropy-driven mixing of the alternative molecular configurations.

The order parameter

Two-state models cannot microscopically explain the existence of locally-favored states corresponding to LDL-like tetrahedral structures, and this has hindered attempts to build a two-state model from purely microscopic information. The phenomenological order parameter in the two-state model is the extent of the "reaction" between the two alternative structures [109] (see Fig. 13). Thermodynamically this order parameter belongs to the Ising model universality class and it is a non-conserved dynamic property [208].

The most popular order parameters used in microscopic two-state models of water are the tetrahedral order parameter [109, 172] (defined in Eq. 3), $g_5(r)$ (the average density of fifth-nearest neighbor) [122], ζ (the distance between the first and second shell) [220], and the local structure index (LSI) [221–225].

The LSI for each molecule i is acquired by putting the distances of the nearest neighbors j from the reference molecule i in increasing order, i.e. $r_1 < r_2 < r_3 < ... < r_{n(i)} < 3.7$Å $< r_{n(i)+1}$, where $n(i)$ is the number of molecules within 3.7Å from molecule i (using the positions of the oxygen atoms). The LSI distinguishes molecules with well-separated first and second coordination shells from molecules in a disordered environment, containing molecules

in interstitial positions, using the parameter $I(i)$ defined by

$$I(i) = \frac{1}{n(i)} \sum_{j=1}^{n(i)} [\Delta(j;i) - \Delta_{mean}(i)]^2. \quad (4)$$

Here $\Delta(j;i) = r_{j+1} - r_j$ and $\Delta_{mean}(i)$ is the average of $\Delta(j;i)$ over all neighbors j of molecule i within the cutoff. A low LSI value indicates a disordered local environment (HDL), and a high LSI value indicates a highly structured, tetrahedrally coordinated environment (LDL).

Here we consider several properties of supercooled liquid water that can be defined using the order parameter. In reference to a possible liquid-liquid phase transition in water, evidence has been found that there are two different forms of liquid water that differ in the structure of their second-nearest neighbor shell [57]. The low-energy state is characterized by an open tetrahedral structure, and the high-energy state by a collapsed second-nearest neighbor shell with substantial shell interpenetration [33]. The microscopic pathway to the crystallization of supercooled water is also relevant in that hydrogen bonding causes water to acquire a high degree of translational order prior to crystallization, i.e. the supercooled water molecules progressively organize themselves in well-defined shells. In contrast, simple liquids such as hard-sphere fluids have a high degree of orientational order prior to crystallization and acquire translational order only after a liquid-to-solid transition [226]. Thus to detect locally-favored, LDL-like states in water, the order parameter must take into account the structure up to the second-nearest neighbor shell, defined in terms of the network of hydrogen bonds, and be based on translational order rather than orientational order. Thus tetrahedral order only takes into account the first coordination shell and is obtained from bond angles rather than bond distances, and $g_5(r)$ ignores the underlying hydrogen bond network. We thus next consider ζ [220], which measures the distance between the shells of the second and first nearest neighbors. This is obtained by reconstructing the network of hydrogen bonds and then computing for each water molecule the difference between the radial distance of the closest oxygen in the second shell and the radial distance of the farthest oxygen atom in the first shell. Locally favored LDL-like states are represented by a gaussian population centered around a finite value of ζ, and the disordered state is characterized by a gaussian population centered around a null value of ζ, with substantial shell interpenetration ($\zeta < 0$).

Figure 15(a) shows that by decomposing the two populations for many state points it is possible to extract the fraction of locally-favored states s, which is the order parameter that indicates the degree of structural order in water. This fraction can then be fitted with

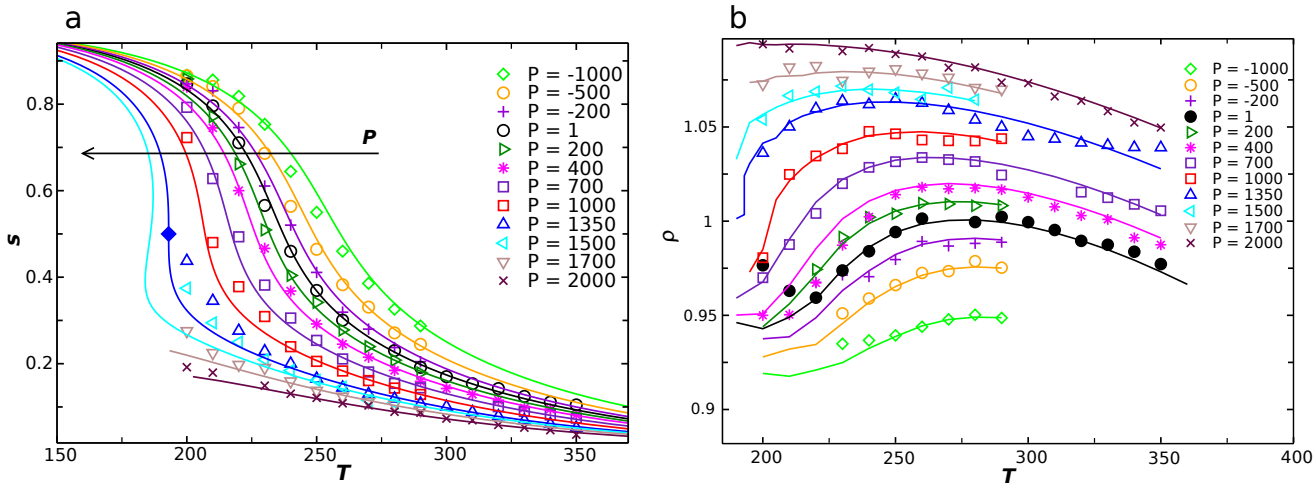

FIG. 15. Two-state model for TIP4P/2005 water. a) Values of the fraction of the locally favored S state (s) as function of temperature for all simulated pressures. The symbols mark the values obtained by decomposition of the order parameter distribution, $P(\zeta)$, at the corresponding state point. Continuous lines are fits according to the two-state model. b) Temperature dependence of density for several pressures. Continuous lines are simulation results, while symbols are obtained from the two-state model. Reproduced from Ref. [220].

a two-state model [see the lines in Fig. 15(a)], which is obtained soley from microscopic information. Note that the isobars become mechanically unstable at high pressure and low temperature, indicating the presence of a liquid-liquid critical point (full symbol).

The structural order parameter estimated using microscopic measurements enables us to predict quantitatively the magnitude of the anomalies and compare them with those obtained in simulations. Figure 15(b) compares the simulations (lines) with the two-state model predictions (symbols) for the density anomaly of TIP4P/2005. The two-state model agrees with the measured anomalies, indicating that a microscopic two-state description of the phase behavior of water is possible. Reference [220] carries out extended analyses for both the TIP4P/2005 and TIP5P models of water.

Although it was recently proposed that a liquid-liquid phase separation can only occur on time-scales shorter than the equilibration time of the simulated (or real) liquid—and thus only liquid-solid transitions are possible [35, 36]—results from several water models showing strong fluctuations between high- and low-density liquid indicate the presence of an HDL-LDL transition [111, 122, 127]. The extensive study by Palmer et al. [121] using several

different computational protocols verifies a metastable liquid-liquid coexistence for the ST2 model. For other simulation models the situation is less clear. The studies above were performed in the deeply supercooled and pressurized region of the phase diagram while water anomalies set in already under ambient conditions. As already discussed, these anomalies find a simple description in a two-state model and evidence of a bimodal distribution of local, instantaneous structures has been found in ambient real water both from x-ray spectroscopies [141, 147, 162, 163] and from measurements of the optical Kerr effect [168]. However, no molecular dynamics simulation has so far shown a bimodal structural distribution under ambient conditions. On the other hand, Sciortino and coworkers [223, 225] applied the local-structure index (LSI) of Shiratani and Sasai [221, 222] to the *inherent* structure of SPC/E water and found that the resulting distribution of this order parameter was bimodal in terms of HDL and LDL at all investigated temperatures. The inherent structure [227] is obtained by removing thermal disorder, i.e. quenching the instantaneous structure to the nearest local minimum through minimizing the energy in an optimization of the geometry. The LSI measures the degree of order in the pair-correlation function out to the second shell for a given oxygen; a high value indicates a highly structured, locally favored tetrahedral or LDL-like, local environment while a low value indicates a highly disordered, more close-packed or HDL-like structure [221, 222]. A connection between the inherent structure of the more realistic TIP4P/2005 water model and the phase diagram of water was made by Wikfeldt et al. [224]. They found a perfectly bimodal distribution of structures separated at the same LSI value for all temperatures and pressures (Fig. 14A-C). The fraction in each distribution is plotted in Fig. 14D where a weak dependence on temperature is seen in the ambient regime but as the temperature is decreased into the supercooled regime an accelerated conversion of low-LSI (HDL) species into high-LSI (LDL) is observed fully consistent with recent measurements on micron-sized water droplets where a continuous, but accelerated transformation to a highly tetrahedral liquid was observed down to 227 K [210]. Interestingly, the 3:1 ratio between HDL- and LDL-like local environments in the inherent structure at ambient conditions is very close to what has been concluded from spectroscopic measurements [141, 147, 162, 163, 168].

A direct connection with thermodynamics is found for the crossing point, i.e. where the populations in the two distributions are equal. At each investigated pressure this coincides with the Widom line (see the definition in section VIII) in the model where fluctuations

are maximal. A further observation regarding the inherent structure can be made from the temperature dependence within each distribution where, with increasing temperature, the low-LSI (HDL-like) species exhibit increasing disorder (shift to lower LSI values) while the maximum of the high-LSI (LDL-like) distribution remains at fixed LSI value while the magnitude decreases. This is consistent with the temperature-dependence of the two lone-pair peaks in x-ray emission spectroscopy [141, 162, 163] as well as the temperature evolution of x-ray absorption spectra of water [149]. However, in simulations of ambient water published so far the bimodality of the inherent structure becomes smeared out and more of an average is observed.

VI. MODE COUPLING THEORY AND DYNAMICAL CROSSOVERS

The dynamical behavior of bulk water simulated upon supercooling [228, 229] fits in the framework of the idealized version of mode coupling theory (MCT) [230]. The normal diffusive behavior of a liquid is Brownian. At t=0 the single particle starts with a ballistic diffusion and then switches to a Brownian regime. When a simple liquid is cooled below the melting line the dynamics starts to be dominated by the "cage effect". After the initial ballistic behavior the particle is trapped by the transient caging of its first neighbors and rattles in this cage until the cage relaxes and the particle is free to diffuse away and restore the Brownian regime. Upon supercooling the relaxation time of the cages become longer and longer and relaxation times of the liquid stretch by orders of magnitude. The ideal version of the theory predicts that at the MCT crossover temperature T_C all cages are frozen. If structural relaxations were the only relaxation channels for having an ergodic liquid then T_C would be the glass transition temperature. When the relaxation time of the cage is stretched enough, already slightly above T_C, hopping processes start and the liquid does not lose ergodicity also below T_C where cages are frozen and these activated processes become the only source of diffusion.

Glass former liquids which are described by MCT show relaxation times with a super-Arrhenius behavior. This behavior can either be phenomenologically fitted with the Vogel-Fulcher-Tamman (VFT) relation [231]

$$\tau = \tau_0 e^{\frac{BT_0}{T-T_0}} \tag{5}$$

or with the MCT power law [230],

$$\tau \sim (T - T_C)^{-\gamma} \tag{6}$$

and this behavior is termed "fragile". Below T_C, according to the idealized version of MCT, the system is frozen but since in real structural glasses, hopping processes restore ergodicity, around T_C the liquid turns its behavior to that of a strong liquid [230, 346]. The relaxation time of strong liquids increases upon decreasing temperature with an Arrhenius behavior [232].

$$\tau = \tau_0 e^{\frac{E_A/K_B}{T}} \tag{7}$$

The crossover from non-Arrhenius to Arrhenius behavior is referred to as a fragile-to-strong (FTS) crossover and it is a feature of many glass formers.

The MCT crossover temperature, which falls close to the FTS transition temperature, is very close to the singular temperature T_s [228, 229] which is the temperature where thermodynamic and dynamic quantities show power law divergencies [1, 12]. This finding points to a connection between dynamics and thermodynamics for water.

Experimental observations demonstrated that bulk water behaves as a fragile liquid, [4, 233]. The translational region of Raman spectra of water has been interpreted in terms of scaling behavior predicted by MCT with a T_C close to T_S [234]. Relaxation times from time resolved spectroscopy follow MCT predictions [235] and show a T_C close to T_S in agreement with simulations [228, 229]. However, we note that very recently Dehaoui et al. [366] found that viscosity and diffusivity are not coupled as predicted by MCT.

It is important to stress that in water, a network-forming liquid, the caging phenomenon is due to the breaking and re-forming of the hydrogen bond local network [236].

The change in behavior from fragile to strong in water was experimentally found in 1999 and discussed [237] also pointing out that the FTS crossover in water is connected to the presence of a thermodynamic event. An FTS crossover in water was also observed later the same year in computer simulations for SPC/E water [238]. We will discuss further the fragile to strong transition in water and the connection between dynamics and thermodynamics in Sec.s VIII, X and XI.

VII. NUCLEATION OF ICE FROM SUPERCOOLED WATER

Below the melting point, water is metastable and will eventually freeze into its thermodynamically stable phase (ice). The transformation involves overcoming a free energy barrier so that the freezing is an activated process. Often the transformation into ice occurs on the surface of solid impurities (heterogeneous nucleation). Some solid compounds, such as AgI [239], or feldspar [240] are quite efficient in reducing the free energy barrier for nucleation. Dust particles of the Sahara desert play a key role in the freezing of water in the upper atmosphere [240]. In the absence of impurities, metastable liquid water can survive even at temperatures well below the melting point, until a critical nucleus of ice appears in the bulk (homogeneous nucleation). By condensing micrometer-sized water droplets (microdroplets) in expansion cloud chambers, it has been possible to prepare metastable liquid water at temperatures down to 232 K [241–243]. Below this temperature (known as the homogeneous nucleation temperature T_H) water freezes too quickly for traditional measurement techniques.

From the fraction of droplets containing ice as a function of time at a given temperature, it is possible to experimentally determine the nucleation rate, J, i.e. the number of critical ice clusters per unit of volume and time. Classical nucleation theory (CNT) has often been used to describe the experimental results. According to CNT, J is given by [244–246] $J = K^* exp(-\Delta G^*/(k_B T))$ where K^* is a kinetic prefactor related to the time required for a particle of the fluid to be incorporated into a solid cluster and ΔG^* is the free energy barrier. In CNT ΔG^* is related to the interfacial free energy γ_{sl} between the two phases, ice Ih and liquid, and to their chemical potential dfference $\Delta\mu$ and is given by the relation $\Delta G^* \propto (\gamma_{sl})^3/(\Delta\mu)^2$. $\Delta\mu$ is well known from experiments and increases as the temperature decreases (thus reducing the free energy barrier), but the experimental value of γ_{sl} for the ice Ih-water interface is not so well known (values between 25 and 35 mN/m have been reported [247, 248]). By inserting solid clusters of ice Ih (seeds) in simulations of supercooled water, and using CNT to interpret the results it has been possible to estimate J from computer simulations [249, 250] in a range of temperatures larger than previous studies [251–257].

Various experimental techniques to determine J are compared in Fig. 16. Above T_H, 232 K, microdroplets have been produced in (water-in-oil) emulsions using microfluidic devices by Stan et al. [258] and Riechers et al. [259], whereas Stöckel et al. [268] levitated single

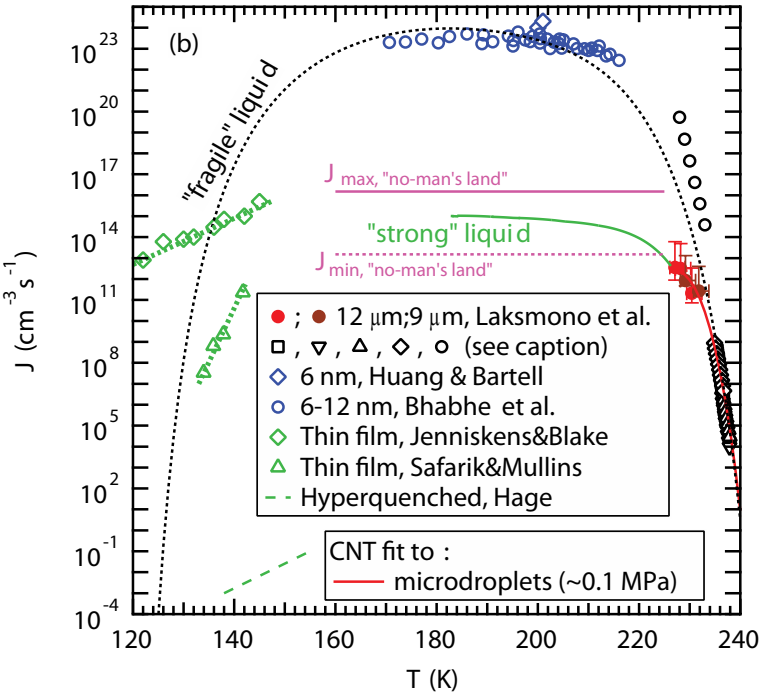

FIG. 16. Comparison of experimentally determined nucleation rates J of water using microdroplets (black hollow markers [258–260, 268, 269] and red and brown filled dots [261]), nanodroplets (blue hollow markers [262, 263]), thin films (black filled diamonds and triangles [264, 265], and hyperquenched water [266, 267]). The data of microdroplets (red solid line) and nanodroplets (blue symbols) follow different trajectories where the nanodroplet data might be affected by the large surface area to volume ratio and elevated internal pressure. An upper limit for the nucleation rate maximum within "no-man's land" J_{max} (pink solid line) and a corresponding lower limit J_{min} (pink dashed line) were calculated from hyperquenching experiments on microdroplets [72, 212–215]. The expected CNT behavior for a "fragile" (black dotted line) and a "strong" (green solid line) liquid are included as guides to the eye. We follow Jenniskens and Blake [264] to obtain the "fragile liquid" CNT curve and also include an expected extension nucleation rate into "no-man's land" (green curve) based on the requirement to lie between the upper and lower limits from hyperquenched microdroplets. Figure adapted from Ref. [261].

water droplets in an electrodynamic balance and Murray et al. [269] determined the nucleation rate from microdroplets supported on a hydrophobic substrate. All these techniques agree within the error of the experiments [269] and have determined J within an order of

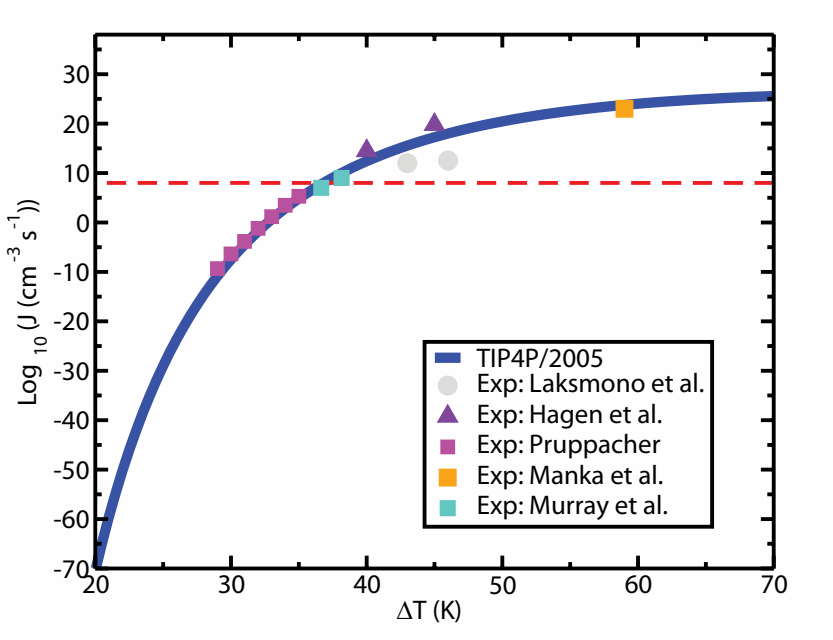

FIG. 17. Nucleation rate J as determined for the TIP4P/2005 model (blue solid line) compared to experiments (filled squares) of Pruppacher [270], Murray et al. [269] and Manka et al. [271]. Experimental results from Laksmono et al. [261] (filled circles) and from Hagen et al. [260] (filled triangles) were also included. The horizontal line corresponds to $Log_{10}\ J\ (\mathrm{cm}^{-3}\mathrm{s}^{-1}) = 8$ which is the approximate value of J at the homogeneous nucleation temperature in experiments (i.e. 38 K below the melting point). Figure adapted from Ref. [250].

magnitude between 235 K and 244 K to 7×10^8 $\mathrm{cm}^{-3}\mathrm{s}^{-1}$ and 5×10^{10} $\mathrm{cm}^{-3}\mathrm{s}^{-1}$, respectively [258, 259, 268–270]. If CNT is applied to the experimental data in this temperature regime, the fit closely resembles that of a "fragile" liquid. Below 232 K, however, non-conventional techniques that cool water rapidly and simultaneously detect ice nucleation have to be applied to overcome the homogeneous nucleation temperature, which has resulted in that various measurements do not agree. Hagen et al. [260] used an expansion cloud chamber to nucleate microdroplets between 228 K and 233 K, and obtained J of 2×10^{17} $\mathrm{cm}^{-3}\mathrm{s}^{-1}$ and 2×10^{12} $\mathrm{cm}^{-3}\mathrm{s}^{-1}$, respectively. Hagen et al. relied on using a droplet growth model [260] that may introduce large uncertainties in the estimation of the temperature and droplet size [269]. Very recently, Sellberg et al. [210] exploited the intense and fully coherent 50 fs x-ray pulses from the Linac Coherent Light Source (LCLS) free-electron x-ray laser to measure the structure of water in microdroplets evaporatively cooled in vacuum to a range of tempera-

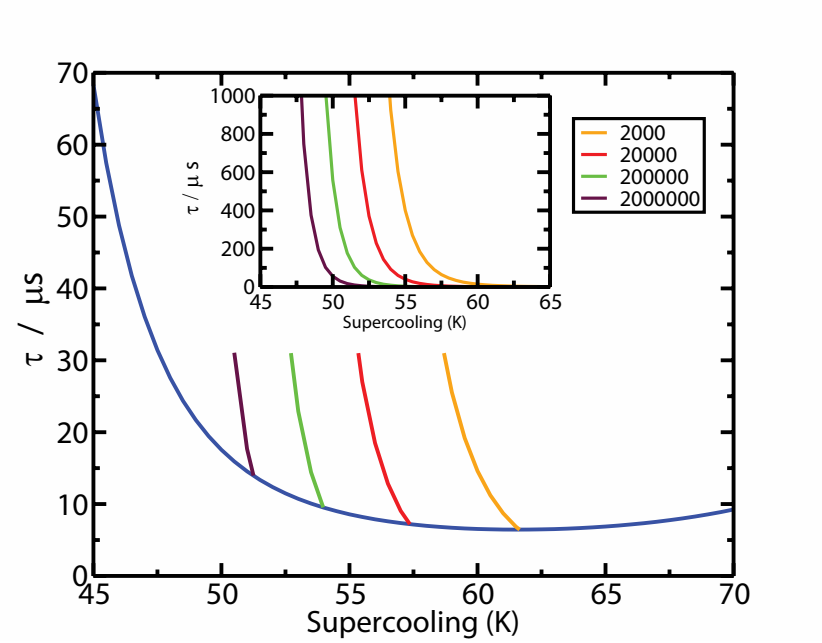

FIG. 18. τ_X for $\phi = 0.7$ for the TIP4P/2005 model as a function of the supercooling. τ_X is the time necessary to crystallize 70% of the system in an infinitely large system (blue line). Inset: plot of the nucleation time, τ_ν, versus the supercooling for systems having different numbers, N, of molecules of water. Figure taken from Ref. [250].

tures down to 227 K, i.e. 5 degrees below T_H. Based on these data Laksmono et al. [261] analyzed the ice fraction and obtained J ranging from 2×10^{11} cm^{-3}s^{-1} to 4×10^{12} cm^{-3}s^{-1} as the temperature decreased from 232 K to 227 K [261]. Sellberg et al. and Laksmono et al. determined the droplet diameters through *ex situ* optical microscopy and scanning electron microscopy, but were forced to rely on Knudsen theory of evaporation, which was calibrated toward reference data above 250 K to determine the droplet temperature as well as to MD simulations of droplet cooling to verify the Knudsen model [210].

Huang and Bartell [262], Manka et al. [271], and Babhe et al. [263] used a different approach and condensed water vapor in a supersonic flow, which reduced the droplets to nanometer-sized dimensions (nanodroplets). This reduces the probability of nucleation, but also increases the surface-to-volume ratio and internal Laplace pressure and therefore may not be representable of bulk water at ambient pressure [261]. These measurements have yielded J of $\sim 10^{23}$ cm^{-3}s^{-1} between 170 K and 215 K with nearly no temperature dependence [262, 263, 271], which would be the expected behavior if water behaves as

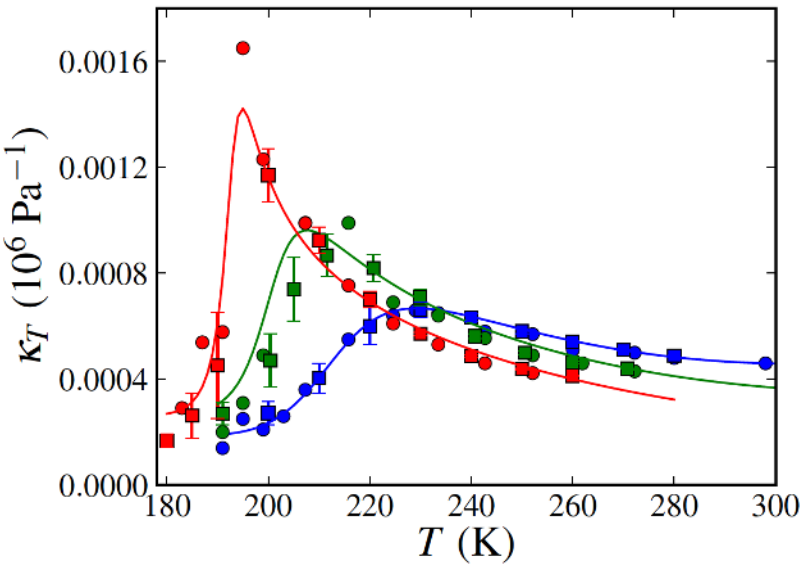

FIG. 19. Isothermal compressibility of TIP4P/2005 water at 1 (blue), 70 (green) and 1200 bar (red) as function of temperature. The symbols indicate the simulated values: squares (with error bars) obtained by Bresme et al. [277] and circles (without error bars) obtained previously by Abascal and Vega [98]. The curves represent values calculated from the two-structure equation of state. Figure taken from Ref.[277]

a "fragile" liquid in this temperature regime. However, additional information obtained from hyperquenching experiments using micrometer-sized water droplets can be used to place upper and lower limits on the maximum nucleation rate [72, 212–215] at temperatures further into "no-man's land". These limits can be defined based on the observation that essentially *all* droplets crystallize in huge ensembles of droplets of 3 μm in diameter, when they are cooled at 10^4 K/s, whereas crystallization was *not detected* when cooled at 10^7 K/s through the 70 K broad "no-man's land" [72, 212–215]. These limits are included in Fig. 16.

Finally, the crystallization rate has also been measured in the temperature range between 122 K and 143 K using thin films of amorphous ice created by vapor deposition. Jenniskens and Blake [264] obtained J ranging from 4×10^{12} cm^{-3}s^{-1} to 7×10^{14} cm^{-3}s^{-1} between 122 K and 140 K, respectively, in support of water behaving as a "strong" liquid around the glass transition temperature of 136 K [69, 71, 272] and in agreement with dielectric relaxation and calorimetric measurements [81]. In contrast, Safarik and Mullins [265] obtained much

lower values of J ranging from 3×10^7 cm^{-3} s^{-1} to 2×10^{11} cm^{-3} s^{-1} between 134 K and 142 K. These measurements are clearly inconsistent with each other and may be affected by the growth rate that limits the crystallization rate at these temperatures and therefore renders it difficult to obtain J.

Results for the TIP4P/2005 model of water are shown in Fig. 17. The agreement with experiment is good. From the computer simulation, it has been estimated that K^* is of the order of 10^{31} cm^{-3}s^{-1} at 235 K, and γ_{sl} of about 29 mN/m at the melting point (decreasing slightly with temperature). At moderate supercooling, the growth rate of ice, u, is fast, so that the limiting step for crystallizing a certain fraction of the sample ϕ into ice is the time, τ_ν, required for the formation of a critical cluster. However, at low T, u is small [273] and the time τ_X required to crystallize a certain fraction ϕ of the sample provides an important measure. According to Avrami's equation [2, 274] this time depends on J and u as $\tau_x \propto (Ju^3)^{-1/4}$. Since J increases while u decreases as the temperature becomes lower, the time scale τ_x has a minimum. The existence of this minimum has been obtained from brute force simulations for the mW model of water [108]. It has also been estimated for the TIP4P/2005 model for which results are presented in Fig. 18. For this model τ_x reaches a value of 10 μs at the minimum. To avoid crystallization one must cross the 50 K region around this minimum at least 10 times faster, which means that the cooling rate must be about 50 K/(1μs) = 5×10^7 K/s. This estimate is in reasonable agreement with the experimental finding that to form water in the glassy state (thus avoiding crystallization) the liquid phase must be cooled at rates higher than 10^6-10^7 K/s [72] and is also consistent with the maximum J in "no-man's land" discussed in connection with Fig. 16.

Obviously, water is not an easy glass former as one requires high cooling rates to form the glass (i.e. amorphous water). In computer simulations it has been found that certain response functions (as compressibility, heat capacity) reach a maximum when the liquid is cooled at constant pressure. For TIP4P/2005 (at 1 bar) a maximum in the isothermal compressibility has been found [98, 275–277] at 232 K indicating crossing of the Widom line (see the definition and discussion about the Widom line in water in sec. VIII). Results for this maximum are shown in Fig. 19 where it is shown that the results of several groups are in agreement. As discussed above, for this model Wikfeldt et al. [224] have evaluated the amount of HDL and LDL as a function of T at room pressure with assignment based on the inherent structure. At 232 K, the populations of the two species cross. An issue

with simulations at low temperatures is equilibration and whether this maximum may be due to the transient formation of ice [36]. However, as can be seen in Fig. 17, the value of J at 232 K and 1 bar (where the maximum in compressibility occurs and 20 K below the melting point of the model) is terribly small (i.e. 10^{-70} $cm^{-3}s^{-1}$) so that no ice formation is observed in the simulations. In fact a key question concerning the possible existence of a liquid-liquid critical point in supercooled water [13, 112, 121] (and/or the existence of a Widom line in response functions), is if the liquid can be equilibrated before it freezes. Limmer and Chandler [35] have pointed out that a relevant magnitude is the ratio between τ_x and τ_e (i.e. the time required to equilibrate the system). If this ratio is large/small, the system can/cannot be equilibrated before it freezes. It is also important to point out that both τ_x and τ_e may depend on the system size [278]. For the mW model the maximum in the compressibility at ambient pressure cannot be reached since water freezes first. This is a clear case where the ratio of τ_x to τ_e is close to one and one cannot observe some of the water anomalies because water simply freezes first. However, for TIP4P/2005 water at room pressure this seems not to be the case and the maximum in compressibility occurs without any indication of ice formation. It would be of interest to analyze this ratio at higher pressures. Thus it is difficult to establish definite conclusions. The fact that two different water models behave differently means that "chemistry matters" and one cannot expect universal behavior for all water models. Further studies both from experiment and from simulations determining both equilibration and nucleation times in droplets between the nanometer and the micrometer scale would be very useful to clarify the value of the ratio between τ_x and τ_e in real water.

Local structural ordering in water has an impact on ice nucleation

Structural ordering in water involves both translational and orientational ordering, reflecting the nature of hydrogen bonding that selects not only distance but also orientation. It has been proposed that the local structural ordering in water controls not only water's anomaly but also ice nucleation and that this feature may be generic to so-called water-type liquids [27, 28].

An analysis of locally favored, LDL-like structures in simulated water reveals that a large fraction of second nearest neighbors participates in five-membered rings of hydrogen

bonded molecules, and that this fraction increases with decreasing temperature and pressure. These five-membered rings, being absent in the stable crystalline phases of ice (the cubic and hexagonal polytypes), have been proposed to be responsible for the long lifetime of the locally favored LDL-like states [28, 201], and act as a source of frustration against crystallization to ice I [220, 257]. As the temperature decreases, the lifetime of hydrogen bonds increases, and the opening of five-membered rings to form six-membered rings becomes increasingly rare. This partly explains why water has such a large metastability gap, in which, in absence of impurities, it can persist in its liquid form down to 40 degrees (°C or K) from the melting temperature.

Work by Molinero and collaborators has shown that homogeneous crystal nucleation starts from tetrahedrally ordered regions inside the liquid phase [108]. In the language of two-state models, crystallization should thus be initiated from locally favored, LDL-like structures, which already have the full translational symmetry of the crystal up to the second shell. These locally favored structures have long lifetimes at supercooled conditions due to the inclusion of five-membered rings of hydrogen bonded molecules, which severely constrains the orientational degrees of freedom of the involved water molecules, and thus stops the development of the orientational order necessary to trigger the liquid-to-ice I transition. The differences in local structure between the supercooled liquid phase and the ice I phase can be measured with quantities such as the dipole-dipole spatial correlation, or the topology of hydrogen bond loops (see Fig. 20).

To overcome frustration effects, the pathway to crystallization can occur through intermediate steps, in line with Ostwald's empirical step rule of phases [279] (see, e.g., Ref. [280] for a theoretical basis in terms of minimum entropy production). In fact, in many molecular and soft-matter systems, crystallization does not occur directly into the stable crystalline phase, but instead involves one or more intermediate steps where the melt crystallizes first in metastable phases [279]. These metastable crystals are structurally more similar to the melt than to the stable phase. This structural similarity leads to a significant reduction of the interfacial energy, although the bulk free energy of metastable states is only intermediate between the one of the melt and of the stable phase.

The idea of two-step water crystallization involving a metastable phase was recently put forward in Ref. [257]. The authors identified a novel metastable phase, called ice 0, with a tetragonal unit cell with 12 molecules, the thermodynamic and structural properties of

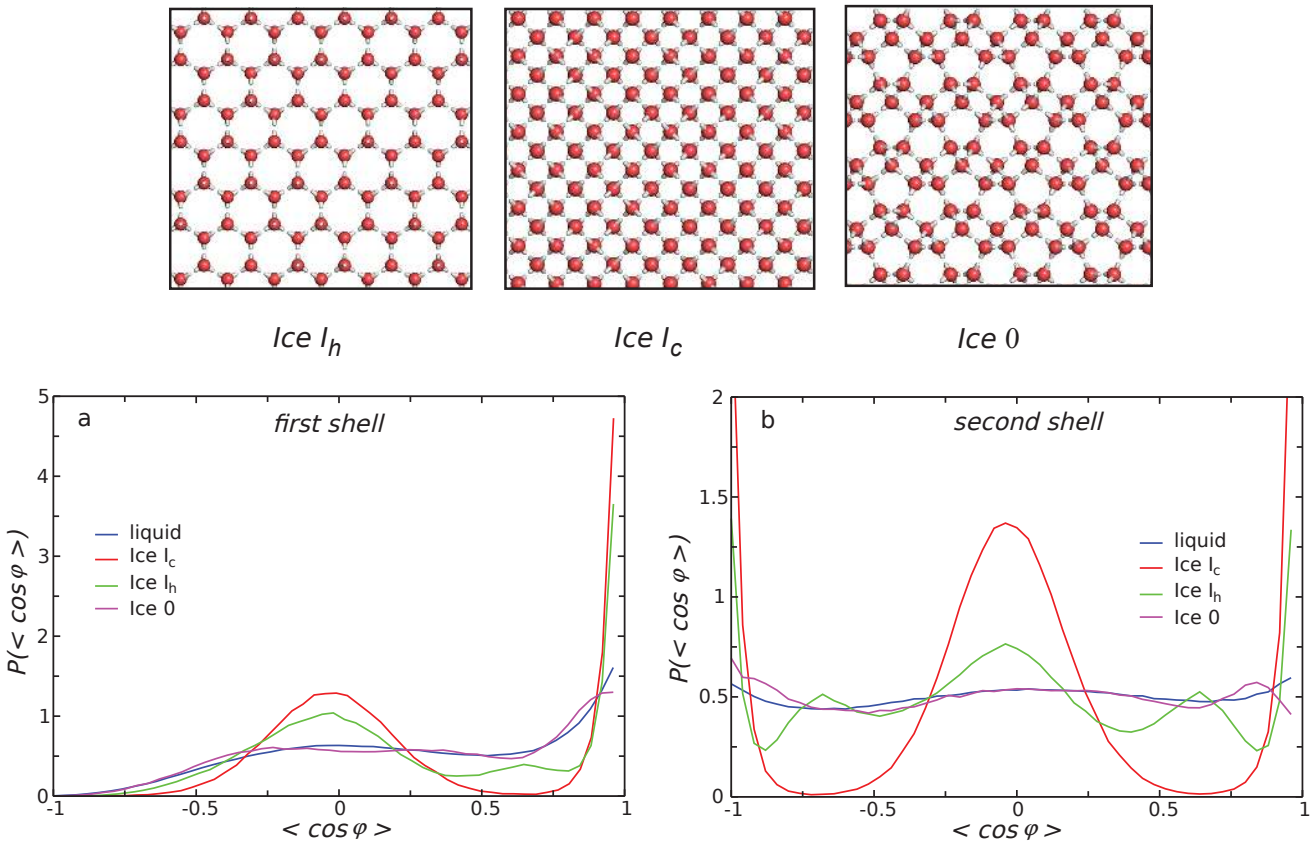

FIG. 20. (top row) Crystal planes for the stable phases and ice 0. (left panel) Distribution of the average angle $\langle \cos\theta \rangle$ between the dipole moment of a molecule and its hydrogen-bonded neighbors for TIP4P/2005 water at $T = 200$ K and $P = 1$ bar in the liquid phase and the ice I_c, I_h and ice 0 phases. (right panel) The same as in the left panel but for second nearest neighbors. Adapted from Ref. [257].

which are intermediate between the melt and the solid crystalline phase. This is shown for example in Fig. 20, where the average dipole-dipole orientation is computed between molecules which are first neighbors (left panel) and second nearest neighbors (right panel). The angle distribution is very similar between the supercooled phase and ice 0, in contrast with the distributions of both the hexagonal and cubic ice forms. Moreover, ice 0 is rich in five-membered rings, which are also very common within the locally favored LDL-like structures where crystallization first originates.

The structural similarity between supercooled water and the metastable ice 0 form, plays

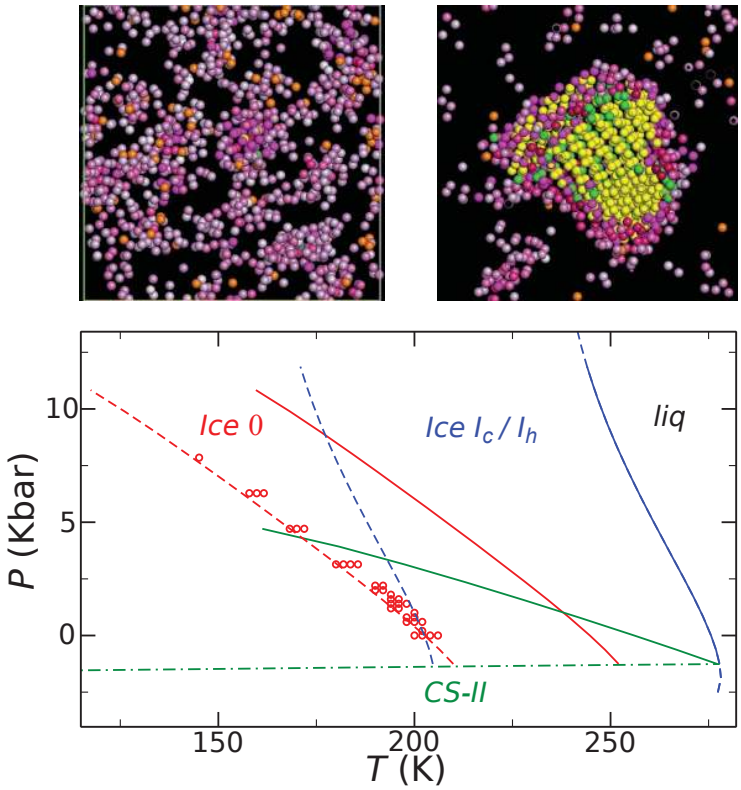

FIG. 21. (top row) Snapshot of two configurations with the birth of a small crystalline nucleus (left panel) and a section of a nucleus of critical size (right panel). The color code is: yellow for ice I_c, green for ice I_h, and magenta for ice 0. (bottom) P-T phase diagram of mW water. Continuous lines indicate coexistence between the liquid phase and different crystal structures: ice Ih/Ic (blue), ice 0 (red) and clathrate CS-II (green). Dashed lines indicate constant chemical potential differences between the liquid and ice Ih/Ic ($\beta\Delta\mu = -0.721$, in blue), and the liquid and ice 0 ($\beta\Delta\mu = -0.365$, in red). The green dashed-dotted line is the Ic/CS-II coexistence line. The red open circles indicate state points where homogeneous nucleation is observed in simulations. Adapted from Ref. [257].

an important role in homogeneous ice nucleation. According to Ostwald's step rule of phases, first a small nucleus of the metastable phase should form, which later converts to the stable ice I form. It is thus natural to expect that, close to the homogeneous nucleation line, where the size of the critical nucleus is negligible, the rate of ice nucleation should be controlled by the thermodynamic properties of ice 0. Reference [257] has indeed shown that the homogeneous nucleation line for the mW model of water coincides with a line of constant

thermodynamic driving force with respect to ice 0 (i.e. the homogeneous nucleation line is the locus of constant chemical potential difference between the melt and ice 0). This scenario was confirmed both by direct simulations and by computation of the nucleation rates of ice.

In Fig. 21 the phase diagram of mW water is reported, with dots representing the locus of homogeneous nucleation, and the dashed line of constant driving force with respect to ice 0. This suggests that it is possible to derive the homogeneous nucleation line from purely thermodynamic arguments. Furthermore, by adopting translational order of the second shell as the order parameter, it is possible to describe the phase behavior of liquid water to a good approximation from purely microscopic information.

Locally favored, LDL-like states are stabilized by five-membered rings of hydrogen bonded molecules, which act as a source of frustration against crystallization to ice I. This dynamical pathway reflects in the crystallization transition, in which the metastable crystalline phase can play an important role. In particular, there is evidence that a novel metastable phase, ice 0, being structurally similar to the supercooled melt, can act as an intermediate step during crystallization. Water would first transform into small nuclei of this phase, that then grow into the stable crystalline phases. According to this scenario, the homogeneous nucleation line would then be controlled by the thermodynamic properties of ice 0.

VIII. RELATION BETWEEN DYNAMICS AND THERMODYNAMICS

Though simulation studies and experimental results approaching the "no-man's land" region of bulk water have shown evidence supporting the existence of LLPT, advanced experimental techniques are still needed to reach this "no-man's land" region [210, 281], in order to establish whether an LLPT exists in deeply supercooled water. Experiments of water in confinement showed that a FTS line as a function of pressure was pointing to where the LLCP is supposedly located [281]. Based on the simulation study on the two-scale Jagla model with an accessible LLCP, Xu et al. proposed an alternative way to detect the LLCP from the one-phase region above the LLCP at higher temperature and lower pressure [34, 94, 110, 282]. Generally speaking in a fluid, when moving away from a critical point into the single-phase region, the correlation length keeps a maximum reminiscent of the critical divergence. On approaching the critical point from this region, thermodynamic quantities such as the specific heat and the isothermal compressibility show

maxima that are expected to merge on a pseudo-critical single line terminating at the critical point. The maxima of those response functions collapse on the same line on approaching the critical point because they become proportional to power laws of the correlation length. This line, called the Widom line, defines this locus of maxima extending from the critical point into the single-phase region. Moving away from the critical point into the single-phase region, the maxima are smeared out progressively and their values decrease [283]. If a second critical point exists in water, the system undergoes a continuous transition from HDL-like to LDL-like liquid upon cooling at constant pressure in the one-phase region [34, 94, 110, 282]. Thermodynamic response functions, such as isobaric heat capacity C_P, isothermal compressibility κ_T and thermal expansion coefficient α, show extrema in this region, the loci of which asymptotically approach one another and converge to the Widom line in the vicinity of the LLCP. This phenomenon in water has been clearly detected in numerous simulation studies: the Widom line pointing to the LLCP has been found for the ST2 and Jagla potentials [34, 94, 110, 282], for the TIP4P potential [107, 284], and for the TIP4P/2005 potential [98]. It has also been found in simulations of aqueous solutions [107, 284, 285] as discussed in Sec. XI. In experiments on supercooled water, the Widom line is of particular interest since it can be used to trace the hypothesized LLCP from the one-phase region, thus avoiding the two-phase region where crystallization occurs easily. Across the Widom line not only the structural response functions but also dynamic properties change and a unified picture of slow dynamics and thermodynamics emerges where a FTS dynamic crossover happens for water upon crossing the Widom line as explicitely found in bulk water for ST2 and Jagla potentials [34, 110, 282], TIP4P potential [287] and more recently for the TIP4P/2005 potential[288]. A recent study of the Van Hove self correlation function for TIP4P/2005 water explicitely connects the freezing of the structural relaxations and the start of activated processes with the FTS transition [289]. This coincidence between the FTS and the Widom line also persists in solutions [286, 290] (see discussion in Sec. XI).

We note here that these findings clarify the connections between glassy dynamics and thermodynamics that is peculiar of water and that was hypothesized from the past studies discussed in Sec. VI.

Xu et al. [291] and later Wikfeldt et al. [224] showed that the populations of LDL-like and HDL-like structures in simulated water change upon crossing the Widom line and, due to these structural changes the system shows the dynamic crossover from non-Arrhenius

(fragile) behavior at higher temperature to Arrhenius (strong) behavior at lower temperature [34, 94, 110, 282, 286, 287, 290].

The structural change is observed experimentally by infrared (IR), Nuclear Magnetic Resonance (NMR), Quasi-Elastic Neutron Scattering (QENS) experiments on confined water, and by x-ray scattering measurements in bulk water [210] at ambient pressure. This is consistent with the results of model studies upon crossing the Widom line from the one-phase region in water. Using QENS and NMR on water confined in MCM-41, Liu et al. observed a cusp-like dynamic transition [281], from non-Arrhenius (fragile) behavior at high T to Arrhenius (strong) behavior at low temperature. This transition was linked to the FTS transition upon crossing the Widom line in the vicinity of the LLCP with the high- and low-temperature liquids corresponding to the HDL and LDL, respectively. The picture of water confined in MCM41 undergoing a FTS was reproduced, linked to bulk water and framed in the MCT context by a simulation study [293–295] (see also the section on confined water here below). Fourier Transform InfraRed (FTIR) experiments on confined water also showed that an HDL-like to LDL-like continuous transition occurs upon crossing the Widom line [291]. According to these experiments, we should be able to trace the LLCP – if it exists – as the terminal point of the dynamic crossover in the one-phase region, located at $P_c = 1600 \pm 400$ bar and $T_c = 200 \pm 10$ K. However, it must be noted that the cited pressure is that applied to water using a fluid outside the pores. The actual pressure in water might be different, and even negative due to the Laplace pressure effect [292].

A convenient conceptual bridge connecting thermodynamic and dynamic properties of dense fluids is also provided by excess entropy scaling relationships for transport properties. In dense fluids, diffusion proceeds by a combination of binary collisions and cage relaxations. Transport properties can be conveniently reduced to dimensionless form using reduction factors based on kinetic theory. Rosenfeld and others [296–311] showed that for a wide range of simple liquids, the following semi-empirical scaling relationship was valid: $X^* = Aexp(\alpha S_e)$ where X^* are dimensionless transport properties, including diffusivity, viscosity and thermal conductivity. The scaling parameters A and α depend on both the nature of the interactions and the transport property.

For example, for simple liquids, the scaled diffusivity, $D_R^* = Dr^{1/3}/(k_BT/m)^{1/2}$, obeys excess entropy scaling with quasiuniversal values of A and α. Rosenfeld-type exponential scaling relationships between transport properties and excess entropies hold for a much wider

variety of dense liquids in the stable and supercritical regimes than was originally assumed, including liquid metals, molecular fluids, ionic melts, core-softened model fluids, chain fluids, room temperature ionic liquids and colloidal fluids, even though the exact scaling parameters may vary substantially. Deviations from Rosenfeld-scaling behavior arise as a consequence of cooperative effects, but for a large number of fluids, transport properties from a wide range of state points scale with the excess entropy.

Given the idea behind Rosenfeld scaling, it was shown in a recent study on TIP4P water that if s_e is approximated with s_2, i.e. the two-body term of the excess entropy, the same FTS transition of the diffusion coefficient is found for s_2 [198, 199]. This result can be tested experimentally by measuring the radial distribution function. The relation between s_2 and the radial distribution function is in fact straightforward and for a one-component fluid it is:

$$s_e \approx s_2 = -2\pi\rho k_B \int \{g(r)ln[g(r)] - [g(r) - 1]\} r^2 dr \tag{8}$$

where g(r) for water is the Oxygen-Oxygen $g(r)$.

We note also that the phenomenon of the Widom line extends its interest also in the supercritical state i.e. in the the one-phase region above the well known liquid gas critical point both in water [312] and in other liquids [313, 314]. In supercritical water the Widom line it is clearly found both in experiments and in simulations [312, 315]. A dynamic crossover passing through the Widom line has been also shown to exists in the supercritical state of water where change of trends in diffusion coefficient and viscosity have been observed upon crossing this line on isobaric paths [312, 315].

IX. STRETCHED WATER

Water, like any liquid, can resist mechanical traction and become metastable with respect to its vapor [2]. We will not be able to claim that we understand the "most anomalous liquid" properly until we have learned to measure the properties of water and its solutions accurately in the negative pressure domain. In particular, the behavior of the line of density maxima (LDM) at negative pressure can help discriminate between the proposed theoretical scenarios, depending on whether, when the pressure decreases, the LDM reaches a maximum temperature, or its temperature keeps increasing. Moreover, a region exists, at negative pressure and temperature below the melting point of ice, where water is doubly metastable,

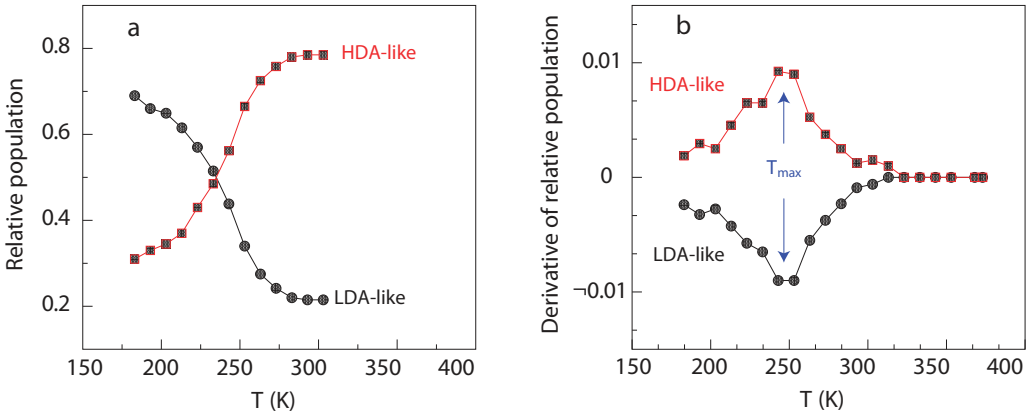

FIG. 22. Experimental IR results for structural change of confined water upon crossing the Widom line (adapted from ref. [291]). (a) Relative population of HDA-like and LDA-like water species as function of temperature. (b) Derivative of the relative population for HDA-like and LDA-like water species. The maximal change occurs at the temperature T_{max} where the Widom line is crossed.

with respect to both ice and vapor. Is it possible to observe the Widom line (or one of the lines of maxima in a thermodynamic response function) in the doubly metastable region? A comparison between the experimental line of homogeneous nucleation of ice and simulations with the TIP4P/2005 potential (Fig. 23) suggests that it might be possible [38, 317].

Whereas negative pressures are routinely accessible in simulations, experiments are notoriously difficult because a small perturbation can trigger the rupture of the liquid by nucleation of a bubble (cavitation). The most documented quantity is the largest negative pressure that could be reached. For water, all experimental techniques but one are limited to -30 MPa [317–319]. Negative pressure studies seem to come into focus about every twenty years. In 1950 Briggs [335] reached -25 MPa (compared with -50 MPa for mercury), while Winnick and Cho [336] developed a clever centrifugal force method in 1971, but were unable to get beyond Briggs' limit. Henderson and Speedy's outstanding works of 1987 were slightly ahead of the pattern. They reported the line of density maxima to -20.3 MPa [320] and the melting temperature of ice to -24 MPa [321]. They both lie on a natural extension of the positive pressure data, but cavitation prevented to follow these properties to larger negative pressure.

The 20 year cycle for negative pressure studies was restored in 1991 by Green et al. [337], and Zheng et al. [325, 338] who broke new ground. They showed that, with a

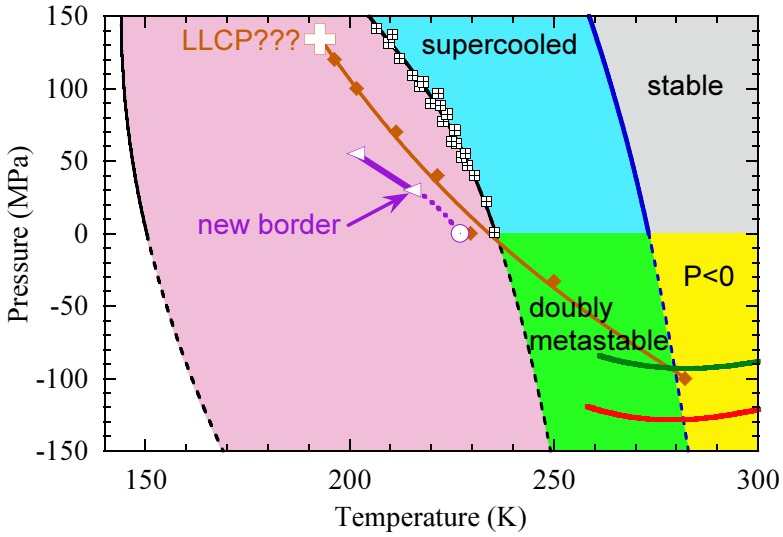

FIG. 23. Pressure-temperature phase diagram of water from Ref. [38]. Colored areas are used to identify the different possible states for liquid water. The melting line of ice I_h is shown at positive pressure by a solid blue curve and its extrapolation to negative pressure by a dashed blue curve. The black crossed squares show the experimental supercooling limit [316]. They define the experimental homogeneous nucleation line (solid black curve), which is extrapolated here to negative pressure (dashed black curve). The ρ_1 and ρ_2 isochores of TIP4P/2005 water are shown by the red circles and curve, and green diamonds and curve, respectively. Simulations of TIP4P/2005 water are performed to find the maximum κ_T along several isobars (white triangles), defining the line of maxima in κ_T (brown curve), that might emanate from an LLCP (white plus symbol). Because the predictions of TIP4P/2005 are in satisfactory agreement with the reported experimental results in the supercooled region [275], this figure seems to indicate that the line of maxima in κ_T (and other extrema in the response functions) might be accessible to experiment only in the doubly metastable region.

microscopic version of the original (1850) Berthelot tube approach, unprecedented tensions, in the vicinity of -150 MPa, could be reached before their water-filled $\simeq$ 5 by 15 μm dimension vesicles in quartz crystals, cavitated. Since these tensions are close to the values predicted for the same temperature 40-47 °C by classical nucleation theory nearly 70 years ago [339] and quantitatively supported by more recent theory [105], it appeared that a major barrier had been crossed.

What was of high significance in the 1990s era studies was the finding of a tension maxi-

mum, identified by the "schizophrenic" behavior at 40-47 °C of the vesicles in a preparation of density 0.91 g/cm^3, and the failure to cavitate at any temperature for inclusions of higher densities. {Different vesicles in the same sample which, at other densities would all behave in the same manner, would sometimes cavitate during cooling but at different temperatures in the range 40-47 °C, and sometimes not at all. Any inclusion that survived cavitation to 40 °C would never cavitate, making it clear that a tension maximum, very close to the limiting tension for that sample, had been traversed.} This suggested the existence of a density maximum at this low density. However, since the cavitation probability depends on a combination of negative pressure and surface tension, a more refined analysis is needed, see below. In the measurements of the 90s era were also the first direct measurements of a physical property in the new high tension range made available by the micro-Berthelot tube. Alvarenga et al. [326] showed it was possible, using micro-Brillouin scattering methods, to obtain the isochoric velocity of sound and hence the adiabatic compressibility along the isochore.

After a further two decade lapse, a new set of experiments has emerged since 2010 from the Caupin laboratory. Using an acoustic wave to stretch water, an experimental equation of state was measured at ambient temperature to -26 MPa [322]. It agrees with the extrapolation of the recommended formulation of the equation of state measured at positive pressure [323, 324]. Later, using the same autoclaving method established by geochemists [341] and used by Zheng et al. [325] and Schmulovich et al. [327], El Mekki et al. [328] obtained a perfectly formed vesicle with which they were able to study the statistics of cavitation in a single vesicle as function of temperature and thereby to estimate the temperature of the minimum energy barrier for cavitation, around 320 K. This must be corrected for the variation of surface tension with temperature, in order to locate the temperature of the tension maximum for the isochore of the studied density, 922 kg/m^3. The correction depends on the model chosen to express the energy barrier for cavitation. Using classical nucleation theory with a Tolman length correction to the surface tension, the results are not inconsistent with the extrapolation of the positive pressure equation of state [323, 324], that is a temperature of density maximum near 296 K at 922 kg/m^3. Obviously more direct measurements would be useful.

Another line of research uses the fact that some of the water inclusions are able to survive cooling without any bubble nucleation [38, 325], which gives access to the doubly

metastable region. Revisiting the work of Alvarenga et al. [326], Pallares et al. recently measured the sound velocity in two doubly metastable samples [38]. An estimate of the path followed in the phase diagram is given in Fig.23. This study suggests that: (i) the experimental equation of state deviates from the extrapolation of positive pressure data at low temperature, (ii) the adiabatic compressibility passes through a maximum when the temperature varies at constant density, and (iii) the sound velocity vs. density at constant temperature becomes non-monotonic at low temperature. These features are consistent with the liquid-liquid critical point scenario [13] and the singularity-free interpretation [23]. It has also been suggested that the experiments might have found the liquid-liquid transition [329]; although not impossible, this possibility does not seem likely [38]. More measurements on water in the doubly metastable region would certainly help to shed light on the origin of its anomalies.

X. THERMODYNAMICS AND DYNAMICS OF CONFINED WATER

The dynamical properties of water in restricted geometries and at interfaces have been studied intensely because of the important effects in systems of interest to biology, chemistry, and geophysics, the behavior of which depends on how the pore size and structure influence the diffusion of water. Those properties are particularly relevant in understanding phenomena like the mobility of water in biological channels or the dynamics of hydrated proteins [8–10] also in connection with cryopreservation, see for example ref. [342].

Of all this vast field we here focus only on the relation between dynamics and thermodynamics in confinement and in particular to what extent confinement can be of help to shed light on the thermodynamics of bulk water in the supercooled region.

Molecular dynamics studies on water confined in hydrophilic silica porous glasses like Vycor [343, 344] and MCM-41 [293–295] upon supercooling evidentiated that for this kind of pores and hydrophilic surfaces the dynamics of water can be split in two ranges: (i) the dynamics of the bound water, close to the surface of the pores, and (ii) the dynamics of the inner water, often called free water, which is more bulk-like. The dynamics of the bulk-like inner part follows the MCT in the region of mild supercooling and upon further supercooling shows a FTS [293–295, 343, 344].

Experiments show that it is easier to supercool water in confinement than in bulk. In

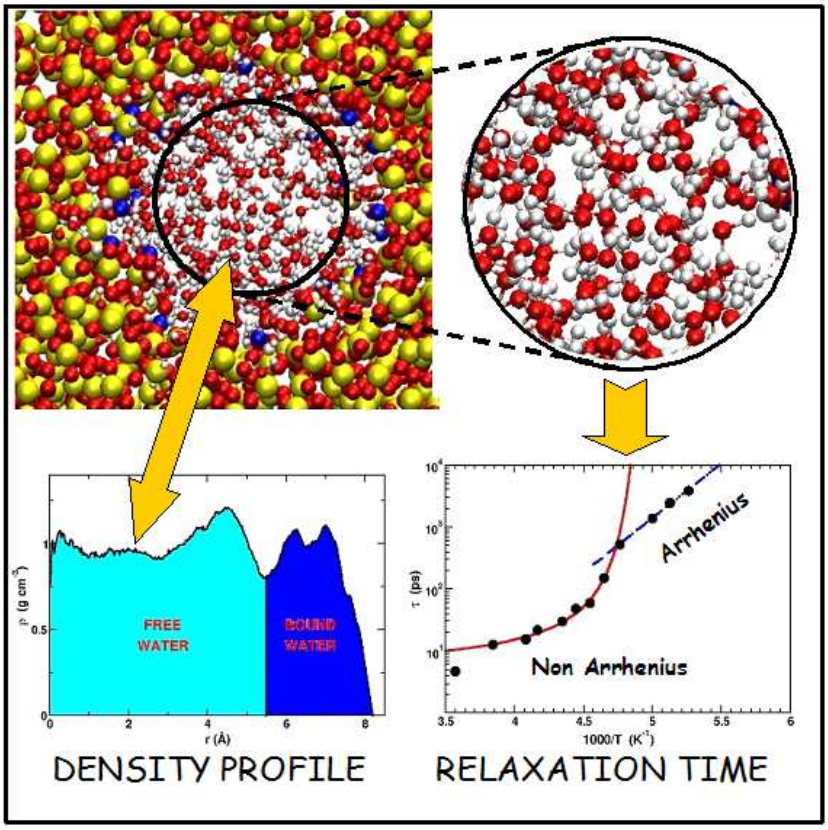

FIG. 24. Molecular dynamics simulations of water in MCM-41. In the picture we can see the difference between bound and free water which show distinct dynamical behavior and the behavior of the relaxation time of free water that shows the FTS transition that coincides with the Widom line (not shown). Reproduced from ref. [293].

particular, by confining water in nanopores of mesoporous silica MCM-41-S with cylindrical pores of 14 Å diameter it was possible to study its dynamical behavior in a temperature range down to 160 K, without crystallization [281, 345].

Quasielastic neutron scattering (QENS) is the most suitable technique to study translational dynamics as its cross section is directly related to the (Q, ω) Fourier transform of the density-density correlation function. Care must instead be taken when analyzing relaxation times with techniques that probe orientational degrees of freedom as the FTS transition is only translational in nature. QENS experiments are sensitive only to the more mobile water contained in the inner part of the pores as the sluggish water close to the surface of the strongly hydrophilic pores gives a signal which is buried in the resolution of the instrument. The experiments performed on supercooled water in confinement found evidence of a FTS

dynamic crossover [281, 345] already hypothesized in bulk water, and in analogy with other network-forming liquids [346].

Most important is that it was found that the FTS line, as function of pressure, points to the zone where the LLCP is supposed to exist [34, 281, 347]. After that the FTS transition line was identified to coincide with the Widom line in simulations of bulk water [34], Gallo et al. simulated water in MCM-41 and obtained the same results as in the experiments, see Fig. 24, further finding that the FTS crossover coincides with a peak in the specific heat that identifies the Widom line [293, 295] and thus bridging the gap between experiments in confinement [281, 345] and MD results in the bulk [34]. This link between Widom line and FTS crossover described in these last two sections shows that for water the Widom line appears to also be a switching line for hopping, favored on the side where water is less dense. Another typical feature of glass forming materials that has recently been related to the crossing of the Widom line [348] is the appeareance of the Boson peak. The Boson peak is an excess of intensity in the low-frequency range of the vibrational spectrum.

XI. THERMODYNAMICS AND DYNAMICS OF AQUEOUS SOLUTIONS

In this section we will discuss how and to what extent aqueous solutions can be used as route to reach the "no-man's land". Similar to confinement, many aqueous solutions have the invaluable advantage that they can be supercooled more than the bulk [349–351]. Besides, in the natural environment water is almost always found as solvent in mixture of two or more components.

Archer and Carter showed that in NaCl(aq) the heat capacity and the density anomalies are still present in dilute solutions [352, 353], however at higher concentration of NaCl the heat-capacity anomaly disappears, as seen in Fig. 25. This fact does not contradict the possibility of liquid-liquid transitions in supercooled aqueous solutions of NaCl, stemming from the liquid-liquid transition in pure water. Moreover, the suppression of the heat-capacity anomaly measured at constant composition is predicted by thermodynamics and, as seen in Fig. 25, is well described by the two-state model [134].

Later Mishima performed experiments on LiCl aqueous solutions where the observed decompression-induced volumetric change of dilute LiCl aqueous solution can be interpreted by the polyamorphic viewpoint about the solvent water and can be regarded as the expected

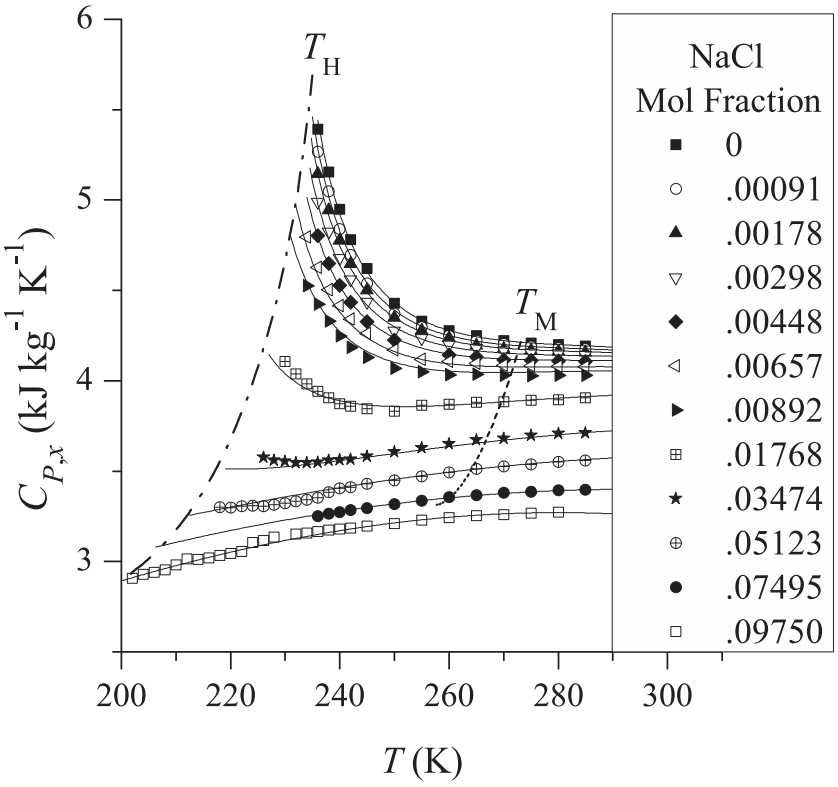

FIG. 25. Suppression of the anomaly of the heat capacity in aqueous solutions of sodium chloride. Symbols: experimental data of Archer and Carter [352, 353]. Solid curves: predictions based on two-state thermodynamics [134]. Dashed curve shows the positions of the melting temperatures. Dashed-dotted curve shows the temperatures of homogeneous ice formation.

polyamorphic phase separation [354, 355]. This finding is supported by later experiments [356] and by simulations [357, 358]. Kobayashi and Tanaka [169, 170] studied the glass-forming ability of LiCl-water mixtures and found that it is maximized near the eutectic point. Furthermore, it was demonstrated that the dependence of the viscosity and the Raman spectra on salt concentration can be explained by a simple two-state model.

Chatterjee and Debenedetti studied the thermodynamics of solvophobic aqueous-like solutions. In the presence of an LLCP for the aqueous-like component, critical lines will stem from the LLCP of the pure substance upon increasing the solute content [359, 360].

Given these evidences, if an LLCP in water exists then it could be found with a properly tuned aqueous solution. Indeed, a LLCP was claimed for the glycerol-water system by Suzuki and Mishima at 0.12–0.15 mole fraction, 150 K and 30–50 MPa [361]. Murata and Tanaka have also reported the observation of a liquid-liquid transition in supercooled aqueous

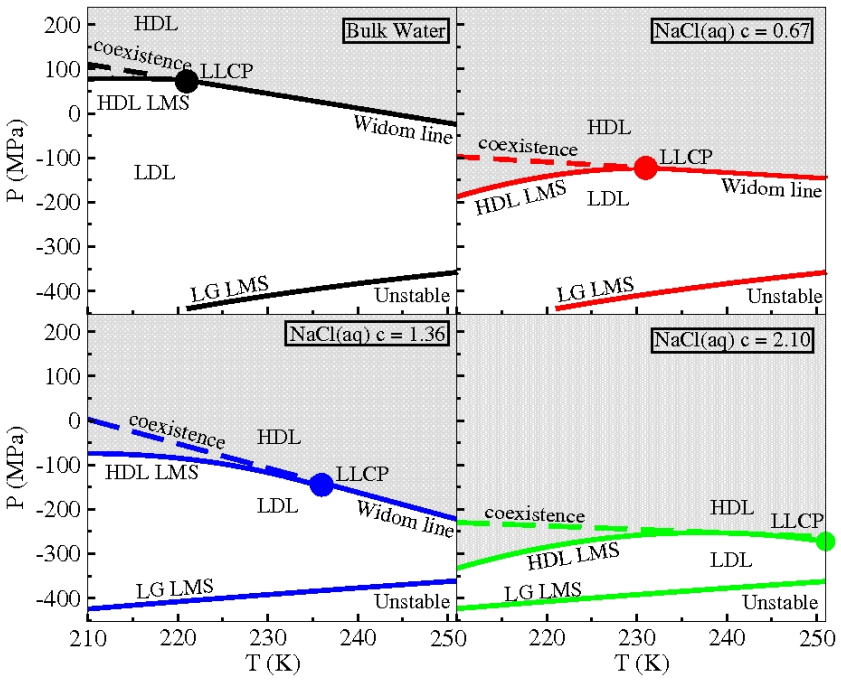

FIG. 26. Phase diagram of NaCl aqueous solutions of supercooled water as obtained from molecular dynamics simulations properly matched to the experimental data. Upon increasing salt content the LDL region shrinks and the LLCP is shifted to lower pressures and higher temperatures. Reproduced from ref. [284]

solutions of glycerol [362] and also in many other aqueous organic solutions [363]. This interpretation has been questioned for water-glycerol mixtures and ice formation suggested as the origin [364, 365].

Corradini et al. studied with MD simulations NaCl dissolved in TIP4P water with concentrations ranging from c=0.67 to 2.10 mol/kg [107, 284]. The liquid-liquid critical point is present both in the bulk and in the solutions and its position in the thermodynamic plane shifts to higher temperature and lower pressure upon adding salt. Comparison with available experimental data allowed to produce the phase diagrams of both bulk water and the aqueous solution as should be measurable in experiments as shown in Fig. 26. Given the position of the liquid-liquid critical point in the solution as obtained in these simulations, the experimental determination of the hypothesized liquid-liquid critical point of water in aqueous solutions of salts appears possible. For the experimental c=0.67 mol/kg NaCl(aq) the LLCP is predicted to be at around $T_c = 230$ K and $P_c = -120$ MPa. In NaCl(aq) with concentration c=0.8 mol/kg experiments have shown that rupture occurs at P = -140 MPa

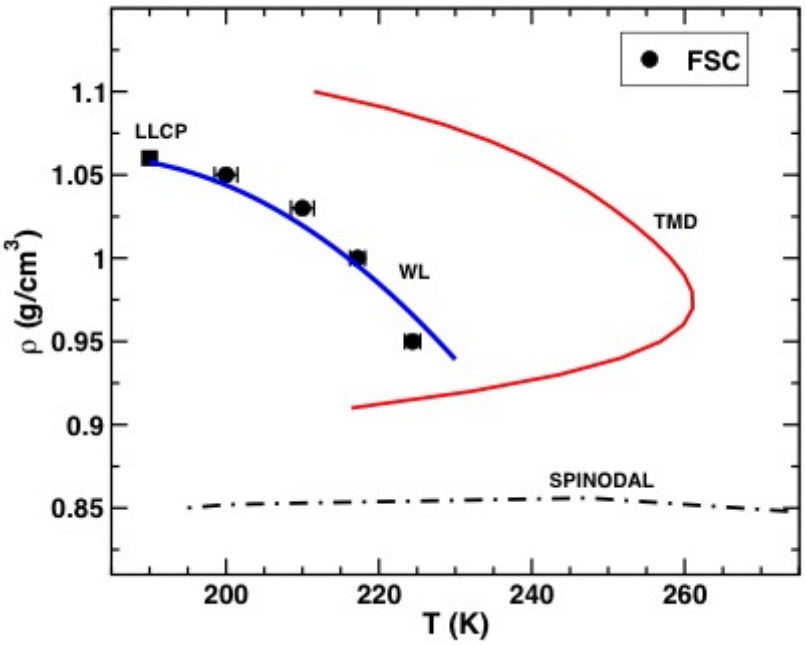

FIG. 27. FTS transition points (circles) and Widom line (line) in a NaCl aqueous solution as obtained from molecular dynamics simulations. The nose-shaped line is the TMD [286].

[337]. More recently a series of aqueous solution was studied [327] and cavitation pressures beyond -100 MPa were also observed. From refs. [316] and [367] the homogeneous nucleation temperature position can be estimated to be slightly below that of the LLCP of c=0.67 mol/kg.

Upon further adding salt (Fig. 26) the LDL region shrinks more and more as ions are more favorably solvated by the high density liquid [358, 368].

To complete the picture of low concentration solutions of NaCl in water an MCT behavior and a FTS transition was found upon supercooling and the FTS transition happens on crossing the Widom line, see Fig. 27, confirming also for the solution the link between dy-

namics and thermodynamics found in the bulk [286, 287]. The excess entropy approximated by the two-body terms extracted from MD simulations of NaCl(aq) shows the same FTS transition as the diffusion coefficient [198] and this means that from a direct experimental measurement of the g(r) the FTS should be measureable also in solutions.

Small angle x-ray scattering experiments of NaCl aqueous solutions also demonstrate the persistence of the anomalous behavior in the solution since they show that the correlation length can be fit with a power law, similar to the bulk, upon cooling [369].

Biddle et al. [134] have compared their equation of state for solutions based on the ideas described in sec. IV, with the MD results of NaCl(aq) [107, 284] and found agreement.

Recent experiments on melting of precipitated ice IV in supercooled LiCl-H_2O solution by Mishima [370, 371] can be explained presuming existence of polymorphism in water, and by the simple assumption that LiCl is dissolved mainly in high-density liquid water as also found in simulation on NaCl(aq) [368].

A similar picture to that of electrolytes appears for the phase diagram of the small amphiphilic methanol molecule. The phase diagram is shifted down in pressure (but not in temperature) and the LLCP is still found for low concentrations [372]. A FTS was measured in methanol solutions at different concentrations [373].

Also a model potential like Jagla shows, upon addition of a solvophobic solute, the same phenomenology described so far. In particular, solutions of Jagla water upon insertion of hard spheres show a shift of the LLCP to higher pressures and lower temperatures and a dynamic transition upon crossing the Widom line [285, 290].

Experiments, theory and simulations thus indicate that aqueous solutions are a viable route to solve the mysteries of supercooled water.

XII. FUTURE DIRECTIONS

The foregoing review makes clear that, despite many, often highly sophisticated, experimental and computational efforts to obtain a full understanding of the complex behavior of water, there remain many gaps in our knowledge and understanding of this most anomalous liquid. In this section we seek to identify the most serious of these gaps, and to explore how they might be dealt with. The biggest problem faced is that of the "crystallization curtain" that has until recently blocked our knowledge of behavior below the homogeneous

nucleation temperature. How best to capitalize on the success of Nilsson and coworkers [210] in penetrating this barrier by means of microdroplet streams and pulsed x-ray laser interrogation, is obviously one line of study to be explored and this is the first issue that will be considered below.

But there are other possibilities for circumventing the crystallization problem to be considered. Each has its own set of difficulties and uncertainties but also promise. There is, for instance the approach outlined by Koop and coworkers [382] to effectively mimic the raising of pressure on water by introduction of second components. Although this usually results in the wiping-out of the anomalies at the same time as it removes the crystallization event (Figs. 25 and 26), it now seems it is possible to decouple the two effects by using the right kind of solute. This approach should be worthy of detailed study since it is basically simple.

Then there is the prospect raised by recent studies of water under high tension [38, 317], which have suggested that the anomalous domain can be elevated above the fast crystallization domain, perhaps due to competition between ice Ih and various empty clathrate structures that frustrate the generation of critical nuclei of any one crystal form. The negative pressure domain is the only remaining unexplored region of metastable water's existence, and although the challenges in sample production, and in exploring anything other than isochoric behavior are many, the rewards might be great. It has been argued [317, 332] that it is in this domain that the observations needed to distinguish between the different scenarios of section II, will need to be made.

Also, of course, there are developments and refinements in the field of computer simulations that are much needed for the understanding of deeply supercooled water. The need is illustrated by a comparison of laboratory data for the fundamental thermodynamic properties, isothermal compressibility and constant pressure heat capacity, with those determined by calculations with the best pair potential currently available. The comparison of ambient pressure compressibility obtained with the pair-potential given most attention in this review, viz. TIP4P/2005 is shown in Figure 28. The agreement is quite good for the first 20°C of supercooling, but then becomes rapidly poorer at lower temperatures where the simulations go through a mild maximum and the experimental quantity shows a strong tendency to diverge at about the same temperature. The power law behavior is seen not only for the compressibility, but also for the heat capacity (Fig. 1), and even more clearly for various transport properties such as viscosity, dielectric relaxation, spin-lattice relaxation and the

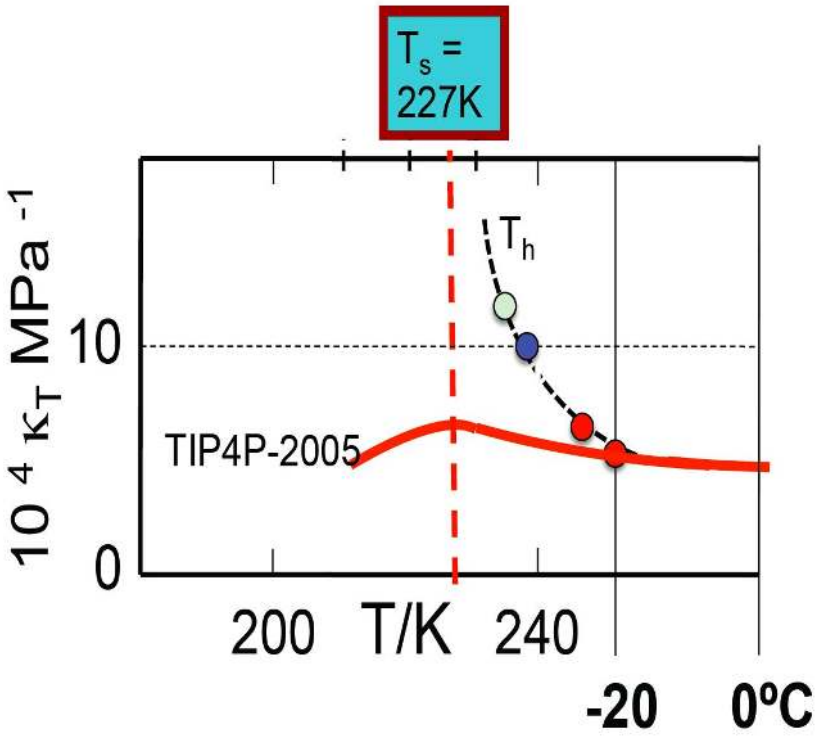

FIG. 28. Comparison of the compressibility-temperature relation at 0.1 MPa obtained with the TIP4P/2005 pair-potential (heavy red curve), with the experimental findings and their extensions, as follows: -20 °C (253 K): combination of fluctuation based data (Huang et al.) and direct p-V data (Speedy et al.) that are in close agreement: -24 °C (249 K) lowest temperature direct measurement of Speedy et al. (239 K limit of Holten and Anisimov extrapolation of ambient pressure fitted data: 235 K (based on low T limit of heat capacity measurements, that follow the power law with same divergence temperature).

related reorientation relaxation time, all measured by different authors, so is probably a reliable representation of the observable data. The divergence temperature which has not been confirmed because it lies in "no-man's land", falls in the range 223-228 K, depending on range of data fitted and nature of background corrections.

We now consider each of these in sequence.

A. Ultrafast probing.

As described in section V there has been a development in terms of a general method for studying liquid structures below T_H based on fast cooling and ultrafast probing using femtosecond short x-ray pulses by exploiting the unique capabilities of the x-ray laser LCLS [210, 261]. This needs to be further developed to allow other types of measurements both at ambient pressures and eventually at elevated pressures. It will be essential to measure the thermodynamic response functions, such as C_P and κ_T, on small water droplets into "no-mans land" and also the correlation length (ξ). If direct temperature measurements can be developed and a heat source to induce a temperature rise, then potentially C_P could be determined. SAXS is the most direct probe of density variations or fluctuations on different length scales in a liquid and from such measurements both κ_T and the correlation length (ξ) could be determined using x-ray lasers. There is a thermodynamic relationship that relates κ_T to the structure factor at $q = 0$ as $S(0) = nk_BT\kappa_T$, where k_B is the Boltzmann constant, T is the absolute temperature, and n is the molecular number density [374]. We can then test the hypothesis that neither ξ, C_P nor κ_T will diverge to infinity but will reach a maximum at T_s i.e., within the LLCP hypothesis, at the Widom line. Depending on how flat the temperature-dependent region around T_s is, this could provide further insight into the validity of the various scenarios and if there exists an LLCP. It will also be essential to follow ξ and κ_T to lower temperature beyond T_s. Furthermore it would be valuable to conduct the experiment using D_2O in order to probe isotope effects as well as use NaCl solution since the latter has an effect similar to pressure [369, 375] as discussed in section XI. It could also be possible to determine the density variation from Wide-Angle X-ray Scattering (WAXS) at very high q. The scattering intensity will have weak q-dependence and become proportional to the density of the liquid. From such measurements it could also be possible to derive the thermal expansivity α. Here it will be essential to observe if there is a minimum in α close to the Widom line. Eventually all these classes of experiments should be developed to also involve higher pressures. This will become a major experimental challenge but it is essential that an effort will be devoted to this since it could provide a final answer to which of the various scenarios best describes real water.

Another essential question to address is the proposed scenario that there is only a liquid to solid transition and that an LDL liquid crystallizes faster than the relaxation time of the

liquid [35, 108]. Could we then observe at which temperature the time-scale of liquid equilibration becomes longer than the time scale for ice crystallization? By directly comparing these time scales we could establish if and at which temperature the liquid could no longer equilibrate relative to fast ice nucleation. We would expect that the structural fluctuations significantly slow down entering into the supercooled regime and maybe in the "no-man's land" region could become on the order of 10 ps or 100 ps. This could also be related to the much discussed fragile to strong transition in the temperature dependence of the viscosity of water both above and below "no-man's land" [24, 235, 237, 291, 376]. It has been suggested that there is a dynamic transition at 228 K that would coincide with the temperature of the T_s or Widom line [237].

B. Second component studies.

Koop et al. [382] showed that ice nucleation commences at a temperature determined by the water activity irrespective of whether the water activity is reduced by increase of pressure or by addition of a second component that dissolves in the water. The more hydrophilic the solute the less of it is required to reduce the nucleation temperature to a target value, or alternatively to remove the possibility of crystallization altogether.

Hydrophilic solutes like LiCl or $MgCl_2$ lower the nucleation temperature rapidly, leading to non-crystallizing solutions. On computational time scales, NaCl behaves the same way [284]. The general consequence of high hydrophilicity is that the structures responsible for the interesting anomalies of water are quickly dismantled (or at least are pushed out of sight to negative pressures (see Fig. 26, and ref. [284])). There are other solutes, however, which do not lower the activity of water very rapidly, in fact lead to demonstrably ideal solution behavior according to melting point depression criteria, and it is found that in these cases the low temperature behavior retains the anomalies of water, indeed in enhanced form. This behavior is only recently recognized, and not yet much exploited. It might provide a convincing demonstration of how water would behave during cooling in absence of crystallization. Its relation to the studies of Murata and Tanaka [363] needs to be clarified in future work. However, because second component incorporation is a proxy for increasing pressure, neither provides clear answers to the burning question of pure water behavior at ambient pressure, in absence of crystallization. This may be more easily approached from

the other end of the pressure scale, namely at high states of tension or negative pressure.

C. Studies at negative pressure.

Studies of water at large negative pressures have been sparse because of the difficulty of preparing the microscopic samples of water in mineral matrices needed to evaluate the behavior of water in this exotic state, and the difficulty of studying them once successfully formed. Regrettably the fluid inclusion strategy seems to offer the only feasible way of obtaining samples suitable for evaluating the behavior of water in this interesting domain. The constraint to constant volume over the temperature range of study is another problem. Nevertheless the difficulties have been mastered by different groups, and Caupin and coworkers, [38, 317] in particular, have given evidence that the anomalous behavior can emerge from, and be studied outside of, the fast crystallization zone (no-man's land"), see section IX. Clearly this provides a challenge to future workers to perform measurements additional to the velocity of sound studies that have so far been performed, and to design sampling procedures that permit more variable pVT conditions.

Although most workers are of the opinion that the critical zonein real water lies fully at positive pressures, and that scenario B of section II is the appropriate description of real water behavior, the issue is not yet settled. Although it has not been discussed in the body of the review, there is a powerful argument by Binder (see ref. [384]) to the effect that in a metastable system a true critical point cannot exist because the diverging time scale needed for its ergodic manifestation would cross the finite lifetime for the liquid imposed by crystallization kinetics. This difficult-to-deny argument which, however, only concerns the immediate vicinity of the critical point, leads us to refer to a critical "zone" within which ergodicity in principle cannot be established, but on either side of which a liquid-liquid line or a Widom line could exist and could play a role in the physics of the liquid.

The arguments given by Speedy for an essentially continuous line of compressibility infinities from a negative pressure extreme to strong positive pressures, and the similarity to the engineering equations of state, coupled with the lack of any isochore crossing point for the available isochores from the IAP-WS95 equation of state in the positive pressure range (such as that seen so clearly for ST2 water [94]), leaves the situation with real water in some doubt. While this can be rationalized by locating the critical point very close to ambient

pressure, as fitted by Holten and Anisimov [31], the fact that the "most likely" second critical point pressure has moved steadily to lower pressures with passing time over some two decades, keeps the final location of the critical point and liquid-liquid line, or HDL spinodal vs Widom line at ambient pressure, a matter for continuing debate and future work. An important part of this debate concerns the behavior of the line of density maxima (LDM), which itself passes through a maximum at negative pressures according to all pair-potential models, but does the opposite in the case of the empirical equations of state and the scenario C of section II. A positive identification of the behavior of the LMD is badly needed as the TMD claimed in the original study of Zheng et al. 1991 is now subject to adjustment by a surface tension argument given earlier in section IX. Two possibilities are identified here for future work.

Firstly, the existence of a density maximum can be identified directly from the Brillouin light scattering measurement by the vanishing of the central line intensity since the Landau-Placzek ratio must go to zero at a density maximum. The Landau-Placzek ratio connects the intensities of the Brillouin peaks, I_B, and of the elastic peak, I_R, in light scattering with the specific heat at constant volume and that at constant pressure according to the following equation:

$$\frac{I_R}{2I_B} = \frac{C_P - C_V}{C_V} \tag{9}$$

However, in the quartz inclusion milieu presently used, the stray light is far too intense for this observation to be a possibility. Further developments of stray light cancelling strategies, or ways of producing a single perfect vesicle in a perfect quartz crystal, may eventually permit this simple measurement to generate an unambiguous line of density maxima that will end the debate one way or another.

Secondly, and more immediately, the introduction of small reporter dye molecules, sensitive to pressure, offer the possibility of direct spectroscopic determination of a density maximum. For instance, there is the water-soluble dyestuff molecules of the type recently used for analyzing friction patterns on sliding surfaces [377]. These studies depended on the sensitivity of the fluorescence spectrum to pressure or viscosity or both [378].

The fluorescence intensity of molecule 1 of Fig. 29A is depicted in Fig. 29B. The sensitivity to pressure is seen to be quite high, and although the isochoric nature of the projected experiment will possibly complicate the interpretation, the likelihood of a null

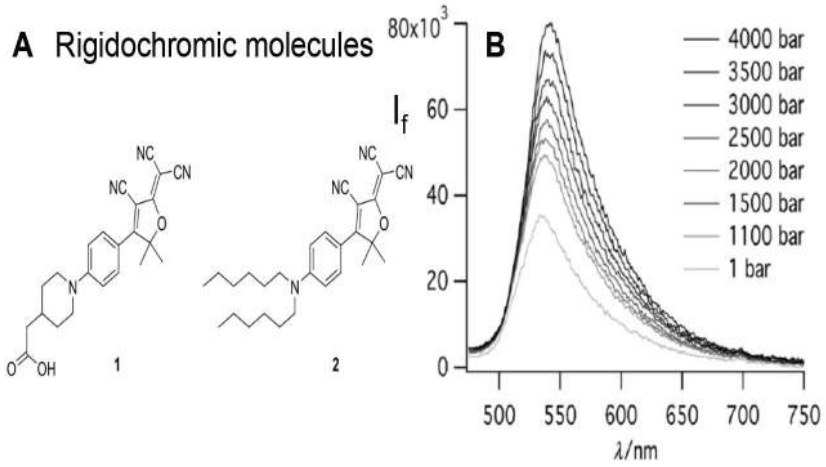

FIG. 29. **A**. Fluorescent molecules whose intensities I_f have high sensitivity to pressure or viscosity. **B**. Pressure dependence of the fluorescence intensity of molecule 1 in 1M solution in acetone. Reproduced from Ref. [378] with permission.

result at the tension maximum seems small. In any case, this is not the only pressure sensitive dyestuff that is available. If the pressure sensitivity is due to a pressure dependent viscosity, so much the better since the diffusivity of water is known to decrease with great rapidity as pressure decreases in the direction of the tensile domain [379].

Of course, the molecule must first survive the autoclaving procedure used to produce the samples but there is precedence for this in the successful introduction of a water-insoluble polyphenyl, orthoterphenyl, into the vesicles prepared by Zheng (and only reported in ref. [381]). We expect that a water soluble version of the molecule seen in Fig. **??** will likewise survive as it need only be present in very low concentrations.

If the temperature of maximum density detected by such fluorescence intensity studies confirms the reversal of TMD trajectory in pressure, then the existence of the second critical point at zero pressure or thereabouts will be confirmed and other scenarios can be put to rest.

But what will it imply if such a study confirms the high values of the TMD reported from the original inclusion measurements or their successor studies? Firstly, it will confirm the great sensitivity of the equation of state parameters to the choice of L-L coexistence data which was pointed out by the authors of ref. [31], and secondly it will support the qualitative validity of engineering equations of state for water, which to date have been given little credence by the metastable water community.

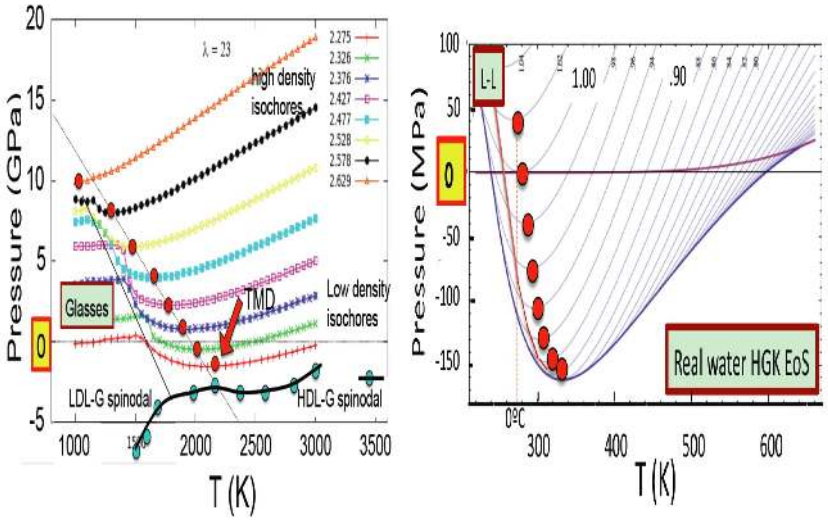

FIG. 30. **LH panel**. Behavior of the isochores, and the TMD, with isochore density in the tuned S-W model with λ parameter = 23. The TMD does not reverse as it does for the silicon potential λ= 21 The flattened segments at lower temperatures correspond to broken ergodicity states (glasses on the simulation time scale). **RH panel**. Isochores and density maxima behavior of the HGK equation of state for water.

The origin of the sensitivity can be found in the way the TMD is approaching the liquid-gas spinodal limit. This can be seen from the work of Vashist et al. [117] on liquid Si in the Stillinger-Weber (S-W) model where the point of reversal of the TMD with increasing tension is extremely close to the spinodal limit for the liquid state. Since the latter cannot be penetrated, the said reversal must suddenly switch in the opposite direction if the λ parameter of the S-W model is made any larger. Indeed if it is raised to the value 23 used by Molinero and Moore [124] in their successful adaptation of the S-W form of potential to the description of water, then the isochore minima, *which determine the TMD*, no longer reverse their direction with increasing temperature, but rather behave in the manner given by, for instance, the HGK, or IAP-WS95 equations of state for water. This is demonstrated by current assessments of the isochores of the tuned S-W model seen in Fig. 30 LH panel which no longer cross at a critical point as they do for values of λ of 21 and lower (Kapko and Angell to be published).

More importantly, it might also require recognition that, not only have the critical point-related anomalies emerged from "no-man's land" (as suggested by the negative pressure

studies of Caupin and co-authors [38, 317]), but that the critical point itself has disappeared into the liquid-gas spinodal and become a virtual phenomenon. It would mean that the Widom line does not exist but rather that the anomalies of water are provoked by close approach to a line of spinodal instabilities of the high density liquid that lies just a few K on the low temperature side of a line of liquid-liquid transitions that itself lies close to but below the line of homogeneous nucleation temperatures. This is now called the "critical point-free" scenario [24] (diagram C in Fig. 2).

Thus in light of Figure 1 above and the latter challenges, there seems to be a need for more work on water models that will provide better agreement with experiment in these extreme conditions.

Why have pair-potential models not yet acquired the ability to show the above sequence of possibilities ? According to the x-ray laser data shown in Fig. 12, the TIP4P-2005 model is not "going tetrahedral" quickly enough with decreasing temperature (see Fig. 12). Perhaps, as in mW water [108] they need the additional drive to tetrahedrality that is provided by potentials of the S-W form, in which a departure from tetrahedrality is penalized by a repulsive energy component that opposes the pairwise additive attraction component of the total potential. In water this would act on the O-O-O alignments which need to be tetrahedral in an LDA-like structure. While such possibilities as the above remain uninvestigated, water is likely to maintain its mystique as the most anomalous and least understood liquid.

XIII. ACKNOWLEDGEMENTS

This review was initiated during the Nordita (Nordic Institute for Theoretical Physics) scientific program "Water - the Most Anomalous Liquid". Additional financial support for this program was provided by the Royal Swedish Academy of Sciences through its Nobel Institutes for Physics and Chemistry, by the Swedish Research Council and by the Department of Physics at Stockholm University. We would like to acknowledge helpful suggestions by Prof. Pablo Debenedetti. We are grateful to Stephan Fuhrmann for providing Fig. 3. CAA wishes to acknowledge support from the NSF under collaborative grant No. CHE 12-13265. TL is grateful for funding to the European Research Council (ERC Starting Grant SULIWA), the Austrian Science Fund FWF (bilateral project I1392) and the Alexander von Humboldt Foundation (Bessel award). AZP would like to acknowledge support

for this work by the Department of Energy, Office of Basic Energy Sciences, under Award No. DE-SC0002128. XLM acknowledges the support from National Science Foundation of China (Grant No.: 11174006, 11290162, 11525520) and MOST (Grant No.: 2012CB921404, 2015CB856801). FC acknowledges funding by the European Research Council under the European Community's FP7 Grant Agreement 240113, and by the Agence Nationale de la Recherche Grant 09-BLAN-0404-01.

---

[1] Angell, C. A. Water and Aqueous Solutions at Subzero Temperatures, in *Water: A Comprehensive Treatise* Vol.7. New York: Plenum, 1982.

[2] Debenedetti, P. G. *Metastable Liquids: Concepts and Principles.* Princeton: Princeton University Press, 1996.

[3] Franks, F. *Water: A Matrix of Life.* Cambridge: Royal Society of Chemistry, 2000.

[4] Debenedetti, P. G. Supercooled and glassy water. *J. Phys: Condens Matter* **2003**, *15*, R1669–R1726.

[5] Debenedetti, P. G.; Stanley, H. E. Supercooled and Glassy Water. *Physics Today* **2003**, *56*, 40–46.

[6] Angell, C. A. Amorphous water. *Ann. Rev. Phys. Chem.* **2004**, *55*, 559–583.

[7] Ball, P. Water as an active constituent in cell biology. *Chem. Rev.* **2008**, *108*, 74–108.

[8] Bellissent-Funel, M.-C. *Hydration Processes in Biology: Theoretical and Experimental Approaches.* Amsterdam: ISO Press, 1999.

[9] Robinson, G. W.; Zhu, S. B.; Singh, S.; Evans, M. W. *Water in Biology, Chemistry, and Physics: Experimental Overviews and Computational Methodologies*. Singapore: World Scientific, 1996.

[10] Workshop on "Water": Structure and Dynamics of Water and Aqueous Solutions — Anomalies and their Possible Implications in Biology. Grenoble: Proc. of Inst. Laue-Langevin, 1984.

[11] Angell, C. A.; Shuppert, J-; Tucker, J. C. Anomalous properties of supercooled water. Heat capacity, expansivity, and proton magnetic resonance chemical shift from 0 to -38°C. *J. Phys. Chem.* **1973**, *77*, 3092–3099.

[12] Speedy, R. J.; Angell, C. A. Isothermal compressibility of supercooled water and evidence for a thermodynamic singularity at 45°C. *J. Chem. Phys.* **1976**, *65*, 851–858.

[13] Poole, P. H.; Sciortino, F.; Essmann, U.; Stanley, H.E. Phase Behavior of Metastable Water. *Nature* **1992**, *360*, 324–328.

[14] Stanley, H. E. *Introduction to phase transitions and critical phenomena*. New York: Oxford University Press, 1971.

[15] Kumar, P.; Stanley, H. E. Thermal conductivity minimum: A new water anomaly. *J. Phys. Chem. B* **2011**, *115*, 14269–14273.

[16] Angell, C. A.; Oguni, M.; Sichina, W. J. Heat capacity of water at extremes of supercooling and superheating. *J. Phys. Chem.* **1982**, *86*, 998–1002.

[17] Sato, H.; Watanabe, K.; Levelt-Sengers, J. M. H.; Gallagher, J. S.; Hill, P. G.; Straub, J.; Wagner, W. Sixteen Thousand evaluated experimental thermodynamic property data for water and steam. *J. Phys. Chem. Ref. Data* **1991**, *20*, 1023–1044.

[18] Conde, O.; Teixeira, J.; Papon, P. Analysis of sound velocity in supercooled H_2O, D_2O, and water-ethanol mixtures. *J. Chem. Phys.* **1982**, *76*, 3747–3753.

[19] Kanno, H.; Angell, C. A. Water: Anomalous compressibilities to 1.9 kbar and correlation with supercooling limits. *J. Chem. Phys.* **1979**, *70*, 4008–4016.

[20] Poole, P. H.; Sciortino, F.; Essmann, U.; Stanley, H. E. The Spinodal of Liquid Water. *Phys. Rev. E* **1993**, *48*, 3799–3817.

[21] Poole, P. H.; Essmann, U.; Sciortino, F.; Stanley, H. E. Phase Diagram for Amorphous Solid Water.*Phys. Rev. E* **1993**, *48*, 4605–4610.

[22] Sciortino, F.; Poole, P. H.; Essmann, U.; Stanley, H. E. Line of Compressibility Maxima in the Phase Diagram of Supercooled Water. *Phys. Rev. E* **1997**, *55*, 727–737.

[23] Sastry, S.; Debenedetti, P. G.; Sciortino, F.; Stanley, H. E. Singularity-Free Interpretation of the Thermodynamics of Supercooled Water. *Phys. Rev. E* **1996**, *53*, 6144–6154.

[24] Angell, C. A. Insights into liquid water phases from study of its unusual glass-forming properties. *Science* **2008**, *319*, 582–587.

[25] Speedy, R. J. Stability-limit conjecture. *J. Phys. Chem.* **1982**, *86*, 982–989.

[26] Tanaka, H. Simple physical model of liquid water. *J. Chem. Phys.* **2000**, *112*, 799–809.

[27] Tanaka, H. Simple view of waterlike anomalies of atomic liquids with directional bonding. *Phys. Rev. B* **2002**, *66*, 064202.

[28] Tanaka, H. Bond orientational order in liquids: Towards a unified description of water-like anomalies, liquid-liquid transition, glass transition, and crystallization. *Eur. Phys. J. E* **2012**, *35*, 113.

[29] Fuentevilla, D. A.; Anisimov, M. A. Scaled equation of state for supercooled water near the liquid-liquid critical point. *Phys. Rev. Lett.* **2006**, *97*, 195702.

[30] Bertrand, C. E.; Anisimov, M. A. Peculiar thermodynamics of the second critical point in supercooled water. *J. Phys. Chem. B* **2011**, *115*, 14099–14111.

[31] Holten, V.; Anisimov, M. A. Entropy-driven liquid-liquid separation in supercooled water. *Sci. Rep.* **2012**, *2*, 713.

[32] Stanley, H. E.; Kumar, P.; Franzese, G.; Xu, L.; Yan, Z.; Mazza, M. G.; Buldyrev, S. V.; Chen, S.-H.; Mallamace, F. Liquid Polyamorphism: Possible Relation to the Anomalous Behavior of Water. *Eur. Phys. J. Special Topics* **2008**, *161*, 1–17.

[33] Mishima, O.; Stanley, H. E. The relationship between liquid, supercooled and glassy water. *Nature* **1998**, *396*, 329–335.

[34] Xu, L.; Kumar, P.; Buldyrev, S. V.; Chen, S.-H.; Poole, P. H.; Sciortino, F.; Stanley, H. E. Relation between the Widom line and the dynamic crossover in systems with a liquid-liquid phase transition. *Proc. Natl. Acad. Sci. (USA)* **2005**, *102*, 16558–16562.

[35] Limmer, D.T.; Chandler, D. The putative liquid-liquid transition is a liquid-solid transition in atomistic models of water. *J. Chem. Phys.* **2011**, *135*, 134503.

[36] Limmer, D. T.; Chandler, D. The putative liquid-liquid transition is a liquid-solid transition in atomistic models of water. II. *J. Chem. Phys.* **2013**, *138*, 214504.

[37] Poole, P. H. ; Sciortino, F.; Grande, T.; Stanley, H. E.; Angell, C. A. Effect of Hydrogen Bonds on the Thermodynamic Behavior of Liquid Water. *Phys. Rev. Lett.* **1994**, *73*, 1632–1635.

[38] Pallares, G.; El Mekki Azouzi, M.; González, M. A.; Aragones, J. L.; Abascal, J. L. F.; Valeriani, C.; Caupin, F. Anomalies of water at negative pressure. *Proc. Natl. Acad. Sci. (USA)* **2014**, *111*, 7936–7941.

[39] Mishima, O.; Stanley, H. E. Decompression-Induced Melting of Ice IV and the Liquid-Liquid Transition in Water. *Nature* **1998**, *392*, 164–168.

[40] Sciortino, F.; La Nave, E.; Tartaglia, P. Physics of the liquid-liquid critical point. *Phys. Rev. Lett.* **2003**, *91*, 155701.

[41] Sivakumar, T. C.; Rice, S. A.; Sceats, M. G. Raman spectroscopic studies of the OH stretching region of low density amorphous solid water and of polycrystalline ice Ih. *J. Chem. Phys.* **2000**, *69*, 3468–3476.

[42] Maruyama, S.; Wakabayashi, K.; Oguni, M. Thermal properties of supercooled water confined within silica gel pores. *American Institute of Physics Conference Proceedings* **2004**, *708*, 675–676.

[43] Mishima, O.; Calvert, L. D.; Whalley, E. 'Melting ice' I at 77 K and 10 kbar: a new method of making amorphous solids. *Nature* **1984**, *310*, 393–395.

[44] Mishima, O.; Calvert, L. D.; Whalley, E. An apparently first-order transition between two amorphous phases of ice induced by pressure. *Nature* **1985**, *314*, 76–78.

[45] Mishima, O.; Takemura, K.; Aoki, K. Visual Observations of the Amorphous-Amorphous Transition in H_2O Under Pressure. *Science* **1991**, *254*, 406–408.

[46] Finney, J. L.; Bowron, D. T.; Soper, A. K.; Loerting, T.; Mayer, E.; Hallbrucker, A. Structure of a New Dense Amorphous Ice. *Phys. Rev. Lett.* **2002**, *89*, 205503.

[47] Bellissent-Funel,M.-C.; Bove, L.E.; Nilsson, A.; Paciaroni, A.; Schlesinger, D.; Skinner, L.B.; Amann-Winkel, K. X-ray and Neutron Scattering of Water, *Chem. Rev.* **2015**, *XX*, YY–ZZ.

[48] Whiting, H. A new theory of cohesion applied to the thermodynamics of liquids and solids,*Proc. Am. Acad. Arts Sci.* **1884**, *19*, 353–431.

[49] Röntgen, W. K. Ueber die constitution des flüssigen wassers. *Ann. Phys.* **1892**, *45*, 91–97.

[50] Davis, C. M., Jr.; Litovitz, T. A. Two-State Theory of the Structure of Water. *J. Chem. Phys.* **1965**, *42*, 2563–2576.

[51] Angell, C. A. Two-state thermodynamics and transport properties for water from "bond lattice" model, *J. Phys. Chem.* **1971**, *75*, 3698–3705.

[52] Vedamuthu, M.; Singh, S.; Robinson, G. W. Properties of Liquid Water: Origin of the Density Anomalies. *J. Phys. Chem.* **1994**, *98*, 2222–2230.

[53] Mishima, O. Reversible first-order transition between two H_2O amorphs at 0.2 GPa and 135K. *J. Chem. Phys.* **1994**, *100*, 5910–5912.

[54] Bellissent-Funel, M.- C.; Bosio, L.; Hallbrucker, A.; Mayer, E.; Sridi-Dorbez, R. X-ray and neutron scattering studies of the structure of hyperquenched glassy water. *J. Chem. Phys.* **1992**, *97*, 1282–1286.

[55] Bellissent-Funel, M.- C.; Bosio, L. A neutron scattering study of liquid D_2O under pressure and at various temperatures. *J. Chem. Phys.* **1995**, *102*, 3727–3735.

[56] Anderson, O. Glass-liquid transition of water at high pressure. *Proc. Natl. Acad. Sci. (USA)* **2011**, *108*, 11013–11016.

[57] Soper, A. K.; Ricci, M. A. Structures of high-density and low-density water. *Phys. Rev. Lett.* **2000**, *84*, 2881–2884.

[58] Bellissent-Funel, M. C. Is there a liquid-liquid phase transition in supercooled water? *Europhys. Lett.* **1998**, *42*, 161–166.

[59] Head-Gordon, T.; Stillinger, F. H. An Orientational Perturbation Theory for Pure Liquid Water. *J. Chem. Phys.* **1993**, *98*, 3313–3327.

[60] Stanley, H. E.; "Mysteries of Water" [Opening Course, 1998 Les Houches School], in Hydration Processes in Biology: Theoretical and Experimental Approaches [Proc. NATO Advanced Study Institutes, Vol. 305), edited by M.-C. Bellissent-Funel (IOS Press, Amsterdam, 1999), Chapter 1.

[61] Giovambattista, N.; Loerting, T.; Lukanov, B. R.; Starr, F. W. Interplay of the glass transition and the liquid-liquid phase transition in water. *Sci. Rep.* **2012**, *2*, 1–8.

[62] Loerting, T.; Fuentes-Landete, V.; Handle, P. H.; Seidl, M.; Amann-Winkel, K.; Gainaru, C.; Böhmer, R. The glass transition in high-density amorphous ice. *J. Non-Crystalline Solids* **2015**, *407*, 423–430.

[63] Mishima, O.; Suzuki, Y. Propagation of the polyamorphic transition of ice and the liquid-liquid critical point. *Nature* **2002**, *419*, 599–603.

[64] Klotz, S.; Strässle, Th.; Nelmes, R. J.; Loveday, J. S.; Hamel, G.; Rousse, G.; Canny, B.; Chervin, J. C.; Saitta, A. M. Nature of the Polyamorphic Transition in Ice under Pressure. *Phys. Rev. Lett.* **2005**, *94*, 025506.

[65] Yoshimura, Y.; Mao, H. K.; Hemley, R. J. An in situ Raman spectroscopic study on the reversible transition between low-density and high-density amorphous ices at 135 K. *J. Phys.: Condens. Matter* **2007**, *19*, 425214 .

[66] Winkel, K.; Elsaesser, M. S.; Mayer, E.; Loerting, T. Water polyamorphism: reversibility and (dis)continuity. *J. Chem. Phys.* **2008**, *128*, 044510.

[67] Winkel, K.; Mayer, E.; Loerting, T. Equilibrated high-density amorphous ice and its first-order transition to the low-density form. *J. Phys. Chem. B* **2011**, *115*, 14141–14148.

[68] Andersson, O. Glass-liquid transition of water at high pressure.*Proc. Natl. Acad. Sci. (USA)* **2011**, *108*, 11013–11016.

[69] Johari, G. P.; Hallbrucker, A.; Mayer, E. The glass-liquid transition of hyperquenched water. *Nature* **1987**, *330*, 552–553.

[70] Hallbrucker, A.; Mayer, E.; Johari, G. P. Glass-liquid transition and the enthalpy of devitrification of annealed vapor-deposited amorphous solid water - A comparison with hyperquenched glassy water. *J. Phys. Chem.* **1989**, *93*, 4986–4990.

[71] Elsaesser, M. S.; Winkel, K.; Mayer, E.; Loerting, T. Reversibility and isotope effect of the calorimetric glass – liquid transition of low-density amorphous ice. *Phys. Chem. Chem. Phys.* **2010**, *12*, 708–712.

[72] Kohl, I.; Bachmann, L.; Hallbrucker, A.; Mayer, E.; Loerting, T. Liquid- like Relaxation in Hyperquenched Water at $\leq$140 K. *Phys. Chem. Chem. Phys.* **2005**, *7*, 3210–3220.

[73] Angell, C. A.; Moynihan, C. T.; Hemmati, M. 'Strong' and 'superstrong' liquids, and an approach to the perfect glass state via phase transition. *J. Non-Crystalline Solids* **2000**, *274*, 319–331.

[74] Shephard, J. J.; Evans, J. S. O.; Salzmann, C. G. Structural Relaxation of Low-Density Amorphous Ice upon Thermal Annealing. *J. Phys. Chem. Lett.* **2013**, *4*, 3672–3676.

[75] Smith, R. S.; Kay, B. D. The existence of supercooled liquid water at 150 K. *Nature* **1999**, *398*, 788–791.

[76] Fisher, M.; Devlin, J. P. Defect activity in amorphous ice from isotopic exchange data - Insight into the glass-transition. *J. Phys. Chem.* **1995**, *99*, 11584–11590.

[77] Angell, C. A. Glass transition dynamics in water and other tetrahedral liquids: 'order-disorder' transitions versus 'normal' glass transitions. *J. Phys.: Condens. Matter* **2007**, *19*, 205112.

[78] Capaccioli, S.; Ngai, K. L. Resolving the controversy on the glass transition temperature of water? *J. Chem. Phys.* **2011**, *135*, 104504.

[79] Amann-Winkel, K.; Böhmer, R.; Fujara, F.; Gainaru, C.; Geil, B.; Loerting, T. Water's Controversial Glass Transitions, *Rev. Mod. Phys.* **2015**, in press.

[80] Sepulveda, A.; Leon-Gutierrez, E.; Gonzalez-Silveira, M.; Rodriguez-Tinoco, C.; Clavaguera-Mora, M. T.; Rodriguez-Viejo, J. Glass transition in ultrathin films of amorphous solid water. *J. Chem. Phys.* **2012**, *137*, 244506.

[81] Amann-Winkel, K.; Gainaru, C.; Handle, P. H.; Seidl, M.; Nelson, H.; Böhmer, R.; Loerting, T. Water's second glass transition. *Proc. Natl. Acad. Sci. (USA)* **2013**, *110*, 17720–17725.

[82] Gainaru, C.; Agapov, A. L.; Fuentes-Landete, V.; Amann-Winkel, K.; Nelson, H.; Köster, K. W.; Kolesnikov, A. I.; Novikov, V. N.; Richert, R.; Böhmer, R.; Loerting, T.; Sokolov, A. P. Anomalously large isotope effect in the glass transition of water. *Proc. Natl. Acad. Sci. (USA)* **2014**, *111*, 17402–17407.

[83] Mishima, O.; Suzuki, Y. Vitrification of emulsified liquid water under pressure. *J. Chem. Phys.* **2001**, *115*, 4199–4202.

[84] Mishima, O. The glass-to-liquid transition of the emulsified high-density amorphous ice made by pressure-induced amorphization. *J. Chem. Phys.* **2004**, *121*, 3161–3164.

[85] Andersson, O. Relaxation time of water's high-density amorphous ice phase. *Phys. Rev. Lett.* **2005**, *95*, 205503.

[86] Andersson, O.; Inaba, A. Dielectric properties of high-density amorphous ice under pressure. *Phys. Rev. B* **2006**, *74*, 184201.

[87] Seidl, M.; Elsaesser, M. S.; Winkel, K.; Zifferer, G.; Mayer, E.; Loerting, T. Volumetric study consistent with a glass-to-liquid transition in amorphous ices under pressure. *Phys. Rev. B* **2011**, *83*, 100201.

[88] Handle, P. H.; Seidl, M.; Loerting, T. Relaxation Time of High-Density Amorphous Ice. *Phys. Rev. Lett.* **2012**, *108*, 225901.

[89] Floriano, M. A.; Handa, Y. P.; Klug, D. D.; Whalley, E. Nature of the transformations of ice-I and low-density amorphous ice to high-density amorphous ice. *J. Chem. Phys.* **1989**, *91*, 7187–7192.

[90] Xu, L; Buldyrev, S. V.; Giovambattista,N.; Angell, C. A; Stanley, H. E. A monatomic system with a liquid-liquid critical point and two distinct glassy states. *J. Chem. Phys.* **2009**, *130*, 054505.

[91] Xu, L.; Giovambattista, N.; Buldyrev, S. V.; Debenedetti, P. G.; Stanley, H. E. Waterlike glass polyamorphism in a monoatomic isotropic Jagla model. *J. Chem. Phys.* **2011**, *134*, 064507

[92] Harrington, S.; Poole, P. H.; Sciortino, F.; Stanley, H. E. Equation of state of supercooled water simulated using the extended simple point charge intermolecular potential. *J. Chem. Phys.* **1997**, *107*, 7443–7450.

[93] Yamada, M.; Mossa, S.; Stanley, H. E.; Sciortino, F. Interplay between Time-Temperature-Transformation and the Liquid-Liquid Phase Transition in Water. *Phys. Rev. Lett.* **2002**, *88*, 195701.

[94] Poole, P. H.; Saika-Voivod, I.; Sciortino, F. Density minimum and liquid-liquid phase transition. *J. Phys.: Condens. Matter* **2005**, *17*, L431–L437.

[95] Paschek, D. How the liquid-liquid transition affects hydrophobic hydration in deeply supercooled water. *Phys. Rev. Lett.* **2004**, *94*, 217802.

[96] Paschek, D.; Rüppert, A.; Geiger, A. Thermodynamic and structural characterization of the transformation from a metastable low-density to a very high-density form of supercooled TIP4P-Ew model water. *Chem. Phys. Chem.* **2008**, *18*, 2737–2741.

[97] Liu, Y.; Panagiotopoulos, A. Z.; Debenedetti, P. G. Low-temperature fluid-phase behavior of ST2 water. *J. Chem. Phys.* **2009**, *131*, 104508.

[98] Abascal, J. L. F.; Vega, C. Widom line and the liquidliquid critical point for the TIP4P/2005 water model. *J. Chem. Phys.* **2010**, *133*, 234502.

[99] Meyer, M.; Stanley, H. E. Liquid-liquid phase transition in confined water: A Monte-Carlo study. *J. Phys. Chem. B* **1999**, *103*, 9728–9730.

[100] Stokely, K.; Mazza, M. G.; Stanley, H. E.; Franzese, G. Effect of Hydrogen Bond Cooperativity on the Behavior of Water. *Proc. Natl. Acad. Sci. (USA)* **2010**, *107*, 1301–1306.

[101] Li, Y.; Li, J.; Wang, F. Liquid-liquid transition in supercooled water suggested by microsecond simulations. *Proc. Natl. Acad. Sci. (USA)* **2013**, *110*, 12209–12212.

[102] Corsetti, F.; Artacho, E.; Soler, J. M.; Alexandre, S. S.; Fernández-Serra, M.-V. Room temperature compressibility and the diffusivity anomaly of liquid water from first principles.*J. Chem. Phys.* **2013**, *139*, 194502.

[103] Jeffery, C. A.; Austin, P. H. A new analytic equation of state for liquid water. *J. Chem. Phys.* **1999**, *110*, 484–496.

[104] Kiselev, S. B. Physical Limit of Stability in Supercooled Liquids. *Int. J. Thermophys.* **2001**, *22*, 1421–1433.

[105] Kiselev, S. B.; Ely, J. F. Parametric crossover model and physical limit of stability in supercooled water. *J. Chem. Phys.* **2002**, *116*, 5657–5665.

[106] Kalová, J.; Mares, R. Crossover Equation and the Vapor Pressure of Supercooled Water. *Int. J. Thermophys.* **2010**, *31*, 756–765.

[107] Corradini, D.; Rovere, M.; Gallo, P. A route to explain water anomalies from results on an aqueous solution of salt. *J. Chem. Phys.* **2010**, *132*, 134508.

[108] Moore, E. B.; Molinero, V., Structural transformation in supercooled water controls the crystallization rate of ice. *Nature* **2011**, *479*, 506–508.

[109] Holten, V.; Limmer, D. T.; Molinero, V.; Anisimov, M. A. Nature of the anomalies in supercooled liquid state of the mW model of water. *J. Chem. Phys.* **2013**, *138*, 174501.

[110] Xu, L.; Buldyrev, S. V.; Angell, C. A; Stanley, H. E. Thermodynamics and dynamics of the two-scale spherically symmetric Jagla ramp model of anomalous liquids. *Phys. Rev. E* **2006**, *74*, 031108.

[111] Gallo, P.; Sciortino, F. Ising Universality Class for the Liquid-Liquid Critical Point of a One Component Fluid: A Finite-Size Scaling Test. *Phys. Rev. Lett.* **2012**, *109*, 177801.

[112] Liu, Y.; Palmer, J. C.; Panagiotopoulos, A. Z.; Debenedetti, P. G. Liquid-liquid transition in ST2 water. *J. Chem. Phys.* **2012**, *137*, 214505.

[113] Liu, Y.; Panagiotopoulos, A. Z.; Debenedetti, P. G. Low-temperature fluid-phase behavior of ST2 water. *J. Chem. Phys.* **2009**, *131*, 104508.

[114] Franzese, G.; Malescio, G.; Skibinsky, A.; Buldyrev, S. V.; Stanley, H. E. Generic mechanism for generating a liquid-liquid phase transition. *Nature* **2001**, *409*, 692–695.

[115] Smallenburg, F.; Filion, L.; Sciortino, F. Erasing no-man's land by thermodynamically stabilizing the liquid-liquid transition in tetrahedral particles. *Nature Phys.* **2014**, *10*, 653–657.

[116] Saika-Voivod, I.; Sciortino, F.; Poole, P. H. Computer simulations of liquid silica: equation of state and liquid-liquid phase transition. *Phys. Rev. E* **2001**, *63*, 011202.

[117] Vasisht, V. V.; Saw, S.; Sastry, S. Liquid-liquid critical point in supercooled silicon. *Nature Phys.* **2011**, *7*, 549–553.

[118] Glosli, J. N.; Ree, F. H. Liquid-liquid phase transformation in carbon. *Phys. Rev. Lett.* **1999**, *82*, 4659–4662.

[119] Li, R. Z.; Chen, J.; Li, X. Z.; Wang, E. G.; Xu, L. Supercritical phenomenon of hydrogen beyond the liquidliquid phase transition. *New J. Phys.* **2015**, *17*, 063023.

[120] Stillinger, F. H.; Rahman, A. Improved simulation of liquid water by molecular dynamics. *J. Chem. Phys.* **1974**, *60*, 1545–1557.

[121] Palmer, J. C.; Martelli, F.; Liu, Y.; Car, R.; Panagiotopoulos, A. Z.; Debenedetti, P. G. Metastable liquid–liquid transition in a molecular model of water. *Nature* **2014**, *510*, 385–388.

[122] Cuthbertson, M. J.; Poole, P. H. Mixturelike Behavior Near a Liquid-Liquid Phase Transition in Simulations of Supercooled Water. *Phys. Rev. Lett.* **2011**, *106*, 115706.

[123] Poole, P. H.; Bowles, R. K.; Saika-Voivod, I.; Sciortino, F. Free energy surface of ST2 water near the liquid-liquid phase transition. *J. Chem. Phys.* **2013**, *138*, 034505.

[124] Molinero, V.; Moore, E. B. Water Modeled As an Intermediate Element between Carbon and Silicon. *J. Phys. Chem. B* **2009**, *113*, 4008–4016.

[125] Yagasaki, T.; Matsumoto, M.; Tanaka, H. Spontaneous liquid-liquid phase separation of water. *Phys. Rev. E* **2014**, *89*, 020301.

[126] Overduin, S. D.; Patey, G. N. Fluctuations and local ice structure in model supercooled water. *J. Chem. Phys.* **2015**, *143*, 094504.

[127] Kesselring, T. A.; Franzese, G.; Buldyrev, S. V.; Herrmann, H. J.; Stanley, H. E. Nanoscale Dynamics of Phase Flipping in Water near its Hypothesized Liquid-Liquid Critical Point. *Sci. Rep.* **2012**, *2*, 474.

[128] Kesselring, T. A.; Lascaris, E.; Franzese, G.; Buldyrev,S. V.; Herrmann, H. J.; Stanley, H. E. Finite-size scaling investigation of the liquid-liquid critical point in ST2 water and its stability with respect to crystallization. *J. Chem. Phys.* **2013**, *138*, 244506.

[129] Ghiringhelli, L. M.; Valeriani, C.; Los, J.H.; Meijer, E.J.; Fasolino, A.; Frenkel, D. State-of-the-art models for the phase diagram of carbon and diamond nucleation. *Mol. Phys.* **2008**, *106*, 2011–2038.

[130] Smallenburg, F.; Sciortino, F. Tuning the Liquid-Liquid Transition by Modulating the Hydrogen-Bond Angular Flexibility in a Model for Water. *Phys. Rev. Lett.* **2015**, *115*, 015701.

[131] Palmer, J. C.; Debenedetti, P. G.; Car, R.; Panagiotopoulos, A. Z. Response to "Comment [arXiv:1407.6854] on Palmer et al., Nature, 510, 385, 2014". *arXiv*:1407.7884 [cond-mat.stat-mech], **2014**.

[132] Jagla, E. A. Core-softened potentials and the anomalous properties of water. *J. Chem. Phys.* **1999**, *111*, 8980–8986.

[133] Tanaka, H. Thermodynamic anomaly and polyamorphism of water *Europhys. Lett.* **2000**, *50*, 340–346.

[134] Biddle, J. W.; Holten, V.; Anisimov, M. A. Behavior of supercooled aqueous solutions stemming from hidden liquidliquid transition in water. *J. Chem. Phys.* **2014**, *141*, 074504.

[135] Holten, V.; Sengers, J. V.; Anisimov, M. A. Equation of state for supercooled water at pressures up to 400 MPa. *J. Phys. Chem. Ref. Data* **2014**, *43*, 043101.

[136] Hare, D. E.; Sorensen, C. M. The density of supercooled water. II. Bulk samples cooled to the homogeneous nucleation limit. *J. Chem. Phys.* **1987**, *87*, 4840–4845.

[137] Mishima, O. Volume of supercooled water under pressure and the liquid-liquid critical point. *J. Chem. Phys.* **2010**, *133*, 144503.

[138] Sotani, T.; Arabas, J.; Kubota, H.; Kijima, M. Volumetric behaviour of water under high pressure at subzero temperature. *High Temp. High Pressures* **2000**, *32*, 433.

[139] Abascal, J. L. F.; Vega, C. A general purpose model for the condensed phases of water. *J. Chem. Phys.* **2005**, *123*, 234505.

[140] Overduin, S. D.; Patey, G. N. An analysis of fluctuations in supercooled TIP4P/2005 water. *J. Chem. Phys.* **2013**, *138*, 184502.

[141] Huang, C.; Wikfeldt, K. T.; Tokushima, T.; Nordlund, D.; Harada, Y.; Bergmann, U.; Niebuhr, M.; Weiss, T. M.; Horikawa, Y.; Leetmaa, M. et al. The Inhomogeneous Structure of Water at Ambient Conditions, *Proc. Natl. Acad. Sci. (USA)* **2009**, *106*, 15214–15218.

[142] Huang, C.; Weiss, T. M.; Nordlund, D.; Wikfeldt, K. T.; Pettersson, L. G. M.; Nilsson, A. Increasing correlation length in bulk supercooled H_2O, D_2O and NaCl solution determined

from small angle x-ray scattering, *J. Chem. Phys.* **2010**, *133*, 134504.

[143] Huang, C.; Wikfeldt, K.T.; Tokushima, T.; Nordlund, D.; Harada, Y.; Bergmann, U.; Niebuhr, M.; Weiss, T. M.; Horikawa, Y.; Leetmaa, et al. Reply to Soper "Fluctuations in water around a bimodal distribution of local hydrogen bonded structural motifs", *Proc. Natl. Acad. Sci. (USA)* **2010**, *107*, E45.

[144] Soper, A. K.; Teixeira, J.; Head-Gordon, T. Is ambient water inhomogeneous on the nanometer-length scale? *Proc. Natl. Acad. Sci. (USA)* **2010**, *107*, E44.

[145] Clark, G. N. I.; Hura, G. L.; Teixeira, J.; Soper, A. K.; Head-Gordon, T. Small-angle scattering and the structure of ambient liquid water. *Proc. Natl. Acad. Sci. (USA)* **2010**, *107*, 14003–14007.

[146] Overduin, S. D.; Patey, G. N. Understanding the Structure Factor and Isothermal Compressibility of Ambient Water in Terms of Local Structural Environments. *J. Phys. Chem. B* **2012**, *116*, 12014–12020.

[147] Wernet, Ph.; Nordlund, D.; Bergmann, U.; Ogasawara, H.; Cavalleri, M.; Näslund, L.-Å.; Hirsch, T. K.; Ojamäe, L.; Glatzel, P.; Odelius, M.; Pettersson, L. G.M.; Nilsson, A. The structure of the first coordination shell in liquid water. *Science* **2004**, *304*, 995–999.

[148] Myneni, S.; Luo, Y.; Näslund, L.-Å.; Cavalleri,M.; Ojamäe, L.; Ogasawara, H.; Pelmenschikov, A.; Wernet, Ph.; Väterlein, P.; Heske, C.; Hussain, Z.; Pettersson, L. G. M.; Nilsson, A. Spectroscopic probing of local hydrogen bonding structures in liquid water, *J. Phys.: Condens. Mat.* **2002**, *14*, L213–L219.

[149] Nilsson, A.; Nordlund, D.; Waluyo, I.; Huang, N.; Ogasawara, H.; Kaya, S.;H.; Bergmann, U.; Näslund, L.-Å.; Öström, H.; Wernet, Ph.; Andersson, K.; Schiros, T.; Pettersson, L. G. M. X-ray Absorption Spectroscopy and X-ray Raman Scattering of Water; An Experimental View, *J. Electron Spec. Rel. Phen.* **2010**, *177*, 99–129.

[150] Chen, W.; Wu, X.; Car, R. X-ray absorption signatures of the molecular environment in water and ice. *Phys. Rev. Lett.* **2010**, *105*, 017802.

[151] Nordlund, D.; Ogasawara, H.; Andersson, K. J.; Tatarkhanov, M.; Salmerón, M.; Pettersson, L. G.M.; Nilsson, A. Sensitivity of X-ray Absorption Spectroscopy to Hydrogen Bond Topology. *Phys. Rev. B* **2009**, *80*, 233404.

[152] Kühne, T. D.; Khaliullin, R. Z. Electronic signature of the instantaneous asymmetry in the first coordination shell in liquid water. *Nature Commun.* **2013**, *4*, 1450.

[153] Clark, G. N. I.; Cappa, C. D.; Smith, J. D.; Saykally, R. J.; Head-Gordon, T. The structure of ambient water. *Mol. Phys.* **2010**, *108*, 1415–1433.

[154] Fernandez-Serra, M.-V.; Artacho, E. Electrons and hydrogen-bond connectivity in liquid water. *Phys. Rev. Lett.* **2006**, *96*, 016404.

[155] Soper, A. K. Recent Water Myths. *Pure Appl. Chem.* **2010**, *82*, 1855–1867.

[156] Nilsson, A.; Huang, C.; Pettersson, L. G. M. Fluctuations in ambient water. *J. Mol. Liq.* **2012**, *176*, 2–16.

[157] Pettersson, L. G. M.; Nilsson, A. The Structure of Water; from Ambient to Deeply Supercooled. *J. Non-Crystalline Solids* **2015**, *407*, 399–417.

[158] Fuchs, O.; Zharnikov, M.; Weinhardt, L.; Blum, M.; Weigand, M.; Zubavichus, Y.; Bär, M.; Maier, F.; Denlinger, J. D.; Heske,C.; Grunze, M.; Umbach, E. Isotope and temperature effects in liquid water probed by x-ray absorption and resonant x-ray emission spectroscopy. *Phys. Rev. Lett.* **2008**, *100*, 027801.

[159] Weinhardt, L.; Benkert, A.; Meyer, F.; Blum, M.; Wilks, R. G.; Yang, W.; Bär, M.; Reinert, F.; Heske, C. Nuclear dynamics and spectator effects in resonant inelastic soft x-ray scattering of gas- phase water molecules, *J. Chem. Phys.* **2012**, *136*, 144311.

[160] Lange, K. M.; Könecke, R.; Ghadimi, S.; Golnak, R.; Soldatov, M. A.; Hodeck, K. F.; Soldatov, A.; Aziz, E. F. High resolution X-ray emission spectroscopy of water and aqueous ions using the micro-jet technique. *Chem. Phys.* **2010**, *377*, 1-5.

[161] Lange, K. M.; Soldatov, M.; Golnak, R.; Gotz, M.; Engel, N.; Könnecke, R.; Rubensson, J.-E.; Aziz, E. F. X-ray emission from pure and dilute H_2O and D_2O in a liquid microjet: Hydrogen bonds and nuclear dynamics. *Phys. Rev. B* **2012**, *85*, 155104.

[162] Tokushima, T.; Harada, Y.; Takahashi, O.; Senba, Y.; Ohashi, H.; Pettersson, L. G. M.; Nilsson, A.; Shin, S. High Resolution X-ray Emission Spectroscopy of Liquid Water: The Observation of Two Structural Motifs. *Chem. Phys. Lett.* **2008**, *460*, 387–400.

[163] Tokushima, T.; Harada, Y.; Horikawa, Y.; Takahashi, O.; Senba, Y.; Ohashi, H.; Pettersson, L. G. M.; Nilsson, A.; Shin, S. High resolution X-ray emission spectroscopy of water and its assignment based on two structural motifs. *J. Electron Spec. Rel. Phen.* **2010**, *177*, 192–205.

[164] Gilberg, E.; Hanus, M. J.; Foltz, B. Investigation of the electronic structure of ice by high resolution x-ray spectroscopy. *J. Chem. Phys.* **1982**, *76*, 5093–5097.

[165] Pettersson, L. G. M.; Tokushima, T.; Harada, Y.; Takahashi, O.; Shin, S.; Nilsson, A. Comment on "Isotope and Temperature Effects in Liquid Water Probed by X-ray Absorption and Resonant X-ray Emission Spectroscopy". *Phys. Rev. Lett.* **2008**, *100*, 249801.

[166] Fuchs, O.; Zharnikov, M.; Weinhardt, L.; Blum, M.; Weigand, M.; Zubavichus, Y.; Bär, M.; Maier, F.; Denlinger, J. D.; Heske, C.; Grunze, M.; Umbach, E. Reply to Comment on "Isotope and Temperature Effects in Liquid Water Probed by X-Ray Absorption and Resonant X-Ray Emission Spectroscopy". *Phys. Rev. Lett.* **2008**, *100*, 249802.

[167] Nilsson, A.; Tokushima, T.; Horikawa, Y.; Harada, Y.; Ljungberg, M. P.; Shin, S.; Pettersson, L. G. M. Resonant inelastic x-ray scattering of water. *J. Electron. Spectrosc. Relat. Phenom.* **2013**, *188*, 84–100.

[168] Taschin, A.; Bartolini, P.; Eramo, R.; Righini, R.; Torre, R. Evidence of two distinct local structures of water from ambient to supercooled conditions. *Nature Commun.* **2013**, *4*, 2401.

[169] Kobayashi, M.; Tanaka, H. Relationship between the phase diagram, the glass-forming ability, and the fragility of a water/salt mixture. *J. Phys. Chem. B* **2011**, *115*, 14077–14090.

[170] Kobayashi, M.; Tanaka, H. Possible Link of the V-Shaped Phase Diagram to the Glass-Forming Ability and Fragility in a Water-Salt Mixture. *Phys. Rev. Lett.* **2011**, *106*, 125703.

[171] Torquato, S.; Truskett, T. M.; Debenedetti, P. G. Is Random Close Packing of Spheres Well Defined? *Phys.Rev. Lett.* **2000**, *84*, 2064–2067.

[172] Errington, J. R.; Debenedetti, P. G. Relationship between structural order and the anomalies of liquid water. *Nature* **2001**, *409*, 318–321.

[173] Vega, C.; Abascal, J. L. F. Relation between the melting temperature and the temperature of maximum density for the most common models of water. *J. Chem. Phys.* **2005**, *123*, 144504.

[174] Vega, C.; Abascal,J. L. F. ; Conde, M. M.; Aragones, J. L. What ice can teach us about water interactions: a critical comparison of the performance of different water models. *Faraday Discuss.* **2009**, *141*, 251–276.

[175] Agarwal, M.; Alam, M. P.; Chakravarty, C. Thermodynamic, diffusional, and structural anomalies in rigid-body water models. *J. Phys. Chem. B* **2011**, *115*, 6935–6945.

[176] Fine, R. A.; Millero, F. J. The high pressure P V T properties of deuterium oxide. *J. Chem. Phys.* **1975**, *63*, 89–95.

[177] Shell, M. S.; Debenedetti, P. G.; Panagiotopoulos, A. Z. Molecular structural order and anomalies in liquid silica. *Phys. Rev. E* **2002**, *66*, 011202.

[178] Nayar, D.; Chakravarty, C. Water and water-like liquids: relationships between structure, entropy and mobility. *Phys. Chem. Chem. Phys.* **2013**, *15*, 14162–14177.

[179] Barros de Oliveira, A.; Salcedo, E.; Chakravarty, C.; Barbosa, M. C. Entropy, diffusivity and the energy landscape of a waterlike fluid. *J. Chem. Phys.* **2010**, *132*, 234509.

[180] Green, H. S. *The Molecular Theory of Fluids*; North-Holland: Amsterdam, 1952.

[181] Schlitter, and J. R. Estimation of absolute and relative entropies of macromolecules using the covariance matrix. *Chem. Phys. Lett.* **1993**, *215*, 617–621.

[182] Andricioaei, I.; Karplus, M. On the calculation of entropy from covariance matrices of the atomic fluctuations. *J. Chem. Phys.*, **2001**, *115*, 6289–6292.

[183] Lin, S. T.; Blanco, M.; Goddard III, W. A. The two-phase model for calculating thermodynamic properties of liquids from molecular dynamics: Validation for the phase diagram of Lennard-Jones fluids *J. Chem. Phys.* **2003**, *119*, 11792–11805.

[184] Henchman, R. H.; Cockram, S. J. Water's non-tetrahedral side *Faraday Discuss.* **2013**, *167*, 529–550.

[185] Hensen, U.; Gräter, F.; Henchman, R. H. Macromolecular entropy can be accurately computed from force. *J. Chem. Theory Comput.* **2014**, *10*, 4777–4781.

[186] Henchman, R. H.; Irudayam, S. J. Hydrogen-Bond Definition to Characterize the Structure and Dynamics of Liquid Water. *J. Phys. Chem. B* **2010**, *114*, 16792–16810.

[187] Raveché, H. J. Entropy and Molecular Correlation Functions in Open Systems. I. Derivation. *J. Chem. Phys.* **1971**, *55*, 2242–2250.

[188] Mountain, R. D.; Raveché, H. J. Entropy and Molecular Correlation Functions in Open Systems. II Two- and Three-Body Correlations. *J. Chem. Phys.* **1971**, *55*, 2250–2255.

[189] Wallace, D. C. On the role of density fluctuations in the entropy of a fluid. *J. Chem. Phys.* **1987**, *87*, 2282–2285.

[190] Baranyai, A.; Evans, D. J. Direct entropy calculation from computer simulation of liquids. *Phys. Rev. A* **1989**, *40*, 3817–3822.

[191] Arisawa, T.; Arai, T.; Yokoyama, I. Pair and triplet correlation entropies based on the hard sphere solution of the PercusYevick equation. *Physica B* **1999**, *262*, 190–198.

[192] Sastry, S.; Angell, C. A. Liquidliquid phase transition in supercooled silicon. *Nature Mater.* **2003**, *2*, 739–743.

[193] Molinero, V.; Sastry, S.; Angell, C. A. Tuning of Tetrahedrality in a Silicon Potential Yields a Series of Monatomic (Metal-like) Glass Formers of Very High Fragility. *Phys. Rev. Lett.* **2006**, *97*, 075701.

[194] Bhat, M. H.; Molinero, V.; Soignard, E.; Solomon, V. C.; Sastry, S.; Yarger, J. L.; Angell, C. A. Vitrification of a monatomic metallic liquid. *Nature* **2007**, *448*, 787–790.

[195] Hujo, W.; Jabes, B. S.; Rana, V. K.; Chakravarty, C.; Molinero, V. The Rise and Fall of Anomalies in Tetrahedral Liquids *J. Stat. Phys.* **2011**, *145*, 293–312.

[196] Singh, M.; Dhabal, D.; Nguyen, A. H.; Molinero, V.; Chakravarty, C. Triplet Correlations Dominate the Transition from Simple to Tetrahedral Liquids *Phys. Rev. Lett.* **2014**, *112*, 147801.

[197] Dhabal, D.; Singh, M.; Wikfeldt, K. T.; Chakravarty, C. Triplet correlation functions in liquid water. *J. Chem. Phys.*, **2014**, *141*, 174504.

[198] Gallo, P.; Corradini, D.; Rovere, M. Excess entropy of water in a supercooled solution of salt. *Mol. Phys.* **2011**, *109*, 2969–2979.

[199] Gallo, P.; Rovere, M. Relation between the two body entropy and the relaxation time in supercooled water. *Phys. Rev. E* **2015**, *91*, 012107.

[200] Bertrand, C. E.; Anisimov, M. A. , The peculiar thermodynamics of the second critical point in supercooled water. *J. Phys. Chem. B* **2011**, *115*, 14099–14111.

[201] Tanaka, H. Importance of many-body orientational correlations in the physical description of liquids. *Faraday Discuss.* **2013**, *167*, 9–76.

[202] Woodcock, L. V.; Angell, C. A.; Cheeseman, P. Molecular dynamics studies of the vitreous state: Simple ionic systems and silica. *J. Chem. Phys.* **1976**, *65*, 1565–1577.

[203] Lascaris, E. Tunable liquid-liquid critical point in an ionic model of silica. http://arxiv.org/abs/1510.08088 **2015**.

[204] Lascaris, E.; Hemmati, M.; Buldyrev, S. V.; Stanley, H. E.; Angell, C. A. Search for a liquid-liquid critical point in models of silica. *J. Chem. Phys.* **2014**, *140*, 224502.

[205] McMillan, P. F. Polyamorphic transformations in liquids and glasses *J. Mater. Chem.* **2004**, *14*, 1506–1512.

[206] Wilding, M. C.; Wilson, M.; McMillan, P. F. Structural studies and polymorphism in amorphous solids and liquids at high pressure. *Chem. Soc. Rev.* **2006**, *35*, 964–986.

[207] Mishima, O. Polyamorphism in water. *Proc. Jpn. Acad., Ser. B* **2010**, *86*, 165–175.

[208] H. Tanaka, General view of a liquid-liquid phase transition *Phys. Rev. E* **2000**, *62*, 6968-6976.

[209] Harada, Y.; Tokushima, T.; Horikawa, Y.; Takahashi, O.; Niwa, H.; Kobayashi, M.; Oshima, M.; Senba, Y.; Ohashi, H.; Wikfeldt, K. T.; Nilsson, A.; Pettersson, L. G. M.; Shin, S. Selective Probing of OH/OD Stretch Vibrations in Liquid Water using Resonant Inelastic Soft X-ray Scattering. *Phys. Rev. Lett.* **2013**, *111*, 193001.

[210] Sellberg, J. A.; Huang, C.; McQueen, T. A.; Loh, N. D.; Laksmono, H.; Schlesinger, D.; Sierra, R. G.; Nordlund, D.; Hampton, C. Y.; Starodub, D. et al. Ultrafast X-ray probing of water structure below the homogeneous ice nucleation temperature. *Nature* **2014**, *510*, 381–384.

[211] Bowron, D. T.; Finney, J. L.; Hallbrucker, A.; Kohl, I.; Loerting, T.; Mayer, E.; Soper, A. K. The local and intermediate range structures of the five amorphous ices at 80K and ambient pressure: A Faber-Ziman and Bhatia-Thornton analysis. *J. Chem. Phys.* **2006**, *125*, 194502.

[212] Mayer, E. Hyperquenching of Water and Dilute Aqueous Solutions into Their Glassy States: An Approach to Cryofixation. *Cryo-Letters* **1988**, *9*, 66–77.

[213] Mayer, E. New Method for Vitrifying Water and Other Liquids by Rapid Cooling of Their Aerosols. *J. Appl. Phys.* **1985**, *58*, 663–667.

[214] Mayer, E.; Brüggeller, P. Vitrification of Pure Liquid Water by High Pressure Jet Freezing. *Nature* **1982**, *298*, 715–718.

[215] Brüggeller, P.; Mayer, E. Complete Vitrification in Pure Liquid Water and Dilute Aqueous Solutions. *Nature* **1980**, *288*, 569–571.

[216] Tu, Y.; Buldyrev, S. V.; Liu, Z.; Fang, H.; Stanley, H. E.Different water scenarios for a primitive model with two types of hydrogen bonds *Europhys. Lett.* **2012**, *97*, 56005.

[217] Ponyatovsky, E. G.; Sinitsyn, V. V.; Pozdnyakova, T. A. The metastable T–P phase diagram and anomalous thermodynamic properties of supercooled water. *J. Chem. Phys.* **1998**, *109*, 2413–2422.

[218] Moynihan, C. T. Two Species/Nonideal Solution Model for Amorphous/Amorphous Phase Transitions. *Mater. Res. Soc. Symp. Proc.* **1996**, *455*, 411.

[219] Holten, V.; Palmer, J. C.; Poole, P. H.; Debenedetti, P. G.; Anisimov, M. A. Two-state thermodynamics of the ST2 model for supercooled water. *J. Chem. Phys.* **2014**, *140*, 104502.

[220] Russo, J.; Tanaka, H. Understanding waters anomalies with locally favoured structures. *Nature Commun.* **2014**, *5*, 3556.

[221] Shiratani, E.; Sasai, M. Growth and collapse of structural patterns in the hydrogen bond network in liquid water. *J. Chem. Phys.* **1996**, *104*, 7671–7680.

[222] Shiratani, E.; Sasai, M. Molecular scale precursor of the liquid–liquid phase transition of water. *J. Chem. Phys.* **1998**, *108*, 3264–3276.

[223] Appignanesi, G. A.; Rodriguez Fris, J. A.; Sciortino, F. Evidence of a two-state picture for supercooled water and its connections with glassy dynamics. *Eur. Phys. J. E* **2009**, *29*, 305–310.

[224] Wikfeldt, K. T.; Nilsson, A.; Pettersson, L. G. M. Spatially Inhomogeneous Bimodal Inherent Structure in Simulated Liquid Water. *Phys. Chem. Chem. Phys.* **2011**, *13*, 19918–19924.

[225] Accordino, S. R.; Rodriguez Friz, J. A.; Sciortino, F.; Appignanesi, G. A. Quantitative investigation of the two-state picture for water in the normal liquid and the supercooled regime. *Eur. Phys. J. E* **2011**, *34*, 48.

[226] Russo, J.; Tanaka, H. The microscopic pathway to crystallization in supercooled liquids. *Sci. Rep.* **2012**, *2*, 505.

[227] Debenedetti, P. G.; Stillinger, F. H. Supercooled liquids and the glass transition. *Nature* **2001**, *410*, 259–267.

[228] Gallo, P.; Sciortino, F.; Tartaglia, P.; Chen, S.-H. Slow Dynamics of Water Molecules in Supercooled States. *Phys. Rev. Lett.* **1996**, *76*, 2730–2733.

[229] Sciortino, F.; Gallo, P.; ; Tartaglia, P.; Chen, S.-H. Supercooled water and the kinetic glass transition *Phys. Rev. E* **1996**, *54*, 6331–6343.

[230] Götze, W. *Complex Dynamics of Glass-Forming Liquids: A Mode-Coupling Theory*; Oxford University Press: Oxford, 2008.

[231] Angell, C. A. Formation of Glasses from Liquids and Biopolymers. *Science* **1995**, *267*, 1924–1935.

[232] Martinez, L. M.; Angell, C. A.; A thermodynamic connection to the fragility of glass-forming liquids. *Nature* **2001**, *410*, 663–667.

[233] Prielmeier, F. X.; Lang, E. W.; Speedy, R. J.; Lüdemann, H.-D. Diffusion in supercooled water to 300 MPa. *Phys. Rev. Lett.* **1987**, *59*, 1128–1131.

[234] A. P. Sokolov, J. Hurst, and D. Quitmann, Dynamics of supercooled water: Mode-coupling theory approach Phys. Rev. B 51, 12865–12868 (R).

[235] Torre, R.; Bartolini, P.; Righini, R. Structural relaxation in supercooled water by time-resolved spectroscopy. *Nature* **2004**, *428*, 296–299.

[236] Starr, F. W.; Nielsen, Stanley, H. E. Fast and Slow Dynamics of Hydrogen Bonds in Liquid Water. *Phys. Rev. Lett.* **1999**, *82*, 2294–2297.

[237] Ito, K.; Moynihan, C. T.; Angell, C. A. Thermodynamic determination of fragility in liquids and a fragile-to-strong liquid transition in water. *Nature* **1999**, *398*, 492–495.

[238] Starr, F.W.; Sciortino, F. ; Stanley, H.E. Dynamics of simulated water under pressure *Phys. Rev. E* **1999**, *60*, 6757–6768.

[239] Fraux, G.; Doye, J. P. K. Note: Heterogeneous ice nucleation on silver-iodide-like surfaces. *J. Chem. Phys.* **2014**, *141*, 216101.

[240] Atkinson, J. D.; Murray, B. J.; Woodhouse, M. T.; Whale, T. F.; Baustian, K. J.; Carslaw, K. S.; Dobbie, S.; O'Sullivan, D.; Malkin, T. L. The importance of feldspar for ice nucleation by mineral dust in mixed-phase clouds. *Nature* **2013**, *498*, 355–358.

[241] Cwilong, B. M. Sublimation in a Wilson Chamber. *Proc. Roy. Soc. A* **1947**, *190*, 137–143.

[242] Mossop, S. C. The Freezing of Supercooled Water. *Proc. Phys. Soc. B* **1955**, *68*,193–208.

[243] Mason, B. J. The supercooling and nucleation of water. *Adv. Phys.* **1958**, *7*, 221–234.

[244] Kelton, K. F. *Crystal Nucleation in Liquids and Glasses*; Vol. 45 Academic Press: Boston, 1991; p. 75.

[245] Auer, S.; Frenkel, D. Numerical prediction of absolute crystallization rates in hard-sphere colloids. *J. Chem. Phys.* **2004**, *120*, 3015–3029.

[246] Valeriani, C.; Sanz, E.; Frenkel, D. Rate of homogeneous crystal nucleation in molten NaCl. *J. Chem. Phys.* **2005**, *122*, 194501.

[247] Hardy, S. C. A grain boundary groove measurement of the surface tension between ice and water. *Philos. Mag.* **1977**, *35*, 471–484.

[248] Gránásy, L.; Pusztai, T.; James, P. F. Interfacial properties deduced from nucleation experiments: A CahnHilliard analysis. *J. Chem. Phys.* **2002**, *117*, 6157–6168.

[249] Sanz,E.; Vega, C.; Espinosa, J. R.; Caballero-Bernal, R.; Abascal, J. L. F.; Valeriani, C. *J. Am. Chem. Soc.* **2013**, *135*, 15008.

[250] Espinosa, J. R.; Sanz, E.; Valeriani,C.; Vega, C. Homogeneous ice nucleation evaluated for several water models, *J. Chem. Phys.* **2014**, *141*, 18C529.

[251] Matsumoto, M.; Saito, S.; Ohmine, I. Molecular dynamics simulation of the ice nucleation and growth process leading to water freezing. *Nature* **2002**, *416*, 409–413.

[252] Radhakrishnan, R.; Trout, B. L. Nucleation of Crystalline Phases of Water in Homogeneous and Inhomogeneous Environments. *Phys. Rev. Lett.* **2003**, *90*, 158301.

[253] Quigley, D.; Rodger, P. M. Metadynamics simulations of ice nucleation and growth. *J. Chem. Phys.* **2008**, *128*, 154518.

[254] Brukhno, A. V.; Anwar, J.; Davidchack, R.; . Handel, R. Challenges in molecular simulation of homogeneous ice nucleation. *J. Phys.: Condens. Matter* **2008**, *20*, 494243.

[255] Reinhardt, A.; Doye, J. P. K. Free energy landscapes for homogeneous nucleation of ice for a monatomic water model. *J. Chem. Phys.* **2012**, *136*, 054501.

[256] Li, T.; Donadio, D.; Russo, G.; Galli, G. Homogeneous ice nucleation from supercooled water. *Phys. Chem. Chem. Phys.* **2011**, *13*, 19807–19813.

[257] Russo, J.; Romano, F.; Tanaka, H. New metastable form of ice and its role in the homogeneous crystallization of water. *Nature Materials* **2014**, *13*, 733–739.

[258] **Stan, C. A. et al.** A microfluidic apparatus for the study of ice nucleation in supercooled water drops. *Lab. Chip* **2009**, *9*, 2293–2305.

[259] Riechers, B.; Wittbracht, F,.; Hütten, A.; Koop, T. The homogeneous ice nucleation rate of water droplets produced in a microfluidic device and the role of temperature uncertainty. *Phys. Chem. Chem. Phys.* **2013**, *15*, 5873–5887.

[260] Hagen, D. E.; Anderson, R. J.; Kassner, J. L. Homogeneous Condensation–Freezing Nucleation Rate Measurements for Small Water Droplets in an Expansion Cloud Chamber. *J. Atmos. Sci.* **1981**, *38*, 1236–1243.

[261] Laksmono, H.; McQueen, T. A.; Sellberg, J. A.; Loh, N. D.; Huang, C.; Schlesinger, D.; Sierra, R. G.; Hampton, C. Y.; Nordlund, D.; Beye, M. et al. Anomalous Behavior of the Homogeneous Ice Nucleation Rate in "No-Man's Land", *J. Phys. Chem. Lett.* **2015**, *6*, 2826–2832.

[262] Huang, J. F.; Bartell, L. S. Kinetics of Homogeneous Nucleation in the Freezing of Large Water Clusters. *J. Phys. Chem.* **1995**, *99*, 3924–3931.

[263] Bhabhe, A.; Pathak, H.; Wyslouzil, B. E. Freezing of Heavy Water (D_2O) Nanodroplets. *J. Phys. Chem. A* **2013**, *117*, 5472–5482.

[264] Jenniskens, P.; Blake, D. F. Crystallization of Amorphous Water Ice in the Solar System. *Astrophys. J.* **1996**, *473*, 1104–1113.

[265] Safarik, D. J.; Mullins, C. B. The nucleation rate of crystalline ice in amorphous solid water. *J. Chem. Phys.* **2004**, *121*, 6003–6010.

[266] Hage, W.; Hallbrucker, A.; Mayer, E.; Johari, G. P. Crystallization Kinetics of Water below 150 K. *Chem. Phys.* **1994**, *100*, 2743-2747.

[267] Hage, W.; Hallbrucker, A.; Mayer, E.; Johari, G. P. Kinetics of Crystallizing D_2O Water near 150 K by Fourier Transform Infrared Spectroscopy and a Comparison with the Corresponding Calorimetric Studies on H_2O Water. *J. Chem. Phys.* **1995**, *103*, 545–550.

[268] Stöckel, P.; Weidinger, I. M.; Baumgärtel, H.; Leisner, T. Rates of homogeneous ice nucleation in levitated H_2O and D_2O droplets. *J. Phys. Chem. A* **2005**, *109*, 2540–2546.

[269] Murray, B. J.; Broadley, S. L.; Wilson, T. W.; Bull, S. J.; Wills, R. H.; Christenson, H. K.; Murray, E. J. Kinetics of the homogeneous freezing of water. *Phys. Chem. Chem. Phys.* **2010**, *12*, 10380–10387.

[270] Pruppacher, H. R. A New Look at Homogeneous Ice Nucleation in Supercooled Water Drops. *J. Atmosph. Sci.* **1995**, *52*, 1924–1933.

[271] Manka, A.; Pathak, H.; Tanimura, S.; Wolk, J.; Strey, R.; Wyslouzil, B. E. Freezing water in no-man's land. *Phys. Chem. Chem. Phys.* **2012**, *14*, 4505–4516.

[272] McMillan, J. A.; Los, S. C. Vitreous ice: Irreversible transformations during warm-up. *Nature* **1965**, *206*, 806–807.

[273] Rozmanov, D.; Kusalik, P. G. Temperature dependence of crystal growth of hexagonal ice (I_h). *Phys. Chem. Chem. Phys.* **2011**, *13*, 15501–15511.

[274] Avrami, M. Kinetics of Phase Change. I General Theory. *J. Chem. Phys.* **1939**, *7*, 1103–1112.

[275] Abascal, J. L. F.; Vega, C. Note: Equation of state and compressibility of supercooled water: Simulations and experiment. *J. Chem. Phys.* **2011**, *134*, 186101.

[276] Wikfeldt, K. T.; Huang, C.; Nilsson, A.; Pettersson, L. G. M. Enhanced small-angle scattering connected to the Widom line in simulations of supercooled water. *J. Chem. Phys.* **2011**, *134*, 214506.

[277] Bresme, F.; Biddle, J. W.; Sengers, J. V.; Anisimov, M. A. Communication: Minimum in the thermal conductivity of supercooled water: A computer simulation study. *J. Chem. Phys.* **2014**, *140*, 161104.

[278] Berg, B. A.; Dubey, S. Finite Volume Kolmogorov-Johnson-Mehl-Avrami Theory. *Phys. Rev. Lett.* **2008**, *100*, 165702.

[279] Ostwald, W. Studien über die Bildung und Umwandlung fester Körper. *Z. Phys. Chem.* **1897**, *22*, 289–330.

[280] van Santen, R. A. The Ostwald Step Rule. *J. Phys. Chem.* **1984**, *88*, 5768–5769.

[281] Liu, L.; Chen, S. H.; Faraone, A.; Yen, C.-W.; Mou, C.-Y. Pressure Dependence of Fragile-to-Strong Transition and a Possible Second Critical Point in Supercooled Confined Water. *Phys. Rev. Lett.* **2005**, *95*, 117802.

[282] Xu L, Ehrenberg I, Buldyrev S V, Stanley H E. Relationship between the liquid–liquid phase transition and dynamic behavior in the Jagla model. *J. Phys.: Condens. Matter* **2006**, *18*, S2239–S2246.

[283] Franzese, G., Stanley, H. E. The Widom line of supercooled water. *J. Phys. Condens. Matter* **19**, 205126 (2007).

[284] Corradini, D.; Gallo, P. Liquid-Liquid critical point in NaCl aqueous solutions: concentration effects. *J. Phys. Chem. B* **2011**, *115*, 14161–14166.

[285] Corradini, D.; Buldyrev, S. V.; Gallo, P.; Stanley, H. E. Effects of hydrophobic solutes on the liquid-liquid critical point. *Phys. Rev. E* **2010**, *81*, 061504.

[286] Gallo, P.; Corradini, D.; Rovere, M. Fragile to strong crossover at the Widom line in supercooled aqueous solutions of NaCl. *J. Chem. Phys.* **2013**, *139*, 204503.

[287] Gallo, P.; Rovere, M. Mode Coupling and fragile to strong transition in supercooled TIP4P water. *J. Chem. Phys.* **2012**, *137*, 164503.

[288] De Marzio M.; Camisasca G.; Rovere M.; Gallo P. Mode Coupling Theory and Fragile to Strong Transition in Supercooled TIP4P/2005 Water *Submitted* **(2015)**.

[289] De Marzio M.; Camisasca G.; Rovere M.; Gallo P. Connection between Fragile to Strong transition and hopping processes in supercooled TIP4P/2005 water *in preparation* **(2015)**.

[290] Corradini, D.; Gallo, P.; Buldyrev, S. V.; Stanley, H. E. Fragile to strong crossover coupled to liquid-liquid transition in hydrophobic solutions. *Phys. Rev. E* **2012**, *85*, 051503.

[291] Xu, L.; Mallamace, M.; Yan, Z.; Starr, F. W.; Buldyrev, S. V.; Stanley, H. E. Appearance of a fractional Stokes–Einstein relation in water and a structural interpretation of its onset. *Nature Phys.* **2009**, *5*, 565–569.

[292] Soper, A. K. Radical re-appraisal of water structure in hydrophilic confinement. *Chem. Phys. Lett.* **2013**, *590*, 1-15.

[293] Gallo, P.; Rovere, M.; Chen, S.-H. Dynamic crossover in supercooled confined water: understanding bulk properties through confinement. *J. Phys. Chem. Lett.* **2010**, *1*, 729–733.

[294] Gallo, P.; Rovere, M.; Chen, S.-H. Anomalous dynamics of water confined in MCM-41 at different hydrations. *J. Phys.: Condens. Matt.* **2010**, *22*, 284102.

[295] Gallo, P.; Rovere, M.; Chen, S.-H. Water confined in MCM-41: a Mode Coupling Theory analysis. *J. Phys.: Condens. Matter* **2012**, *24*, 064109.

[296] Rosenfeld, Y. Relation between the transport coefficients and the internal entropy of simple systems. *Phys. Rev. A* **1977**, *15*, 2545–2549.

[297] Rosenfeld, Y. A quasi-universal scaling law for atomic transport in simple fluids. *J. Phys.: Condens. Matter* **1999**, *11*, 5415–5427.

[298] Dzugutov, M. A universal scaling law for atomic diffusion in condensed matter. *Nature* **1996**, *381*, 137–139.

[299] Hoyt, J. J.; Asta, M.; Sadigh, B. Test of the Universal Scaling Law for the Diffusion Coefficient in Liquid Metals. *Phys. Rev. Lett.* **2000**, *85*, 594–597.

[300] Sharma, R.; Chakraborty, S. N.; Chakravarty, C. Entropy, diffusivity, and structural order in liquids with waterlike anomalies. *J. Chem.Phys.* **2006**, *125*, 204501.

[301] Errington, J. R.; Truskett, T. M.; Mittal, J. Excess-entropy-based anomalies for a waterlike fluid. *J. Chem. Phys.* **2006**, *125*, 244502.

[302] Agarwal, M.; Singh, M.; Sharma, R.; Alam, M. P.; Chakravarty, C. Relationship between Structure, Entropy, and Diffusivity in Water and Water-Like Liquids. *J. Phys. Chem. B* **2010**, *114*, 6995–7001.

[303] Abramson, E. H. Viscosity of water measured to pressures of 6 GPa and temperatures of 300 °C. *Phys. Rev. E* **2007**, *76*, 051203.

[304] Agarwal, M.; Chakravarty, C. Relationship between structure, entropy, and mobility in network-forming ionic melts. *Phys. Rev. E* **2009**, *79*, 030202(R).

[305] de Oliveira, A. B.; Franzese, G.; Netz, P. A.; Barbosa, M. C. Waterlike hierarchy of anomalies in a continuous spherical shouldered potential. *J. Chem. Phys.* **2008**, *128*, 064901.

[306] Mittal, J.; Errington, J. R.; Truskett, T. M. Relationship between thermodynamics and dynamics of supercooled liquids. *J. Chem. Phys.* **2006**, *125*, 076102.

[307] Krekelberg, W. P.; Kumar, T.; Mittal, J.; Errington, J. R.; Truskett, T. M. Anomalous structure and dynamics of the Gaussian-core fluid. *Phys. Rev. E* **2009**, *79*, 031203.

[308] Goel, T.; Patra, C. N.; Mukherjee, T.; Chakravarty, C. Excess entropy scaling of transport properties of Lennard-Jones chains. *J. Chem. Phys.* **2008**, *129*, 164904.

[309] Malvaldi, M.; Chiappe, C. Excess entropy scaling of diffusion in room-temperature ionic liquids. *J. Chem. Phys.* **2010**, *132*, 244502.

[310] Chopra, R; Truskett, T. M.; Errington, J. R. On the Use of Excess Entropy Scaling to Describe the Dynamic Properties of Water. *J. Phys. Chem. B* **2010**, *114*, 10558–10566.

[311] Chopra, R.; Truskett, T. M.; Errington, J. R. Excess entropy scaling of dynamic quantities for fluids of dumbbell-shaped particles. *J. Chem. Phys.* **2010**, *133*, 104506.

[312] Gallo, P.; Corradini, D.; Rovere, M. Widom line and dynamical crossovers: routes to understand supercritical water. *Nature Commun.* **2014**, *5*, 5806.

[313] Simeoni, G. G.; Bryk, T.; Gorelli, F. A.; Krisch, M.; Ruocco, G.; Santoro, M.; Scopigno, T. The Widom line as the crossover between liquid-like and gas-like behavior in supercritical fluids. *Nature Phys.* **2010**, *6*, 503–507.

[314] Brazhkin, V. V.; Fomin, Yu. D.; Lyapin, A. G.; Ryzhov, V. N.; Tsiok, E. N. Widom Line for the Liquid-Gas Transition in Lennard-Jones System. *J. Phys. Chem. B* **2011**, *115*, 14112–14115.

[315] Gallo, P.; Corradini, D.; Rovere, M. The Widom line and dynamical crossover in supercritical water: Popular water models versus experiments *J. Chem. Phys.* **2015**, *143*, 114502.

[316] Kanno, H.; Speedy, R. J.; Angell, C. A. Supercooling of water to -92 °C under pressure. *Science* **1975**, *189*, 880–881.

[317] Caupin, F. Escaping the no man's land: Recent experiments on metastable liquid water. *J. Non-Crystalline Solids* **2015**, *407*, 441–448.

[318] Caupin, F.; Herbert, E. Cavitation in water: a review, *C. R. Phys.* **2006**, *7* 1000–1017.

[319] Caupin, F.; Stroock, A. D. The stability limit and other open questions on water at negative pressure, in: H.E. Stanley, S. Rice (Eds.), *Liquid Polymorphism*; Advances in Chemical Physics **152**, Wiley: New York, 2013.

[320] Henderson, S. J.; Speedy, R. J. Temperature of maximum density in water at negative pressure. *J. Phys. Chem.* **1987**, *91*, 3062–3068.

[321] Henderson, S. J.; Speedy, R. J. Melting temperature of ice at positive and negative pressures. *J. Phys. Chem.* **1987**, *91*, 3069–3072.

[322] Davitt,K.; Rolley,E.; Caupin, F.; Arvengas, A.; Balibar, S. Equation of state of water under negative pressure. (2010) 174507.

[323] Wagner, W.; Pruß, A. The IAPWS formulation 1995 for the thermodynamic properties of ordinary water substance for general and scientific use. *J. Phys. Chem. Ref. Data* **2002**, *31*, 387–535.

[324] The International Association for the Properties of Water and Steam, Revised Release on the IAPWS Formulation 1995 for the Thermodynamic Properties of Ordinary Water Substance for General and Scientific Use, 2009.

[325] Zheng, Q.; Durben, D. J.; Wolf, G. H.; Angell, C. A. Liquids at large negative pressures: water at the homogeneous nucleation limit. *Science* **1991**, *254*, 829–832.

[326] Alvarenga,A. D.; Grimsditch, M.; Bodnar, R. J. Elastic properties of water under negative pressures. *J. Chem. Phys.* **1993**, *98*, 8392–8396.

[327] Shmulovich, K. I.; Mercury, L.; Thiéry, R.; Ramboz, C.; El Mekki, M. Experimental superheating of water and aqueous solutions. *Geochim. Cosmochim. Acta* **2009**, *73*, 2457–2470.

[328] El Mekki Azouzi, M.; Ramboz, C.; Lenain, J.-F.; Caupin, F. A coherent picture of water at extreme negative pressure. *Nature Phys.* **2013**, *9*, 38–41.

[329] Angell, C. A.; Supercooled water: Two phases? *Nature Materials* **2014**, *13*, 673–675.

[330] Ronceray, P.; Harrowell, P., Favoured local structures in liquids and solids: a 3D lattice model. *Soft Matter* **2015**, *11*, 3322-3331.

[331] Velikov, V.; Borick, S.; Angell, C. A. The glass transition of water, based on hyperquenching experiments. *Science* **2001**, *294*, 2335–2338.

[332] Meadley, S. L.; Angell, C. A. Water and its relatives: The stable, supercooled and particularly the stretched, regimes. Proceedings of the International School of Physics Enrico Fermi: "Water: Fundamentals as the basis for understanding the environment and promoting technology" Course 187, edited by P. G. Debenedetti, M. A Ricci and F. Bruni; IOS Press, Amsterdam; SIF, Bologna, 2015; p 19–44.

[333] Birch, F. Finite Elastic Strain of Cubic Crystals. *Phys. Rev. E* **1947**, *71*, 809–824.

[334] Murnaghan, F. D. The Compressibility of Media under Extreme Pressures. *Proc. Natl. Acad. Sci. (USA)* **1944**, *30*, 244–247.

[335] Briggs, L. J. Limiting negative pressure of water. *J. Appl. Phys.* **1950**, *21*, 721–722.

[336] Winnick, J.; Cho, S. J. PVT behavior of water at negative pressures. *J. Chem. Phys.* **1971**, *55*, 2092–2097.

[337] Green, J. L.; Durben, D. J.; Wolf, G. H.; Angell, C. A. Water and Solutions at Negative Pressure: Raman Spectroscopic Study to -80 Megapascals. *Science* **1990**, *249*, 649–652.

[338] Zheng, Q. Liquids under tension and glasses under stress. Ph. D. Thesis, Purdue University, 1991.

[339] Fisher, J. C. The Fracture of Liquids. *J. Appl. Phys.* **1948**, *19*, 1062–1067.

[340] Davitt, K.; Arvengas, A.; Caupin, F. Water at the cavitation limit: density of the metastable liquid and size of the critical bubble. *Euro. Phys. Lett.* **2010**, *90*, 16002.

[341] Bodnar, R. J.; Sterner, S. M. Synthetic fluid inclusions in natural quartz I. Compositional types synthesized and applications to experimental geochemistry. *Geochim. Cosmochim. Acta* **1984**, *48*, 2659–2668.

[342] Corradini, D.; Strekalova, E.; Stanley, H. E.; Gallo, P. Microscopic mechanism of protein cryopreservation in an aqueous solution with trehalose. *Sci. Rep.* **2013**, *3*, 1218.

[343] Gallo, P.; Rovere, M.; Spohr, E. Supercooled confined water and the Mode Coupling Crossover Temperature. *Phys. Rev. Lett.* **2000**, *85*, 4317.

[344] Gallo, P.; Rovere, M.; Spohr, E. Glass transition and layering effect in confined water: a computer simulation study. *J. Chem. Phys.* **2000**, *113*, 11324–11335.

[345] Faraone, A.; Liu, L.; Mou, C.- Y.; Yen, C.-W.; Chen, S.-H. Fragile-to-strong liquid transition in deeply supercooled confined water. *J. Chem. Phys.* **2004**, *121*, 10843–10846.

[346] Saika-Voivod, I.; Poole,P. H.; Sciortino, F. Fragile-to-strong transition and polyamorphism in the energy landscape of liquid silica. *Nature* **2001**, *412*, 514-517.

[347] Luo, J.; Xu, L.; Lascaris, E.; Stanley, H. E.; Buldyrev, S. V. Behavior of the Widom Line in Critical Phenomena. *Phys. Rev. Lett.* **2014**, *112*, 135701.

[348] Kumar, P.; Wikfeldt, K. T.; Schlesinger, D.; Pettersson, L. G. M.; Stanley, H. E. The Boson peak in supercooled water. *Sci. Rep.* **2013**, *3*, 1980.

[349] Kanno, H.; Angell, C. A. Homogeneous nucleation and glass formation in aqueous alkali halide solutions at high pressures. *J. Phys. Chem.* **1977**, *81*, 2639–2643.

[350] Miyata, K.; Kanno, H.; Niino, T.; Tomizawa, K. Cationic and anionic effects on the homogeneous nucleation of ice in aqueous alkali halide solutions. *Chem. Phys. Lett.* **2002**, *354*,

51–55.

[351] Miyata, K.; Kanno, H. Supercooling behavior of aqueous solutions of alcohols and saccharides. *J. Mol. Liq.* **2005**, *119*, 189–193.

[352] Archer, D. G.; Carter, R. W. Thermodynamic Properties of the NaCl + H_2O System. 4. Heat Capacities of H_2O and NaCl(aq) in Cold-Stable and Supercooled States. *J. Phys. Chem. B* **2000**, *104*, 8563–8584.

[353] Carter, R. W.; Archer, D. G. Heat capacity of $NaNO_3$(aq) in stable and supercooled states. Ion association in the supercooled solution. *Phys. Chem. Chem. Phys.* **2000**, *2*, 5138–5145.

[354] Mishima, O. Application of polyamorphism in water to spontaneous crystallization of emulsified LiCl-H_2O solution. *J. Chem. Phys.* **2005**, *123*, 154506.

[355] Mishima, O. Phase separation in dilute LiCl–H_2O solution related to the polyamorphism of liquid water. *J. Chem. Phys.* **2007**, *126*, 244507.

[356] Guadalupe, N. R.; Bove, L. E.; Corti, H. R.; Loerting, T. Pressure-induced transformations in LiCl–H_2O at 77 K. *Phys. Chem. Chem. Phys.* **2014**, *16*, 18553–18562.

[357] Paschek, D. How the Liquid-Liquid Transition Affects Hydrophobic Hydration in Deeply Supercooled Water. *Phys. Rev. Lett.* **2005**, *94*, 217802.

[358] Le, L.; Molinero, V. Nanophase Segregation in Supercooled Aqueous Solutions and their Glasses Driven by the Polyamorphism of Water. *J. Phys. Chem. A* **2011**, *115*, 5900–5907.

[359] **THIS REFERENCE IS A MIX-UP OF TWO** Chaterjee, S.; Debenedetti, P. G. *J. Chem. Phys.* **2006**, *124*, 154504.

[360] Anisimov, M. A. Cold and supercooled water: a novel supercritical-fluid solvent. *Russ. J. Phys. Chem. B* **2012**, *6*, 861–867.

[361] Suzuki, Y.; Mishima, O. Experimentally proven liquid-liquid critical point of dilute of dilute glycerol-water solutions at 150 K. *J. Chem. Phys.* **2014**, *141*, 094505.

[362] Murata, K.; Tanaka, H. Liquid–liquid transition without macroscopic phase separation in a water–glycerol mixture. *Nature Materials* **2012**, *11*, 436–443.

[363] Murata, K.-I.; Tanaka, H. General nature of liquid–liquid transition in aqueous organic solutions. *Nature Commun.* bf 2013, *4*, 2844.

[364] Popov, I.; Greenbaum (Gutina), A.; Sokolov, A. P.; Feldman, Y. The puzzling first-order phase transition in water–glycerol mixtures. *Phys. Chem. Chem. Phys.* **2015**, *17*, 18063–18071.

[365] Zhao, L.-S.; Cao, Z.-X.; Wang, Q. Glass transition of aqueous solutions involving annealing-induced ice recrystallization resolves liquid-liquid transition puzzle of water. *Sci. Rep.* **2015**, *5*, 15714.

[366] Dehaoui, A.; Issenmann, B.; Caupin, F. Viscosity of deeply supercooled water and its coupling to molecular diffusion. *Proc. Natl. Acad. Sci. (USA)* **2015**, *112*, 1202012025.

[367] Miyata, K.; Kanno, H.; Niino, T.; Tomizawa, K. Cationic and anionic effects on the homogeneous nucleation of ice in aqueous alkali halide solutions, *Chem. Phys. Lett.* **2002**, *354*, 51–55.

[368] Corradini, D.; Rovere, M.; Gallo, P. Structural properties of high density and low density water in supercooled aqueous solutions of salt. *J. Phys. Chem. B* **2011**, *115*, 1461–1468.

[369] Huang, C.; Weiss, T. M.; Nordlund, D.; Wikfeldt, K. T.; Pettersson, L. G. M.; Nilsson, A. Increasing correlation length in bulk supercooled H_2O, D_2O, and NaCl solution determined from small angle x-ray scattering. *J. Chem. Phys.* **2010**, *133*, 134504.

[370] Mishima, O. Melting of the Precipitated Ice IV in LiCl Aqueous Solution and Polyamorphism of Water. *J. Phys. Chem. B* **2011**, *115*, 14064–14067.

[371] Suzuki, Y.; Mishima, O. Sudden switchover between the polyamorphic phase separation and the glass-to-liquid transition in glassy LiCl aqueous solutions. *J. Chem. Phys.* **2013**, *138*, 084507.

[372] Corradini, D.; Su, Z.; Stanley, H. E.; Gallo, P. A molecular dynamics study of the equation of state and structure of supercooled aqueous solutions of methanol. *J. Chem. Phys.* **2012**, *137*, 184503.

[373] Mallamace, F.; Branca, C.; Corsaro, C.; Leone, N.; Spooren, J.; Stanley, H. E.; Chen, S.-H. Dynamical crossover and breakdown of the Stokes-Einstein relation in confined water and in methanol-diluted bulk water. *J. Phys. Chem. B* **2010**, *114*, 1870–1878.

[374] Hendricks, R. W., Mardon, P. G. and Shaffer, L. B. X-Ray Zero-Angle Scattering Cross-Section of Water. *J. Chem. Phys.* **1974**, *61*, 319–322.

[375] Leberman, R.; Soper, A. K. Effect of High-Salt Concentrations on Water-Structure. *Nature* **1995**, *378*, 364–366.

[376] Mallamace, F.; Corsaro, C.; Baglioni, P.; Fratini, E.; Chen, S.-H. The dynamical crossover phenomenon in bulk water, confined water and protein hydration water. *J. Phys.: Condens. Matter* **2012**, *24*, 064103.

[377] Suhina, T.; Weber, B.; Carpentier, C. E.; Lorincz, K.; Schall, P.; Bonn, D.; M., B. A. Fluorescence Microscopy Visualization of Contacts Between Objects. *Angew. Chemie Int. Ed.* **2015**, *54*, 3688–3691.

[378] Holmberg, K.; Andersson, P.; Erdemir, A. Global energy consumption due to friction in passenger cars. *Tribol. Int.* **2012**, *47*, 221–234.

[379] Poole, P. H.; Becker, S. R.; Sciortino, F.; Starr, F. W. Dynamical Behavior Near a Liquid-Liquid Phase Transition in Simulations of Supercooled Water. *J. Phys. Chem. B* **2011**, *115*, 1417614183.

[380] Prielmeier, F. X.; Lang, E. W.; Speedy, R. J.; Lüdemann, H.-D. The Pressure Dependence of Self Diffusion in Supercooled Light and Heavy Water. *Ber. Bunsenges. Phys. Chem.* **1988**, *92*, 1111–1117.

[381] Zheng, Q.; Green, J.; Kieffer, J.; Poole, P. H.; Shao, J.; Wolf, G. H.; Angell, C. A. Limiting tensions for liquids and glasses from laboratory and MD studies. NATO-ASI Series *Liquids under Negative pressure*, Kluwer Academic Pub, 2002; p. 1–46.

[382] Koop, T.; Luo, B.-P.; Tsias, A.; Peter, T. Water activity as the determinant for homogeneous ice nucleation in aqueous solutions. *Nature* **2000**, *406*, 611–614.

[383] Waluyo, I.; Nordlund, D.; Bergmann, U.; Schlesinger, D.; Pettersson, L. G. M.; Nilsson, A. Different View of Structure-Making and Structure-Breaking in Alkali Halide Aqueous Solutions through X-ray Absorption Spectroscopy. *J. Chem. Phys.* **2014**, *140*, 244506.

[384] Binder, K. Simulations clarify when supercooled water freezes into glassy structures. *Proc Natl. Acad. Sci. (USA)* **2014**, *111*, 9374–9375.